Stability Analysis of Periodic Delay-Differential Equations Modeling Machine Tool Chatter

PhD dissertation

Tamás Insperger

Supervisor:
Gábor Stépán, DSc

February, 2002

Contents

List of Figures

Chapter 1

Introduction

Systems governed by delay-differential equations often come up in different fields of science and engineering. One of the most important mechanical application is the cutting process dynamics. After the extensive work of Tlusty *et al.* (1962), Tobias (1965) and Kudinov (1955, 1967), the so-called regenerative effect has become the most commonly accepted explanation for machine tool chatter (see Stépán, 1989, Moon, 1998). This effect is related to the cutting force variation due to the wavy workpiece surface cut one revolution ago. The corresponding mathematical models are delay-differential equations.

Delayed equations also arise in robotics applications, telemanipulation with information delay can be mentioned (see Whitney 1977, Stépán and Steven, 1990, Kim and Bejczy, 1993, Müller and Stépán, 1994, Stépán and Haller, 1995, Insperger and Stépán, 2000d). Time delay also arises in neural network models, where the interactions of the neurons are delayed (see Campbell, 1999, Campbell *et al.*, 1999).

In the case of systems with parametric excitation, some characteristic properties of the system change periodically in time. The governing equations are consequently time periodic equations.

The qualitative investigation of these mechanical systems always includes stability analysis. For engineers, this work can effectively be supported by the so-called stability charts. These charts show those parameter values for which the system is stable or unstable.

Some properties of linear functional differential equations are reviewed in Chapter 2. The basic mathematical background for stability analysis is presented for autonomous and periodic systems, and demonstrated by examples.

In Chapter 3, a special periodic linear functional differential equation, the delayed Mathieu equation is considered as a basic problem. Stability analysis is carried out using Hill's infinite matrix method, and an almost closed form stability chart is constructed. This stability chart makes connection between the Strutt–Ince chart of the

Mathieu equation and the Hsu–Bhatt–Vyshnegradskii chart of the second order delay-differential equation (also called delayed oscillator). The combined chart describes the intriguing stability properties of a class of delayed oscillatory systems subjected to parametric excitation.

In Chapter 4, a special approximation method is introduced for the stability analysis of linear delayed equations. The method is based on the special properties of the so-called Fargue-type delay equations, where the time delay is distributed along the past according to a special weight function. These equations are transformed into a system of ordinary differential equations, for which, the stability properties can be determined by conventional methods. In the approach presented in Chapter 4, these equations are used for approximating delayed equations with discrete time delay.

Chapter 5 presents an efficient numerical method, the so-called semi-discretization, for the stability analysis of periodic linear delayed systems. The method is based on a special kind of discretization technique with respect to the past effect only. The resulting approximate system is delayed and also time periodic, but still, it can be transformed analytically into a high dimensional linear discrete system. The method is applied to determine the stability charts of the Mathieu equation with distributed time delay.

In Chapter 6, the milling process is modeled including the tooth pass excitation effect. The relating time periodic delay-differential equation is analyzed by the semi-discretization method, and stability charts are constructed in the plane of technological parameters. New stability properties are recognized for high speed milling.

In Chapter 7, turning with varying spindle speed is considered. Here, the parametric excitation occurs in the time delay. Consequently, the governing equation is a delay-differential equation with time varying delay. Stability charts are constructed by the semi-discretization method, and new bifurcation phenomena are observed.

Chapter 2

Mathematical background

Hereditary systems are described by functional differential equations (FDEs). According to Myshkis (1955), FDEs are equations involving the function $x(t)$ of one scalar argument t (called time) and its derivatives for several values of argument t. It was Mhyskis (1949), who formulated the initial value problem of delay-differential equations in the mathematically correct form of FDEs for the first time. In this chapter, some special FDEs are reviewed and the main stability properties are summarized.

2.1 Linear autonomous ordinary differential equations

Linear autonomous ordinary differential equations (ODEs) have the general form

$$\dot{\mathbf{y}}(t) = \mathbf{A}\mathbf{y}(t) \,, \tag{2.1}$$

where $\mathbf{y} \in \mathbb{R}^n$, $\mathbf{A}$ is an $n \times n$ matrix, and

$$\dot{\mathbf{y}} = \frac{\mathrm{d}\mathbf{y}}{\mathrm{d}t} = \mathrm{col} \left(\frac{\mathrm{d}y_1}{\mathrm{d}t} \ \frac{\mathrm{d}y_2}{\mathrm{d}t} \ \cdots \ \frac{\mathrm{d}y_n}{\mathrm{d}t} \right) .$$

For a given initial value $\mathbf{y}(0) = \mathbf{y}_0$, the solutions of equation (2.1) can be written in the form

$$\mathbf{y}(t) = \exp(\mathbf{A}t)\mathbf{y}_0 \,, \tag{2.2}$$

where the $\exp(\mathbf{A}t)$ is the exponential of matrix $\mathbf{A}t$, defined by the Taylor series of the exponential function (see e.g. the book of Hirsch and Smale, 1974, or the book of Perko, 1996).

The stability of the solution $\mathbf{y}(t) \equiv \mathbf{0}$ is determined by the eigenvalues λ_j, $j = 1, 2, \ldots, n$ of the coefficient matrix $\mathbf{A}$. These are called characteristic roots of equation (2.1). If all the characteristic roots have negative real parts, i.e. $\mathrm{Re}\,\lambda_j < 0$ for all $j = 1, 2, \ldots, n$, then the trivial solution of system (2.1) is exponentially asymptotically
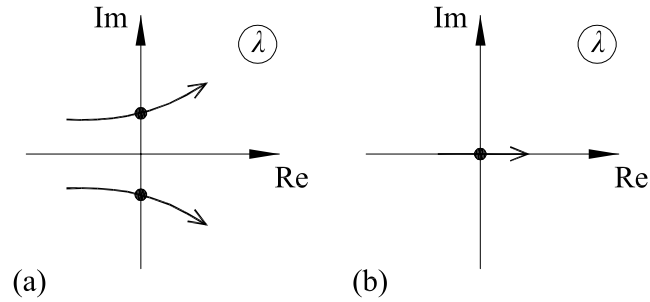
Figure 2.1: Critical characteristic roots for autonomous systems: Hopf bifurcation (a) and saddle-node bifurcation (b)

stable. In a general case, the characteristic roots can be determined by solving the characteristic equation

$$\det(\lambda \mathbf{I} - \mathbf{A}) = 0 \,. \tag{2.3}$$

Development of equation (2.3) results in an nth degree polynomial of λ, and many numerical methods can be used to determine the roots. However, the stability analysis can be done without determining the characteristic roots. The famous Routh–Hurwitz criterion provides an algorithm to check the stability condition by the coefficients of the characteristic polynomial (see Routh, 1877 and Hurwitz, 1895).

According to the location of the critical characteristic roots, there are two basic ways for loss of stability of linear autonomous systems (see Guckenheimer and Holmes, 1983).

1. The critical characteristic roots are complex pair moving from the left-hand side of the complex plane to the right-hand side crossing the imaginary axis, as it is shown by case (a) in Figure 2.1. This case is called *Hopf*, or *Andronov–Hopf* or Poincaré–Andronov–Hopf (PAH) bifurcation of a corresponding nonlinear system. The systematic study of the conditions and the proof of the corresponding bifurcation theorem was done by Andronov and Leontovich (1937) in the two dimensional case, and by Hopf (1942) in the n dimensional case. According to the theory of nonlinear systems, either stable or unstable periodic motion may exist around the equilibrium of the corresponding nonlinear system, called supercritical and subcritical bifurcation, respectively.

2. The critical characteristic root is a real one moving from the left-hand side of the complex plane to the right-hand side crossing the origin, as it is shown by case (b) in Figure 2.1. This case is called *saddle-node* bifurcation of a corresponding nonlinear system.

Example

A simple example for linear autonomous ODEs is the damped oscillator

$$\ddot{x}(t) + b_0\dot{x}(t) + c_0 x(t) = 0 \,. \tag{2.4}$$

Using the so-called Cauchy transformation, this system can be given in the form of equation (2.1), where

$$\mathbf{y}(t) = \begin{pmatrix} x(t) \\ \dot{x}(t) \end{pmatrix} \quad \text{and} \quad \mathbf{A} = \begin{pmatrix} 0 & 1 \\ -c_0 & -b_0 \end{pmatrix} \,. \tag{2.5}$$

The characteristic equation of system (2.4) reads

$$\lambda^2 + b_0\lambda + c_0 = 0 \,. \tag{2.6}$$

This equation can also be obtained by substituting the trial solution $x(t) = K\exp(\lambda t)$ into equation (2.4). The characteristic roots are

$$\lambda_{1,2} = \frac{-b_0 \pm \sqrt{b_0^2 - 4c_0}}{2} \,. \tag{2.7}$$

It can easily be seen, that the condition of asymptotic stability is $c_0 > 0$ and $b_0 > 0$, since in this case $\operatorname{Re}\lambda_{1,2} < 0$. Hopf bifurcation arises at $b_0 = 0$, $c_0 > 0$, saddle node bifurcation occurs at $b_0 > 0$, $c_0 = 0$.

2.2   Linear periodic ordinary differential equations

The general form of a linear periodic ODE reads

$$\dot{\mathbf{y}}(t) = \mathbf{A}(t)\mathbf{y}(t), \quad \mathbf{A}(t) = \mathbf{A}(t+T) \,. \tag{2.8}$$

Here, the coefficient matrix is time periodic in contrast to the constant coefficient matrix of the autonomous system (2.1). The main theorems on general periodic systems are summarized in the book of Farkas (1994).

For periodic ODEs, stability condition is provided by the Floquet Theory. The solution of system (2.8) with the initial condition $\mathbf{y}(0) \equiv \mathbf{y}_0$ is given by $\mathbf{y}(t) = \mathbf{\Phi}(t)\mathbf{y}_0$, where $\mathbf{\Phi}(t)$ is a fundamental matrix of system (2.8). Floquet (1883) showed that the fundamental matrix has the form $\mathbf{\Phi}(t) = \mathbf{P}(t)\exp(\mathbf{B}t)$, where $\mathbf{P}(t) = \mathbf{P}(t+T)$ is a periodic matrix with initial value $\mathbf{P}(0) = \mathbf{I}$, and $\mathbf{B}$ is a constant matrix. The matrix $\mathbf{\Phi}(T) = \exp(\mathbf{B}T)$ is the so-called principal or monodromy or Floquet transition matrix of system (2.8), and it gives the connection between the initial state and the state one principal period later: $\mathbf{y}(T) = \mathbf{\Phi}(T)\mathbf{y}(0)$. The stability conditions for system (2.8) are determined by the eigenvalues of the Floquet transition matrix.

The eigenvalues of $\mathbf{\Phi}(T)$ are the characteristic multipliers $(\mu_j, \; j = 1, 2, \ldots, n)$ calculated from

$$\det(\mu \mathbf{I} - \mathbf{\Phi}(T)) = 0 \,. \tag{2.9}$$

The eigenvalues of matrix $\mathbf{B}$ are the characteristic exponents $(\lambda_j, \; j = 1, 2, \ldots, n)$ given by

$$\det(\lambda \mathbf{I} - \mathbf{B}) = 0 \,. \tag{2.10}$$

Obviously, if μ is a characteristic multiplier, then there is a characteristic exponent λ, such that $\mu = \exp(\lambda T)$, and vice versa.

The trivial solution $\mathbf{y}(t) \equiv \mathbf{0}$ of system (2.8) is asymptotically stable, if and only if all the characteristic multipliers are in modulus less than one, that is, all the characteristic exponents have negative real parts.

Similarly to autonomous systems, the basic types of stability losses can be classified according to the location of the critical characteristic multipliers (see Guckenheimer and Holmes, 1983). For periodic systems, there are three typical ways.

1. The critical characteristic multipliers are a complex pair moving out of the unit circle, i.e. $|\mu| = 1$ and $|\bar{\mu}| = 1$ in the critical case, as it is shown by case (a) in Figure 2.2. This case is topologically equivalent to the Hopf bifurcation of autonomous systems and called as *secondary Hopf* or *Neimark–Sacker* bifurcation. According to the theory of nonlinear systems, either stable (supercritical case) or unstable (subcritical case) quasi-periodic motions exist around the equilibrium of the corresponding nonlinear system.

2. The critical characteristic multiplier is real and moves outside the unit circle at $+1$, as it is shown by case (b) in Figure 2.2. The arising bifurcation is topologically equivalent to the saddle-node bifurcation of autonomous systems and called as *period one* bifurcation of the corresponding nonlinear system.

3. The critical characteristic multiplier is real and moves outside the unit circle at -1, as it is shown by case (c) in Figure 2.2. There is no topologically equivalent type of bifurcation for autonomous systems. This case is called *period two* or *period doubling* or *flip* bifurcation of a corresponding nonlinear system.

Generally, it is hard to apply Floquet's theory for stability calculations, since there is no closed form representation for the principal matrix. For practical applications, approximate methods are used.

Hill (1886) worked out a method like this (sometimes called Hill's Infinite Determinant Method) for the undamped, parametrically forced oscillatory system. Rayleigh (1887) showed, that Hill's method can be applied for more general cases, too. The most
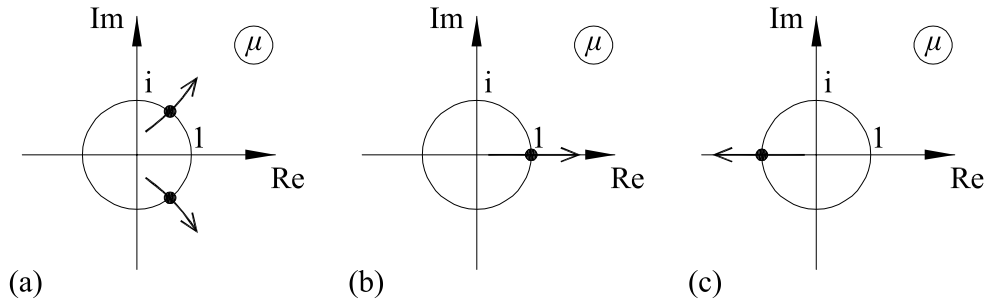
Figure 2.2: Critical characteristic multipliers for periodic systems: secondary Hopf bifurcation (a), period one bifurcation (b) and period two bifurcation (c)

straightforward and less accurate method is the piecewise constant approximation of the coefficient matrix (see, e.g., D'Agelo, 1970 or Insperger and Horváth, 2000). There are other methods described in the book of Nayfeh and Mook (1979): the Lindstedt–Poincare Technique and the Method of Multiple Scales. A novel approach was developed by Sinha and Wu (1991) and improved by Sinha and Butcher (1997). They expanded the state vector and the periodic matrix in terms of Chebyshev polynomials and applied the Floquet Theory to approximate the transition matrix. Their method was used by Szabó and Lóránt (2000) for the analysis of a parametrically excited railway wheelset. The Chebyshev polynomials' approach was also used by Szabó (2001) for the stability analysis of pipes conveying flowing fluids. Bauchau and Nikishkov (2001) worked out a numerical algorithm for extracting the dominant characteristic multipliers without the explicit computation of the transition matrix. They applied their method for rotorcraft stability evaluation.

These examples also show, that the stability analysis of parametrically excited systems is required in many practical applications. Periodic ODEs describe the vibrations of rotating shafts with non-symmetric cross-section (see Ludvig, 1973), the dynamic behaviour of gears (see Márialigeti, 1995, 1997, or Karsai, 1996), or vibrations in belt drives of machine tools (see Patkó and Kollányi, 1999), just to mention a few.

One of the first basic problems of time periodic ODEs was the parametrically excited pendulum and the corresponding Mathieu equation. It was shown by Stephenson (1908), that it is possible to stabilize the upper position of a rigid pendulum by vibrating its pivot point vertically at a specific high frequency. There are many generalizations of this problem. Broer *et al.* (1998) considered the inverted pendulum with periodic forcing as a bifurcation problem. Butcher and Sinha (1998a, 1998b) investigated linear and nonlinear behaviour of the parametrically excited simple pendulum and the double inverted pendulum subjected to periodic follower force. A parametrically excited flexible rod was analyzed by Champneys and Fraser (2000) as an explanation of

the "Indian rope trick". Other generalizations of the Mathieu equation, like nonlinear quasi-periodic or nonlinear noisy Mathieu equation are also in focus of interest (see Namachchivaya *et al.*, 2001, Zounes and Rand, 2001, Ramani *et al.*, 2001).

Example

A simple example for linear periodic ODEs is the parametrically excited damped oscillator

$$\ddot{x}(t) + b_0 \dot{x}(t) + c_0(t)x(t) = 0 , \quad c_0(t) = c_{0\,\delta} + c_{0\,\varepsilon} \cos(t) . \tag{2.11}$$

This equation is called (damped) Mathieu equation. Similarly to equation (2.4), Cauchy transformation can be applied for equation (2.11), but here, the resulted coefficient matrix is time periodic:

$$\mathbf{A}(t) = \begin{pmatrix} 0 & 1 \\ -c_0(t) & -b_0 \end{pmatrix} . \tag{2.12}$$

As mentioned before, the stability conditions cannot be given in closed form even for this simple example.

This time, the stability chart will be determined by the piecewise constant approximation method. Divide the principal period 2π into k time intervals $[t_{i-1}, t_i]$ of length Δt_i, $i = 1, 2, \ldots, k$, so that $\sum_{i=1}^{k} \Delta t_i = 2\pi$. The piecewise constant approximation of function $c_0(t)$ results

$$c_{0i} = c_{0\,\delta} + c_{0\,\varepsilon} \cos(t_i - \Delta t_i/2) , \quad i = 1, 2, \ldots, k , \tag{2.13}$$

and the piecewise constant approximation of the coefficient matrix reads

$$\mathbf{A}_i = \begin{pmatrix} 0 & 1 \\ -c_{0i} & -b_0 \end{pmatrix} , \quad i = 1, 2, \ldots, k . \tag{2.14}$$

By coupling the solutions, an approximated Floquet transition matrix can be given in the form

$$\mathbf{\Phi}(2\pi) = \exp(\mathbf{A}_k \Delta t_k) \exp(\mathbf{A}_{k-1} \Delta t_{k-1}) \cdots \exp(\mathbf{A}_1 \Delta t_1) . \tag{2.15}$$

The boundary curves separating the stable parameter domains from the unstable ones are determined by the eigenvalues μ_1 and μ_2 of the Floquet transition matrix. For some b_0 values, the boundary curves of equation (2.11) can be seen in Figure 2.3. The stable domains are denoted by S, the unstable by $U_{\pm 1}$. By increasing the "damping coefficient" b_0, the stable domains get larger. In the literature, this chart is called Strutt–Ince diagram (van der Pol and Strutt, 1928).

It can easily be shown, that only period one or period two bifurcations can exist for the damped Mathieu equation (2.11). Secondary Hopf bifurcation arises if the
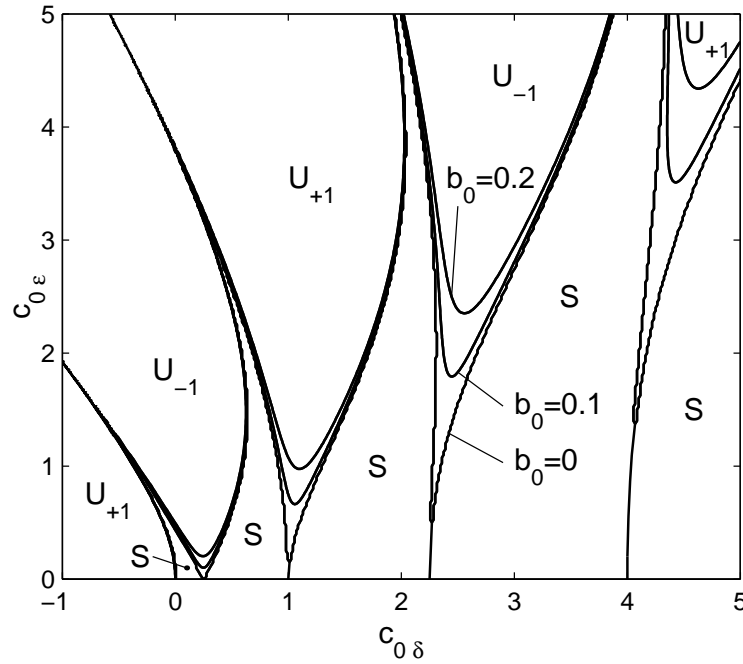
Figure 2.3: Boundary curves for equation (2.11)

characteristic multipliers μ_1 and μ_2 are complex pair in modulus equal to 1 and they cross the unit circle with nonzero velocity as the system parameters $(c_{0\,\delta},\ c_{0\,\varepsilon}$ and $b_0)$ change. This last condition requires that μ_1 and μ_2 are in modulus greater than 1 for some parameters $c_{0\,\delta}$, $c_{0\,\varepsilon}$, b_0.

Liouville's formula (see Farkas, 1994) can be used for equation (2.11) as follows

$$\mu_1\mu_2 = \det \mathbf{\Phi}(2\pi) = \exp \int_0^{2\pi} \text{Tr}A(t)\,\mathrm{d}t = \exp \int_0^{2\pi} -b_0\,\mathrm{d}t = \exp(-2\pi b_0)\,. \qquad (2.16)$$

If $b_0 < 0$, then $\mu_1\mu_2 > 1$, i.e., at least one of the characteristic multipliers is in modulus greater than 1. Consequently, the Mathieu equation (2.11) with negative damping is always unstable.

If $b_0 \geq 0$, then $\mu_1\mu_2 \leq 1$. In this case, there is no secondary Hopf bifurcation, since μ_1 and μ_2 are in modulus not greater than 1 for any parameters $c_{0\,\delta}$, $c_{0\,\varepsilon}$, b_0.

Consequently, only period one or period two bifurcations occur in the damped Mathieu equation (2.11). These curves in Figure 2.3 are the boundaries of the unstable domains denoted by U_{+1} and U_{-1}, respectively.

2.3 Linear autonomous retarded functional differential equations

It has been known for a long time, that several problems can be described by models including past effects. One of the classical examples is the predator-prey model of Volterra (1928), where the growth rate of predators depends not only on the present quality of food (say, prey), but also on the past quantities (in the period of gestation, say). The first delay models in engineering appeared for wheel shimmy (von Schlippe and Dietrich, 1941), and for ship stabilization (Minorsky, 1942). The system, where the rate of change of state is determined by the present and also by the past states of the system, are described by retarded functional differential equations (RFDEs). The initial-value problem of general RFDEs was first correctly formulated by Myshkis (1949). Since then, several books appeared summarizing the most important theorems, see the books of Myshkis (1955), Bellman and Cooke (1963), Halanay (1966), Hale (1977), Kolmanovskii and Nosov (1986), Stépán (1989), Hale and Lunel (1993) and Diekmann *et al.* (1995).

Linear autonomous RFDEs have the general form

$$\dot{\mathbf{y}}(t) = \mathbf{L}(\mathbf{y}_t) \,, \tag{2.17}$$

where $\mathbf{L} : C \to \mathbb{R}^n$ is a continuous linear functional (C is the Banach space of continuous functions). According to the Riesz Representation Theorem (see Hale, 1977), this linear functional $\mathbf{L}$ can be represented in the matrix form

$$\mathbf{L}(\mathbf{y}_t) = \int_{-\sigma}^{0} \mathrm{d}\boldsymbol{\eta}(\vartheta)\mathbf{y}(t+\vartheta) \,, \tag{2.18}$$

where $\boldsymbol{\eta} : [-\sigma, 0] \to \mathbb{R}^{n^2}$ is a matrix function of bounded variation, and the integral is a Stieltjes one, i.e. it contains discrete and continuous time delays as well. The continuous function $\mathbf{y}_t$ is defined by the shift

$$\mathbf{y}_t(\vartheta) = \mathbf{y}(t+\vartheta) \,, \quad \vartheta \in [-\sigma, 0] \,. \tag{2.19}$$

The characteristic function of system (2.17) reads

$$\det\left(\lambda\mathbf{I} - \int_{-\sigma}^{0} \mathrm{e}^{\lambda\vartheta}\mathrm{d}\boldsymbol{\eta}(\vartheta) \right) = 0 \,. \tag{2.20}$$

Opposite to the characteristic polynomial of autonomous ODEs, this characteristic function has, in general, infinite number of zeros in the complex plane, consequently, the corresponding phase space is also infinite dimensional. From this point of view, RFDEs are similar to partial differential equations (PDEs) due to their infinite dimensional nature.

Those RFDEs, where only discrete values of the past have influence on the present rate of change of state, are often called retarded differential-difference equations (RDDEs). A general form for linear autonomous RDDEs reads

$$\dot{\mathbf{y}}(t) = \mathbf{A}\mathbf{y}(t) + \sum_{j=1}^{r} \mathbf{B}_j\, \mathbf{y}(t - \tau_j)\,, \tag{2.21}$$

where $\mathbf{A}$ and $\mathbf{B}_j$'s are $n \times n$ matrices, $\tau_j > 0$ for all j and $r \in \mathbb{Z}^+$.

RFDE and RDDE are mathematical terminologies. In the engineering literature, both RFDEs and RDDEs are usually called delay-differential equations and abbreviated as DDEs.

The necessary and sufficient condition for the asymptotic stability of RFDE (2.17) is that all the infinite number of characteristic roots have negative real parts, and the condition

$$\int_{-\infty}^{0} \mathrm{e}^{-\nu\vartheta}\, |\mathrm{d}\eta_{jk}(\vartheta)| < \infty, \quad j, k = 1, 2, \ldots, n, \quad \nu > 0 \tag{2.22}$$

is satisfied, where $\eta_{jk}(\vartheta)$ are the elements of $\boldsymbol{\eta}(\vartheta)$. Condition (2.22) means that the past effect decays exponentially in the past. Obviously, this condition holds, if the lower limit σ of the integral in equation (2.18) is finite.

Although, there are infinite number of characteristic roots, it is not necessary to compute all of them. There are methods to extract just the critical ones. Moreover, only the signs of the real parts of the critical roots are needed for stability analysis.

The first attempts for determining stability criteria for second order RFDEs was made by Bellmann and Cooke (1963) and by Bhatt and Hsu (1966). They used the D-subdivision method (see Neimark, 1949) combined with a theorem of Pontryagin (1942). The book of Kolmanovskii and Nosov (1986) summarizes the main theorems on stability of RFDEs, and it contains several examples as well. A sophisticated method was developed by Stépán (1989) (generalized also by Hassard, 1997) applicable even for the combination of several discrete and continuous time delays.

Example

An example for linear autonomous RFDEs is

$$\ddot{x}(t) + b_0\dot{x}(t) + c_0 x(t) = c_1 \int_{-\sigma}^{0} w(\vartheta)x(t + \vartheta)\mathrm{d}\vartheta\,, \quad \sigma \in \mathbb{R}^+\,, \tag{2.23}$$

where $w(\vartheta)$ is a weight function. In this case, the Stieltjes integral in equation (2.18) defines a distributed time delay on interval $[-\sigma, 0]$.

By the Cauchy transformation, system (2.23) can be given in the form of equation (2.17), where

$$\mathbf{L}(\mathbf{y}_t) = \begin{pmatrix} 0 & 1 \\ -c_0 & -b_0 \end{pmatrix} \begin{pmatrix} y_1(t) \\ y_2(t) \end{pmatrix} + \begin{pmatrix} 0 \\ c_1 \int_{-\sigma}^{0} w(\vartheta) y_1(t+\vartheta) \mathrm{d}\vartheta \end{pmatrix} \tag{2.24}$$

and

$$\mathbf{y}(t) = \begin{pmatrix} y_1(t) \\ y_2(t) \end{pmatrix} = \begin{pmatrix} x(t) \\ \dot{x}(t) \end{pmatrix} . \tag{2.25}$$

Consider the weight function $w(\vartheta) = f_\delta(\vartheta + \tau)$ with $0 < \tau \le \sigma$, where f_δ is the Dirac distribution. In this case, the time delay is a discrete one, since the Stieltjes integral (2.18) gives

$$\int_{-\sigma}^{0} f_\delta(\vartheta + \tau) x(t+\vartheta) \mathrm{d}\vartheta = x(t - \tau) , \tag{2.26}$$

and the resulting equation is a RDDE of the form

$$\ddot{x}(t) + b_0 \dot{x}(t) + c_0 x(t) = c_1 x(t - \tau) . \tag{2.27}$$

This equation (often called as delayed oscillator) has great importance in applications, since this is the basic governing equation of the regenerative model of machine tool chatter. The Cauchy transformation of system (2.27) results the form of equation (2.21) with $r = 1$, $\tau_1 = \tau$ and

$$\mathbf{A} = \begin{pmatrix} 0 & 1 \\ -c_0 & -b_0 \end{pmatrix} , \quad \mathbf{B}_1 = \begin{pmatrix} 0 & 0 \\ c_1 & 0 \end{pmatrix} . \tag{2.28}$$

Similarly to linear autonomous ODEs, the characteristic equation can be obtained by substituting the trial solution $x(t) = K \exp(\lambda t)$. The characteristic equations of systems (2.23) and (2.27) read

$$\lambda^2 + b_0 \lambda + c_0 = c_1 \int_{-\sigma}^{0} w(\vartheta) \, \mathrm{e}^{\lambda \vartheta} \mathrm{d}\vartheta , \tag{2.29}$$

$$\lambda^2 + b_0 \lambda + c_0 = c_1 \, \mathrm{e}^{-\lambda \tau} , \tag{2.30}$$

respectively. These are transcendent equations with infinitely many complex characteristic roots, as mentioned at the general formula (2.20). Stability conditions can be given by analyzing the roots of equations (2.29) and (2.30).

Now, the stability boundary curves (or D-curves) for equation (2.27) with $\tau = 2\pi$ will be determined through the investigation of its characteristic equation (2.30). At the boundary curves, the critical characteristic root is pure complex or zero. Consequently, the substitution of $\lambda = \mathrm{i}\,\omega$ into the equation (2.30), and the separation of the real and the imaginary parts result the implicit form of the boundary curves as

$$c_0 - \omega^2 - c_1 \cos(2\pi\omega) = 0 , \tag{2.31}$$

$$b_0 \omega + c_1 \sin(2\pi\omega) = 0 . \tag{2.32}$$
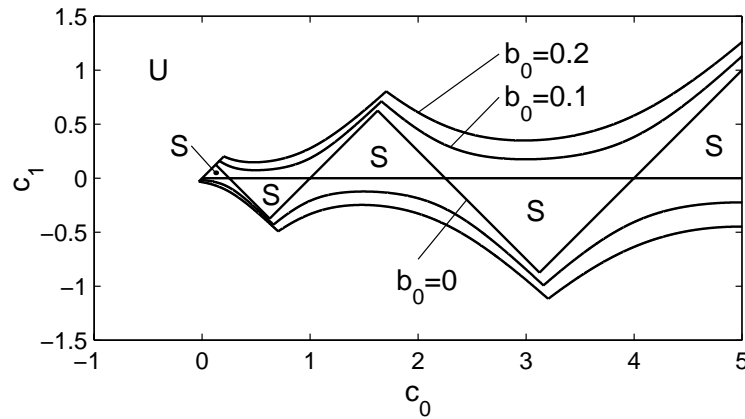
Figure 2.4: Boundary curves for equation (2.27) with $\tau = 2\pi$

When $b_0 = 0$, then equations (2.31) and (2.32) are equivalent to

$$c_1 = 0 \quad \text{with} \quad c_0 \geq 0 \tag{2.33}$$

and

$$c_1 = (-1)^k c_0 - (-1)^k k^2/4 \,, \quad k = 0, 1, \dots \quad (\text{here, } \omega = k/2). \tag{2.34}$$

That is, for $b_0 = 0$, the boundary curves are lines with slope 0 and ± 1.

When $b_0 \neq 0$, then equations (2.31) and (2.32) are equivalent to

$$c_1 = -\frac{b_0 \omega}{\sin(2\pi\omega)} \,, \tag{2.35}$$

$$c_0 = \omega^2 - \frac{b_0 \omega}{\tan(2\pi\omega)} \,, \tag{2.36}$$

where ω is a parameter now, and $\omega \neq k/2$, $k = 0, 1, \dots$.

The boundary curves for some values of b_0 can be seen in Figure 2.4. These curves separate the stable parameter domains from the unstable ones. Further analysis shows, that for the case $b_0 = 0$, the stable domains are inside the triangles, for the cases $b_0 = 0.1$ and $b_0 = 0.2$, the stable domains are those developing from the triangles of the case $b_0 = 0$ (see Hsu and Bhatt, 1966, or Stépán, 1989).

2.4 Linear periodic retarded functional differential equations

Linear periodic RFDEs have the general form

$$\dot{\mathbf{y}}(t) = \mathbf{L}(t, \mathbf{y}_t) \,, \quad \mathbf{L}(t + T, \mathbf{y}_t) = \mathbf{L}(t, \mathbf{y}_t) \,, \tag{2.37}$$

where $\mathbf{L} : \mathbb{R} \times C \to \mathbb{R}^n$ is continuous and linear in $\mathbf{y}_t \in C$. According to the Riesz Representation Theorem, the functional $\mathbf{L}$ can be written in the Stieltjes integral form

$$\mathbf{L}(t, \mathbf{y}_t) = \int_{-\sigma}^{0} \mathrm{d}_\vartheta \boldsymbol{\eta}(t, \vartheta) \mathbf{y}(t + \vartheta) \,, \tag{2.38}$$

where $\boldsymbol{\eta} : \mathbb{R} \times [-\sigma, 0] \to \mathbb{R}^{n^2}$ is a matrix function of bounded variation in $\vartheta \in [-\sigma, 0]$. The continuous function $\mathbf{y}_t$ is defined by the equation (2.19).

Similarly to the autonomous case, linear periodic RDDEs can be defined as

$$\dot{\mathbf{y}}(t) = \mathbf{A}(t)\mathbf{y}(t) + \sum_{j=1}^{r} \mathbf{B}_j(t)\, \mathbf{y}(t - \tau_j) \,, \tag{2.39}$$

$$\mathbf{A}(t + T) = \mathbf{A}(t) \,, \quad \mathbf{B}_j(t + T) = \mathbf{B}_j(t) \,.$$

where $\mathbf{A}(t)$ and $\mathbf{B}_j(t)$'s are $n \times n$ matrices, $\tau_j > 0$ for all j and $r \in \mathbb{Z}^+$.

The Floquet Theory can be extended for RFDEs as it was shown by Halanay (1961), but infinite dimensional linear operators are used instead of the finite dimensional tensors in (2.9) or (2.10). Such a linear operator can be defined by $\mathbf{y}_t = \mathbf{U}(t)\mathbf{y}_0$. While the operator $\mathbf{U}(t)$ plays the role of the fundamental matrix, the role of the principal matrix is taken by the so-called monodromy operator $\mathbf{U}(T)$. The nonzero elements of the spectrum of $\mathbf{U}(T)$ are called the characteristic multipliers of system (2.37), also defined by

$$\mathrm{Ker}(\mu \mathbf{I} - \mathbf{U}(T)) \neq \emptyset \,, \quad \mu \neq 0 \tag{2.40}$$

instead of (2.9). If μ is a characteristic multiplier, and $\mu = \exp(\lambda T)$, then λ is called characteristic exponent.

The necessary and sufficient condition for the asymptotic stability of the periodic RFDE (2.37) is that all the characteristic multipliers are in modulus less than one (that is, all the characteristic exponents have negative real parts), and the condition

$$\int_{-\infty}^{0} \mathrm{e}^{-\nu\vartheta} \, |\mathrm{d}_\vartheta \eta_{jk}(\vartheta, t)| < \infty \,, \quad j, k = 1, 2, \ldots, n, \quad \nu > 0, \quad t \in \mathbb{R}, \tag{2.41}$$

is satisfied, where $\eta_{jk}(\vartheta, t)$ are the elements of $\boldsymbol{\eta}(\vartheta, t)$. Similarly to autonomous RFDEs, condition (2.41) trivially holds if $\sigma < \infty$.

For periodic RFDEs, the difficulty is that the operator $\mathbf{U}(T)$ has no closed form, so no closed form stability conditions can be expected. For practical calculations, only approximations can be applied. Most of the methods were developed with the aim of constructing stability charts for milling processes.

Stability investigations of periodic RFDEs describing milling process are often carried out by numerical simulations (see, e.g., Balachandran, 2001). An alternative of Hill's Infinite Matrix Method combined with a numerical algorithm was developed by

Minis and Yanushevsky (1993), and generalized by Altintas and Budak (1995) and by Seagalman and Butcher (1999). Also, Hill's method was used by Insperger and Stépán (2002a) to determine the closed form stability chart of the delayed Mathieu equation (see Chapter 3). In other works, Insperger and Stépán (2000a, 2001a) approximated the discrete time delay by special continuous ones according to Fargue (1973), and transformed the infinite dimensional eigenvalue problem into an approximate finite dimensional one (see Chapter 4). Temporal finite element method was used by Bayly *et al.* (2001a, 2002) to analyze intermittent cutting and milling operations. A general method, the so-called semi-discretization was developed by Insperger and Stépán (2001b, 2002b) for general periodic RFDEs (see Chapter 5).

Example

A simple example for linear periodic RFDEs can be given via substituting the constant coefficients b_0, c_0 or c_1 in equations (2.23) or (2.27), by time periodic ones.

As a practical example, consider the governing equation of regenerative vibrations in milling processes (see Chapter 6)

$$\ddot{x}(t) + b_0 \dot{x}(t) + c_0(t)x(t) = c_1(t)x(t - \tau) , \tag{2.42}$$

where $c_0(t + \tau) = c_0(t)$, $c_1(t + \tau) = c_1(t)$ and $\tau > 0$. Since the time delay is discrete, this equation is an example for periodic RDDE.

Another example is the governing equation of turning with variable spindle speed (see Chapter 7). In this case, the time delay itself changes periodically in time, consequently, the equation is a periodic RFDE

$$\ddot{x}(t) + b_0 \dot{x}(t) + c_0 x(t) = c_1 x(t - \tau(t)) , \tag{2.43}$$

where $\tau(t + T) = \tau(t)$ and $\tau(t) > 0$, $t \in \mathbb{R}$.

2.5   Other types of linear functional differential equations

There are other types of FDEs than the ones listed in the previous sections. If the rate of change of state depends on its own past values as well, than the corresponding equation is called neutral functional differential equation (NFDE). According to Kolmanovskii and Nosov (1986), linear NFDEs have the general form

$$\dot{\mathbf{y}}(t) = \mathbf{L}(t, \mathbf{y}_t, \dot{\mathbf{y}}_t) , \tag{2.44}$$

where $\mathbf{L} : \mathbb{R} \times C \times C \to \mathbb{R}^n$ is continuous and linear in $\mathbf{y}_t \in C$ and in $\dot{\mathbf{y}}_t \in C$, and can be represented as

$$\mathbf{L}(t, \mathbf{y}_t, \dot{\mathbf{y}}_t) = \int_{-\sigma}^{0} \mathrm{d}_\vartheta \boldsymbol{\eta}_0(t, \vartheta) \mathbf{y}(t + \vartheta) + \int_{-\sigma}^{0} \mathrm{d}_\vartheta \boldsymbol{\eta}_1(t, \vartheta) \dot{\mathbf{y}}(t + \vartheta) \,. \qquad (2.45)$$

where $\boldsymbol{\eta}_{0,1} : \mathbb{R} \times [-\sigma, 0] \to \mathbb{R}^{n^2}$ are matrix functions of bounded variation in $\vartheta \in [-\sigma, 0]$.

Similarly to the previous sections, if $\mathbf{L}(t + T, \mathbf{y}_t, \dot{\mathbf{y}}_t) = \mathbf{L}(t, \mathbf{y}_t, \dot{\mathbf{y}}_t)$, then (2.44) is called linear periodic NFDE. If $\mathbf{L}(t, \mathbf{y}_t, \dot{\mathbf{y}}_t) = \mathbf{L}(\mathbf{y}_t, \dot{\mathbf{y}}_t)$, then (2.44) is a linear autonomous NFDE. Examples for a linear autonomous NFDEs are

$$\dot{x}(t) = \int_{-\sigma}^{0} w_0(\vartheta) x(t + \vartheta) \mathrm{d}\vartheta + \int_{-\sigma}^{0} w_1(\vartheta) \dot{x}(t + \vartheta) \mathrm{d}\vartheta \,, \quad \sigma \in \mathbb{R}^{+}, \qquad (2.46)$$

or

$$\dot{x}(t) = c_1 x(t - \tau) + b_1 \dot{x}(t - \tau) \,. \qquad (2.47)$$

The main theorems on the stability of NFDEs are summarized by Kolmanovskii and Nosov (1986). Similarly to RFDEs, the general stability conditions are determined by infinite number of characteristic roots or characteristic multipliers. Several papers deal with sharp stability criteria for some special NFDEs (see, e.g., Li, 1988, Khusainov and Yun'kova, 1988, Stroinski, 1994, Hu and Hu, 1996, Arino and Nosov, 1998, Park and Won, 2000,).

If the rate of change of state depends on the past values of higher derivatives, than the corresponding equation is called advanced functional differential equation (AFDE). The reason for the phrase "advanced" can be demonstrated in the following simple example. Consider the ADFE

$$\dot{x}(t) = \ddot{x}(t - \tau) \,. \qquad (2.48)$$

By a τ-shift transformation, and by using the new variable $z = \dot{x}$, this equation can be written in the form

$$\dot{z}(t) = z(t + \tau) \,. \qquad (2.49)$$

Here, the rate of change of state is determined by the future values of state, i.e. an advanced state determines the present state. Another example for AFDE is equation (2.43) with alternating negative and positive time delays, i.e., when $\tau(t) < 0$ is also allowed. Although, AFDEs are always unstable and have little physical relevance at the moment, several papers deal with the properties of these systems (see, e.g., Filho, 1997, Zhang and Li, 1998, Kordonis and Philos, 1998, Fiagbedzi, 2001, Listyn and Stavroulakis, 2001).

Mathematicians investigate even more complex cases, like nonautonomous (and even non-periodic) FDEs (see Győri and Pituk, 1997), or systems with time- and state-

dependent delays (see Győri *et al.*, 1995, Péics, 2000). For some of these systems, even the existence and uniqueness of the solutions are not clarified.

NFDEs and AFDEs are mostly in the focus of mathematicians' interest, but they may show up in some practical problems (see Chapter 7).

Chapter 3

Delayed Mathieu equation

In this chapter, the delayed Mathieu equation defined as

$$\ddot{x}(t) + (\delta + \varepsilon \cos t)x(t) = bx(t - 2\pi)$$

is investigated. This is a linear periodic RFDE with a corresponding infinite dimensional phase space, given as the combination of the Mathieu equation and a second order scalar RFDE (the delayed oscillator). A closed form stability condition is given in the form of a three-dimensional stability chart in the parameter space δ, b and ε. This chart describes the intriguing stability properties of a class of delayed oscillatory systems subjected to parametric excitation and also serves as a basic reference for other numerical methods.

3.1   Special cases

In this section we consider the Mathieu equation and the delayed oscillator as the two special limit cases of the delayed Mathieu equation.

The Mathieu equation has the form

$$\ddot{x}(t) + (\delta + \varepsilon \cos t)x(t) = 0 \ . \tag{3.1}$$

This equation was first discussed by Mathieu (1868) in connection with the problem of vibrations of an elliptic membrane. The stability chart, the so called Strutt–Ince diagram was first published by van der Pol and Strutt (1928). This chart shows the stable and unstable domains (denoted by S and $U_{\pm 1}$, respectively in Figure 3.1) in the parameter plane (δ, ε).

Without damping, the system cannot be asymptotically stable. The system is stable in Ljapunov sense, if and only if all the characteristic multipliers are in modulus less than or equal to one, and those with modulus one are simple in the minimal
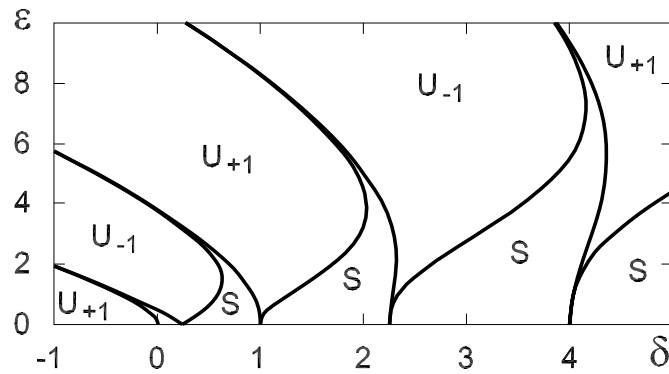
Figure 3.1: The Strutt–Ince stability chart of equation (3.1)

polynomial of the principal matrix. In the stable domains of the Strutt–Ince diagram, this condition holds. Since the system is two dimensional, there are two characteristic multipliers μ_1 and μ_2. From Liouville's formula (2.16), it follows that $\mu_1\mu_2 = 1$ (see also Farkas, 1994). The characteristic multipliers are located in three ways:

1. The characteristic multipliers are a complex pair placed on the unit circle of the complex plane. This case holds for the stable (in Ljapunov sense) domains of the Strutt–Ince diagram.

2. Both characteristic multipliers are real, and $\mu_1 > 1$, $0 < \mu_2 < 1$. This case holds for the unstable domains denoted by U_{+1} in Figure 3.1. At the boundaries, $\mu_1 = \mu_2 = 1$, and there exists a periodic solution with period 2π.

3. Both characteristic multipliers are real, $\mu_1 < -1$ and $-1 < \mu_2 < 0$. This case holds for the unstable domains denoted by U_{-1} in Figure 3.1. At the boundaries, $\mu_1 = \mu_2 = -1$, and there exists a periodic solution with period 4π.

The undamped delayed oscillators are described by the scalar RFDE

$$\ddot{x}(t) + \delta x(t) = bx(t - 2\pi) \,. \tag{3.2}$$

Although, the stability chart in the parameter plane (δ, b) has a very clear structure (see Figure 3.2), it was first published correctly only in 1966 by Hsu and Bhatt. According to Kolmanovskii and Nosov (1986), this chart was also published in the literature in Russian in 1967, often referred there as Vyshnegradskii diagram. The stability boundaries are lines with slope $+1$ and -1. The numbers denote the numbers of characteristic roots with positive real parts. This will be called the number of instabilities. If this number is 0, then the corresponding domain refers to an asymptotically stable system. This will be called the domain of stability, bounded by thick lines in Figure 3.2. The
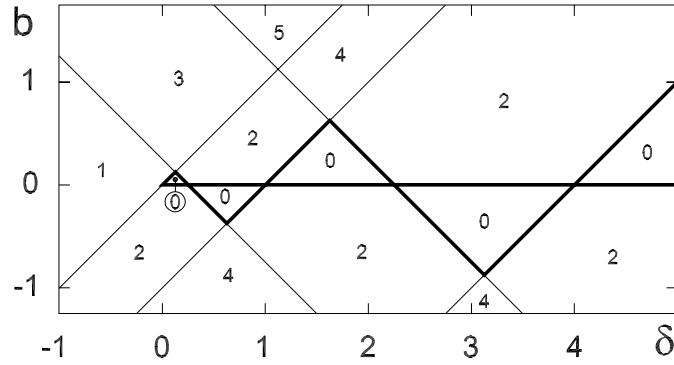
Figure 3.2: The Hsu–Bhatt–Vyshnegradskii stability chart of equation (3.2)

only domains of stability are the triangles attached to the $b = 0$ axis for $\delta > 0$. Along the boundaries where the number of instabilities changes from 0 to 2, Hopf bifurcations occur.

Equations (3.1) and (3.2) are special cases of equations (2.11) and (2.27) with zero damping ($b_0 = 0$) already investigated as examples in Chapter 2.

3.2   The delayed Mathieu equation

The equation in question is the delayed Mathieu equation defined as

$$\ddot{x}(t) + (\delta + \varepsilon \cos t)x(t) = bx(t - 2\pi)\,. \tag{3.3}$$

The time delay is equal to the principal period 2π. We are looking for the stability chart in the space of parameters δ, b, ε. The stability charts for the two special cases $\varepsilon = 0$ and $b = 0$ are presented in the previous section. The stability charts in the plane (δ, b) will be determined for various values of the parameter ε. Geometrically, this means that we follow how the stable triangles of Figure 3.2 vary for $\varepsilon > 0$.

Let us define the stability boundary curves as the set of points in the plane (δ, b), where there is at least one characteristic multiplier in modulus equal to one. The domains bounded by these curves are invariant for the number of instabilities due to the continuous dependence on the parameters.

Our investigation is based on the following two theorems concerning time periodic RFDEs of the form (2.37) (see Farkas, 1994).

Theorem 1 *The trivial solution of system (2.37) is asymptotically stable, if and only if all the (infinite number of) characteristic multipliers are in modulus less than one, that is all the characteristic exponents have negative real parts.*

Theorem 2 $\mu = e^{\lambda T}$ *is a characteristic multiplier of system (2.37), if and only if, there exists a nontrivial solution in the form* $\mathbf{y}(t) = \mathbf{p}(t)\,e^{\lambda t}$, *where* $\mathbf{p}(t) = \mathbf{p}(t + T)$.

Use the trial solution

$$x(t) = p(t)\,e^{\lambda t} + \bar{p}(t)\,e^{\bar{\lambda} t}\,, \tag{3.4}$$

for the delayed Mathieu equation (3.3) according to Theorem 2, where $p(t) = p(t + 2\pi)$ is a periodic function. Note, that λ is characteristic exponent, that is, if $\text{Re }\lambda < 0$, then $x(t) \equiv 0$ is asymptotically stable, as it follows from Theorem 1.

According to Hahn (1961), equation (3.3) may have solutions of the form $t^k p(t)\,e^{\lambda t}$, $k \in \mathbb{Z}^+$ in critical cases. Consequently, if $|\mu| = 1$, i.e. $\text{Re }\lambda = 0$, then the solution $p(t)\,e^{0t}$ is stable in Ljapunov sense, but the solutions $t^k p(t)\,e^{0t}$ are unstable. This case has no importance here, since it may only arise at certain special points of the stability boundaries, while in the present investigation, the domains of asymptotic stability are determined.

Now, expand the periodic function $p(t)$ in (3.4) into Fourier series

$$x(t) = \left(\sum_{k=0}^{\infty} A_k\,e^{i k t} + B_k\,e^{-i k t}\right) e^{\lambda t} + \left(\sum_{k=0}^{\infty} \bar{A}_k\,e^{-i k t} + \bar{B}_k\,e^{i k t}\right) e^{\bar{\lambda} t}\,. \tag{3.5}$$

Using trigonometrical transformations, expression (3.5) can be transformed into

$$x(t) = \sum_{k=-\infty}^{\infty} C_k\,e^{(\lambda + i k)t} + \bar{C}_k\,e^{(\bar{\lambda} - i k)t}\,. \tag{3.6}$$

The substitution into the system (3.3), and the balancing of the harmonics $e^{(\lambda + i k)t}$ and $e^{(\bar{\lambda} - i k)t}$ yield two systems of equations for the coefficients C_k and $\bar{C}_k$, respectively:

$$\frac{\varepsilon}{2}C_{k-1} + c_k C_k + \frac{\varepsilon}{2}C_{k+1} = 0\,, \quad k = -\infty, \dots, \infty\,, \tag{3.7a}$$

$$\frac{\varepsilon}{2}\bar{C}_{k-1} + \bar{c}_k \bar{C}_k + \frac{\varepsilon}{2}\bar{C}_{k+1} = 0\,, \quad k = -\infty, \dots, \infty\,, \tag{3.7b}$$

where

$$c_k = \delta + \left(\lambda + i\,k\right)^2 - b\,e^{-2\pi(\lambda + i\,k)}\,. \tag{3.8}$$

A direct consequence of Theorem 2 is that equations (3.7a) and (3.7b) are satisfied if and only if λ is a characteristic exponent. Equations (3.7a) and (3.7b) are equivalent, so it is enough to analyze (3.7a). There is a nontrivial solution of system (3.7a), if the number zero is an eigenvalue of the so-called Hill's infinite matrix

$$\mathbf{H}(\lambda, \delta, b, \varepsilon) = \begin{pmatrix} \ddots & \ddots & \ddots & \ddots & & \\ \ddots & \varepsilon/2 & c_{-1} & \varepsilon/2 & 0 & \\ & 0 & \varepsilon/2 & c_0 & \varepsilon/2 & 0 \\ & & 0 & \varepsilon/2 & c_1 & \varepsilon/2 & \ddots \\ & & & \ddots & \ddots & \ddots & \ddots \end{pmatrix}\,. \tag{3.9}$$

This matrix represents an unbounded linear operator $\mathbf{H} : l_2^{\mathbb{Z}} \to l_2^{\mathbb{Z}}$. Here, $l_2^{\mathbb{Z}}$ is the Hilbert space of the complex sequences $(\ldots, z_{-1}, z_0, z_1, \ldots)$ with $\sum_{n=-\infty}^{\infty} |z_n|^2 < \infty$. As it is the case for (unbounded) linear operators with compact resolvents, the spectrum of $\mathbf{H}$ consist of a countable number of eigenvalues. All of these eigenvalues are of finite multiplicity. The number zero is an eigenvalue of $\mathbf{H}$ if and only if

$$\mathrm{Ker}\,\mathbf{H}(\lambda, \delta, b, \varepsilon) \neq \emptyset \,. \tag{3.10}$$

Formula (3.10) can be treated as the characteristic equation of (3.3), since its roots are the characteristic exponents. This is a reformulation of (2.40) with $\mu = \exp(2\pi\lambda)$.

In order to carry out calculations, only the truncated system of equations with $k = -N, \ldots, N$ is considered. This reduces the infinite eigenvalue problem of operator $\mathbf{H}$ to the calculation of a finite determinant

$$D(\lambda, \delta, b, \varepsilon) = \det \begin{pmatrix} c_{-N} & \varepsilon/2 & & & \\ \varepsilon/2 & c_{-N+1} & \varepsilon/2 & & \\ & \ddots & \ddots & \ddots & \\ & & \varepsilon/2 & c_{N-1} & \varepsilon/2 \\ & & & \varepsilon/2 & c_N \end{pmatrix} = 0 \,. \tag{3.11}$$

Although, this truncation seems to be a rough approximation, it still has a sound mathematical basis (see Mennicken, 1968, or Denk, 1995). This approximation is just the same as the one applied during the construction of the Strutt–Ince diagram. The operator $\mathbf{H}$ is often called Hill's infinite matrix, and the terminology "infinite determinant" is also used, although, in fact, it is not a determinant of a matrix. In the following, we will construct the boundary curves, then determine the domains of stability for $N \to \infty$.

3.2.1 Stability boundaries

According to the D-subdivision method, the substitution $\lambda = \mathrm{i}\,\omega$ into (3.11) gives an implicit form for the approximate boundary curves of (3.3) in the parameter space (δ, b, ε) with the frequency parameter ω. In this case, the diagonal elements in (3.11) read

$$c_k = \delta - (\omega + k)^2 - b\,\mathrm{e}^{-\mathrm{i}\,2\pi\omega}\,, \quad k = -N, \ldots, N \,. \tag{3.12}$$

Note, that the imaginary part of c_k is not dependent on k

$$\mathrm{Im}\,c_k = b\sin(2\pi\omega)\,, \quad k = -N, \ldots, N \,. \tag{3.13}$$

Disregard the case $b = 0$, which gives the classical Mathieu equation. Then we can state, that $\mathrm{Im}\,c_k = 0$, if and only if $\omega = j/2$, where $j = 0, 1, \ldots$. Examine two cases.

Case $\omega \neq j/2$, $j = 0, 1, \ldots$

In this case, $\mathrm{Im}\, c_k \neq 0$ for any k as it follows from equation (3.13). The Gauss algorithm can be applied for the tridiagonal matrix in equation (3.11) to transform it to an upper triangular matrix having elements d_k in the main diagonal. Clearly, $d_{-N} = c_{-N} \neq 0$. In the $(N + k)$'th step of the Gauss elimination process, Hill's matrix assumes the form

$$
\begin{pmatrix}
d_{-N} & \varepsilon/2 & 0 & \cdots & & & & \\
\vdots & \ddots & \ddots & \ddots & & & & \\
\cdots & 0 & d_{k-1} & \varepsilon/2 & 0 & \cdots & & \\
& \cdots & 0 & d_k & \varepsilon/2 & 0 & \cdots & \\
& & \cdots & 0 & \varepsilon/2 & c_{k+1} & \varepsilon/2 & 0 & \cdots \\
& & & \cdots & 0 & \varepsilon/2 & c_{k+2} & \varepsilon/2 & 0 & \cdots \\
& & & & & \ddots & \ddots & \ddots & \ddots & \ddots
\end{pmatrix} .
\tag{3.14}
$$

Let us suppose that $\mathrm{sgn}(\mathrm{Im}\, d_k) = \mathrm{sgn}(\mathrm{Im}\, c_k)$ for some k. Since $\mathrm{Im}\, c_k \neq 0$, this means that $\mathrm{Im}\, d_k \neq 0$, i.e. $|d_k| \neq 0$. Thus, the subsequent elimination of $\varepsilon/2$ in front of c_{k+1} leads to

$$
d_{k+1} = c_{k+1} - \frac{\varepsilon^2}{4 d_k} = \left(\mathrm{Re}\, c_{k+1} - \frac{\varepsilon^2 \,\mathrm{Re}\, d_k}{4 \,|d_k|^2} \right) + \mathrm{i} \left(\mathrm{Im}\, c_{k+1} + \frac{\varepsilon^2 \,\mathrm{Im}\, d_k}{4 \,|d_k|^2} \right) .
\tag{3.15}
$$

Consequently,

$$
\begin{aligned}
\mathrm{sgn}(\mathrm{Im}\, d_{k+1}) &= \mathrm{sgn}\left(\mathrm{Im}\, c_{k+1} + \left(\frac{\varepsilon}{2\,|d_k|} \right)^2 \mathrm{Im}\, d_k \right) \\
&= \mathrm{sgn}(\mathrm{Im}\, d_k) = \mathrm{sgn}(\mathrm{Im}\, c_k) \neq 0 .
\end{aligned}
\tag{3.16}
$$

Since $\mathrm{Im}\, d_{-N} = \mathrm{Im}\, c_{-N} = b \sin(2\pi\omega) \neq 0$, we have $\mathrm{Im}\, d_k \neq 0$, that is, $|d_k| \neq 0$ is true by induction.

The determinant of Hill's matrix can be calculated as the product of the diagonal elements of the upper triangular matrix. Hence

$$
D(\mathrm{i}\,\omega, \delta, b, \varepsilon) = \prod_{k=-N}^{N} d_k \neq 0 ,
\tag{3.17}
$$

condition (3.11) cannot be satisfied.

This means, that there is no nontrivial solution of system (3.7a), and there are no boundary curves in this case.

Case $\omega = j/2$, $j = 0, 1, \ldots$

In this case, the diagonal elements in (3.11) are real:
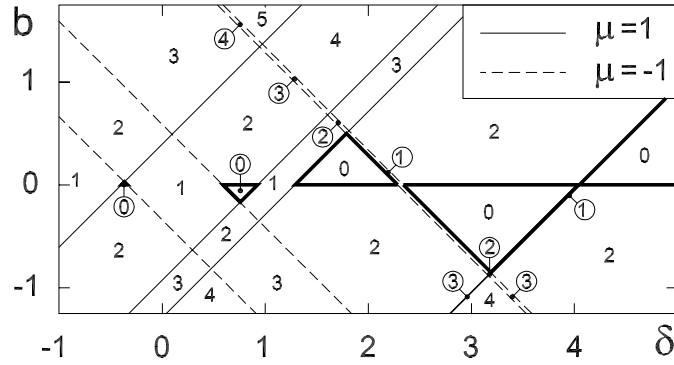
$$
c_k = \delta - (k + j/2)^2 - b(-1)^j .
\tag{3.18}
$$

Figure 3.3: Domains of stability of equation (3.3) for $\varepsilon = 1$ (denoted by 0's)

If j is even, that is $j = 2h$, $h = 0, 1, \ldots$, then $\lambda = \mathrm{i}\, h$ and the corresponding characteristic multiplier is

$$\mu = \mathrm{e}^{\mathrm{i} h 2\pi} = \mathrm{e}^{\mathrm{i} 2\pi} = 1\,. \tag{3.19}$$

In this case, $c_k = \delta - b - (k+h)^2$, and equation (3.11) gives the relation $f_{+1}(\delta - b, \varepsilon) = 0$ for the boundary curves. For the case $b = 0$, the relation $f_{+1}(\delta, \varepsilon) = 0$ serves the $\mu = +1$ stability boundary curves of the classical Mathieu equation defined in the form $\delta = g_{+1}(\varepsilon)$ as shown first by van der Pol and Strutt (1928). This means, that the boundary curves exist for the $b \neq 0$ case, too, in the form $\delta - b = g_{+1}(\varepsilon)$. In the plane (δ, b), these are lines with slope $+1$ (represented by continuous lines in Figure 3.3). Along these boundary curves, there exists a characteristic multiplier $\mu = +1$, and equation (3.3) has a periodic solution of period 2π. This case corresponds to the period one bifurcation.

If j is odd, that is $j = 2h+1$, $h = 0, 1, \ldots$, then $\lambda = \mathrm{i}\,(h+1/2)$ and the corresponding characteristic multiplier is

$$\mu = \mathrm{e}^{\mathrm{i}\,(h+1/2)2\pi} = \mathrm{e}^{\mathrm{i}\,\pi} = -1\,. \tag{3.20}$$

In this case, $c_k = \delta + b - (k+h+1/2)^2$, and equation (3.11) implies the boundary curve relation $f_{-1}(\delta + b, \varepsilon) = 0$. For the same reason as above, the boundary curves exist again in the form $\delta - b = g_{-1}(\varepsilon)$, where $\delta = g_{-1}(\varepsilon)$ gives the $\mu = -1$ stability boundary curves of the classical Mathieu equation. The boundary curves are lines with slope -1 in the parameter plane (δ, b) (represented by dashed lines in Figure 3.3). Along these boundary curves, there exists a characteristic multiplier $\mu = -1$, and equation (3.3) has nontrivial periodic solution of period 4π. This case corresponds to the period two (or flip) bifurcation.

Thus, the boundary curves are lines in the plane (δ, b). For varying parameter ε, these lines pass along the boundary curves of the Strutt–Ince diagram. As mentioned

before, these charts are approximate to the same extent as the Strutt–Ince diagram (N=20 in the figures), and they converge to the exact result for the $N \to \infty$ limit case. This means, that the appearance of the delay in the Mathieu equation does not require any more approximation in the stability analysis, just the same already used in the classical Mathieu equation. The point is, that the parametric excitation in the delayed oscillator does not alter the linearity of the stability boundaries.

3.2.2   Domains of stability

Since the characteristic multipliers and exponents depend continuously on the system parameters, the number of instabilities is constant in each domain separated by the boundary curves. The special case $\varepsilon = 0$ can be treated as a reference regarding the number of instabilities. The domains attached to these triangles of stability in the Hsu–Bhatt–Vyshnegradskii chart (see Figure 3.2) also have zero instability number. Similarly, some domains of instability can also be identified this way, and also the number of instabilities can be given based on the case $\varepsilon = 0$. But there may also be some new domains, which are not connected directly to any domain of the Hsu–Bhatt–Vyshnegradskii chart. To decide the stability of these domains, the sign of Re λ will be investigated near to the boundary curves. The derivative of λ with respect to the parameter b will be determined for $\lambda = \mathrm{i}\, j/2$, $j = 0, 1, \ldots$.

A recursive form for the calculation of the tridiagonal upper left sub-determinants in equation (3.11) can be given as

$$D_{-N} = c_{-N}\,, \tag{3.21}$$

$$D_{-N+1} = c_{-N}c_{-N+1} - \frac{\varepsilon^2}{4}\,, \tag{3.22}$$

$$D_k = c_k D_{k-1} - \frac{\varepsilon^2}{4} D_{k-2}\,, \quad k = -N + 2, \ldots, N\,. \tag{3.23}$$

Let us denote the partial derivative w.r.t. b by comma ($\square' = \partial\square/\partial b$) and the substitution of $\lambda = \mathrm{i}\, j/2$ by hat ($\hat{\square} = \square|_{\lambda=\mathrm{i}\, j/2}$). According to this notation, the partial derivatives of expressions (3.8), (3.21) and (3.22) yield

$$c_k' = 2(\lambda + \mathrm{i}\, k)\lambda' - \mathrm{e}^{-(\lambda+\mathrm{i}\, k)2\pi} + b2\pi\lambda'\,\mathrm{e}^{-(\lambda+\mathrm{i}\, k)2\pi}\,, \tag{3.24}$$

$$\hat{c}_k' = \left(2\pi b\,(-1)^j + \mathrm{i}\,(j + 2k)\right)\lambda' - (-1)^j\,, \tag{3.25}$$

$$\hat{D}'_{-N} = \left(2\pi b\,(-1)^j\,\Gamma_{-N} + \mathrm{i}\,\Omega_{-N}\right)\lambda' - (-1)^j\,\Gamma_{-N}\,, \tag{3.26}$$

$$\hat{D}'_{-N+1} = \left(2\pi b\,(-1)^j\,\Gamma_{-N+1} + \mathrm{i}\,\Omega_{-N+1}\right)\lambda' - (-1)^j\,\Gamma_{-N+1}\,, \tag{3.27}$$

where the coefficients

$$\Gamma_{-N} = 1 \,,$$
$$\Omega_{-N} = j - 2N \,,$$
$$\Gamma_{-N+1} = \hat{c}_{-N} + \hat{c}_{-N+1} \,,$$
$$\Omega_{-N+1} = \hat{c}_{-N}(j - 2N + 2) + \hat{c}_{-N+1}(j - 2N)$$

are real numbers since $\hat{c}_k$ is real for all $k = -N, \ldots, N$. The same differentiation of equation (3.23) yields the recursion

$$\hat{D}'_k = \hat{c}'_k \hat{D}_{k-1} + \hat{c}_k \hat{D}'_{k-1} - \frac{\varepsilon^2}{4} \hat{D}'_{k-2}, \quad k = -N + 2, \ldots, N \,. \tag{3.28}$$

We prove by induction, that equation (3.28) can be expressed in the same form as equations (3.26) and (3.27). For some k, let us suppose that

$$\hat{D}'_{k-2} = \left(2\pi b \, (-1)^j \, \Gamma_{k-2} + \mathrm{i}\, \Omega_{k-2}\right) \lambda' - (-1)^j \, \Gamma_{k-2} \,, \tag{3.29}$$
$$\hat{D}'_{k-1} = \left(2\pi b \, (-1)^j \, \Gamma_{k-1} + \mathrm{i}\, \Omega_{k-1}\right) \lambda' - (-1)^j \, \Gamma_{k-1} \,, \tag{3.30}$$

where Γ_{k-2}, Γ_{k-1}, Ω_{k-2}, Ω_{k-1} are real numbers. Then, by using equation (3.25), equation (3.28) reads

$$\hat{D}'_k = \left(2\pi b \, (-1)^j \, \Gamma_k + \mathrm{i}\, \Omega_k\right) \lambda' - (-1)^j \, \Gamma_k, \quad k = -N + 2, \ldots, N \,, \tag{3.31}$$

where the coefficients

$$\Gamma_k = \hat{D}_{k-1} + \Gamma_{k-1} \hat{c}_k - \frac{\varepsilon^2}{4} \Gamma_{k-2} \,,$$
$$\Omega_k = (j + 2k)\hat{D}_{k-1} + \Omega_{k-1} \hat{c}_k - \frac{\varepsilon^2}{4} \Omega_{k-2}$$

are real numbers, again. Together with equations (3.26) and (3.27), this completes the induction.

The final round of recursion is given by the $k = N$ case. The implicit differentiation of the characteristic exponent in $\hat{D}'_N = 0$ provides the expression of $\mathrm{Re}\,\lambda'$ after a straightforward algebraic calculation from equation (3.31):

$$\mathrm{Re}\,\lambda' = \frac{2\pi \Gamma_N^2}{\left(2\pi b \, (-1)^j \, \Gamma_N\right)^2 + \Omega_N^2} b \,. \tag{3.32}$$

Since the coefficient of b is positive, $\mathrm{sgn}(\mathrm{Re}\,\lambda') = \mathrm{sgn}(b)$ on the boundary curves. That is, moving away from the $b = 0$ axis, each boundary line represents at least one characteristic exponent becoming unstable (i.e. crossing the imaginary axis of the complex plane from the left to the right). So the only domains of stability are the

triangles born from the stable triangles of the $\varepsilon = 0$ case. Since the case $\varepsilon = 0$ is already known (see Figure 3.2), the number of instabilities can be determined for all the domains by equation (3.32) and by topological considerations (see the numbers in the chart of Figure 3.3). The domains of stability are bounded by thick lines. The frame-view of the 3 dimensional stability chart in the space (δ, b, ε) is shown in Figure 3.4.
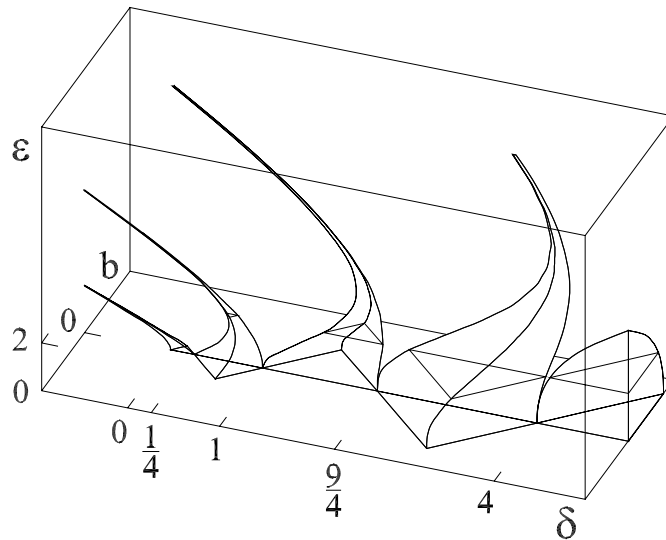
Figure 3.4: Stability chart of the delayed Mathieu equation

3.3 The damped delayed Mathieu equation

In this section, it will be shown that the period one and the period two stability boundaries for the damped delayed Mathieu equation

$$\ddot{x}(t) + \kappa \dot{x}(t) + (\delta + \varepsilon \cos t)x(t) = bx(t - 2\pi) \qquad (3.33)$$

are still lines in the (δ, b) parameter plane for any fixed ε and κ. The investigation is similar to the investigation of the undamped delayed Mathieu equation.

The stability chart of the damped delayed Mathieu equation is a combination of the charts in Figures 2.3 and 2.4. For the classical damped Mathieu equation, there is no secondary Hopf type stability boundary. Similarly to the undamped case, there are either period one or period two stability boundaries, (see the example in Section 2.2 and Figure 2.3).

The substitution of the trial solution (3.4), the use of trigonometrical transformations and the balance of the harmonics result in the system of equations having form

of (3.7a) and (3.7b). Hill's determinant can be defined again as

$$D(\lambda, \delta, b, \varepsilon) = \det \begin{pmatrix} \tilde{c}_{-N} & \varepsilon/2 & & & \\ \varepsilon/2 & \tilde{c}_{-N+1} & \varepsilon/2 & & \\ & \ddots & \ddots & \ddots & \\ & & \varepsilon/2 & \tilde{c}_{N-1} & \varepsilon/2 \\ & & & \varepsilon/2 & \tilde{c}_N \end{pmatrix} = 0 \,. \tag{3.34}$$

but here, the diagonal elements have the form

$$\tilde{c}_k = \delta + (\lambda + \mathrm{i}\,k)^2 + \kappa(\lambda + \mathrm{i}\,k) - b\,\mathrm{e}^{-2\pi(\lambda + \mathrm{i}\,k)} \tag{3.35}$$

instead of c_k defined in equation (3.8).

After the substitution of $\lambda = \mathrm{i}\,\omega$ into (3.35), the imaginary part of $\tilde{c}_k$ reads

$$\mathrm{Im}\,\tilde{c}_k = \kappa(\omega + k) + b\sin(2\pi\omega) \,. \tag{3.36}$$

From this point, the proof of the undamped delayed Mathieu equation cannot be continued, since $\mathrm{Im}\,\tilde{c}_k = 0$ does not fulfill in the cases $\omega = j/2$, $j = 0, 1, \ldots$. This means, that boundary curves may exist even for the case $\omega \neq j/2$, $j = 0, 1, \ldots$, and the critical characteristic multipliers can also be complex pairs of modulus 1. Consequently, secondary Hopf bifurcations may occur in this case, we cannot give the corresponding stability boundaries in closed form, though. However, assume the case when $\omega = j/2$, $j = 0, 1, \ldots$. Then

$$\tilde{c}_k = \delta - (k + j/2)^2 - b(-1)^j + \mathrm{i}\,(k + j/2)\kappa \,, \tag{3.37}$$

and the same classification can be done as in the undamped case.

If j is even, that is $j = 2h$, $h = 0, 1, \ldots$, then $\lambda = \mathrm{i}\,h$ and the corresponding characteristic multiplier is

$$\mu = \mathrm{e}^{\mathrm{i}h2\pi} = \mathrm{e}^{\mathrm{i}2\pi} = 1 \,. \tag{3.38}$$

In this case, $\tilde{c}_k = \delta - b - (k + h)^2 + \mathrm{i}\,(k + h)\kappa$, and equation (3.34) gives the relation $\tilde{f}_{+1}(\delta - b, \varepsilon, \kappa) = 0$ for the boundary curves. For the case $b = 0$, the relation $\tilde{f}_{+1}(\delta, \varepsilon, \kappa) = 0$ serves the $\mu = +1$ stability boundary curves of the classical damped Mathieu equation defined in the form $\delta = \tilde{g}_{+1}(\varepsilon, \kappa)$. This means, that the linear boundary curves exist for the $b \neq 0$ case, too, in the form $\delta - b = \tilde{g}_{+1}(\varepsilon, \kappa)$. In the plane (δ, b), these are lines with slope $+1$ (see Figure 3.5). Along these boundary curves, there exists a characteristic multiplier $\mu = +1$, and equation (3.33) has a periodic solution of period 2π. This case corresponds to the period one bifurcation.

If j is odd, that is $j = 2h+1$, $h = 0, 1, \ldots$, then $\lambda = \mathrm{i}\,(h+1/2)$ and the corresponding characteristic multiplier is

$$\mu = \mathrm{e}^{\mathrm{i}\,(h+1/2)2\pi} = \mathrm{e}^{\mathrm{i}\pi} = -1 \,. \tag{3.39}$$
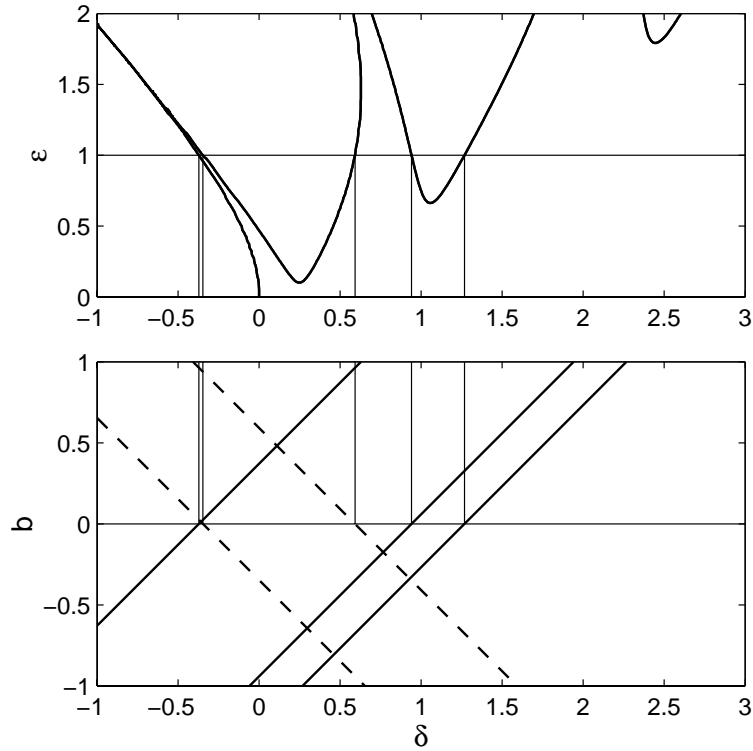
Figure 3.5: Period one and period two boundary lines for equation (3.33) with $\varepsilon = 1$, $\kappa = 0.1$

In this case, $\tilde{c}_k = \delta + b - (k + h + 1/2)^2 + \mathrm{i}\,(k + h + 1/2)\kappa$, and equation (3.34) implies the boundary curve relation $\tilde{f}_{-1}(\delta + b, \varepsilon, \kappa) = 0$. For the same reason as above, the boundary curves exist again in the form $\delta - b = \tilde{g}_{-1}(\varepsilon, \kappa)$, where $\delta = \tilde{g}_{-1}(\varepsilon, \kappa)$ gives the $\mu = -1$ stability boundary curves of the classical damped Mathieu equation. The boundary curves are lines with slope -1 in the parameter plane (δ, b) (see Figure 3.5). Along these boundary curves, there exists a characteristic multiplier $\mu = -1$, and equation (3.33) has nontrivial periodic solution of period 4π. This case corresponds to the period two bifurcation.

This investigation showed that all the period one and period two boundary curves are lines in the (δ, b) plane with slope $+1$ or -1, respectively (see Figure 3.5). However, in addition to these linear boundaries, secondary Hopf type boundary curves may also exist, since λ and consequently μ can also be complex at the loss of stability.

3.4 New results

Thesis 1 *The closed form 3 dimensional stability chart for the delayed Mathieu equation*

$$\ddot{x}(t) + (\delta + \varepsilon \cos t)x(t) = bx(t - 2\pi)$$

was constructed and proved. It was shown analytically, that the boundary curves in the plane (δ, b) are lines for any ε. The number of instabilities was also determined in the domains separated by these lines. At the boundaries with slope $+1$, a characteristic multiplier crosses the unit circle at $+1$, presenting a 2π periodic motion. At the boundaries with slope -1, a characteristic multiplier crosses the unit circle at -1, presenting a 4π periodic motion.

It was also proved, that the damped delayed Mathieu equation also have linear boundary curves in the plane (δ, b) for the period one and period two bifurcations, but secondary Hopf bifurcations may also exist along some non-linear stability boundaries.

Chapter 4

Fargue-type approximation

In this chapter, a special approximation method is introduced for the stability analysis of linear periodic RFDEs. The method is based on the special properties of RFDEs with a Fargue-type delay distribution defined as $\int_{-\infty}^{0} w(\vartheta)x(t+\vartheta)\mathrm{d}\vartheta$, where the weight function is a product of a polynomial and an exponential expression: $w(\vartheta) = C_1 \vartheta^n \, \mathrm{e}^{C_2 \vartheta}$, $C_{1,2} \in \mathbb{R}$, $n \in \mathbb{N}$. It was shown by Fargue (1973), that these RFDEs are equivalent to finite dimensional system of ODEs.

This type of weight function is often used for modeling distributed time delay effects. For example, in population dynamics, delay effects (gestation, digestion) are not so well defined, the delays have some deviations around an average value (see Farkas, 1994, Farkas and Stépán, 1992).

In this section, RFDEs with a Fargue-type delay distribution are used for approximating RFDEs with discrete time delays (i.e. approximating RDDEs).

4.1 Transformation of Fargue-type RFDEs to ODEs

Consider the second order linear periodic RDDE

$$\ddot{x}(t) + b_0 \dot{x}(t) + c_0(t)x(t) = c_1(t)x(t-\tau)\,, \quad c_{0,1}(t+T) = c_{0,1}(t)\,. \tag{4.1}$$

With $T = \tau$, this gives the governing equation of regenerative vibrations in milling processes (see Chapter 6, later). In this chapter, an approximate stability chart for equation (4.1) will be constructed.

The main step of the method is the approximation of the discrete time delay with a distributed one as follows

$$x(t-\tau) \approx \int_{-\infty}^{0} w_n(\vartheta)x(t+\vartheta)\mathrm{d}\vartheta\,, \tag{4.2}$$

31
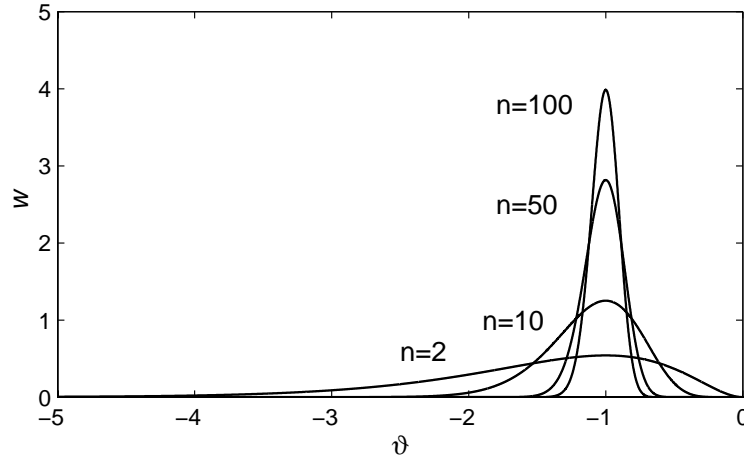
Figure 4.1: The Fargue-type weight function for $\tau = 1$

where $w_n(\vartheta)$ is a special weight function series coming from the product of a polynomial and an exponential expression

$$w_n(\vartheta) = (-1)^n \frac{n^{n+1}}{\tau^{n+1}n!} \vartheta^n \, e^{n\vartheta/\tau} \, . \tag{4.3}$$

The function $w_n(\vartheta)$ satisfies the following properties

$$\int_{-\infty}^{0} w_n(\vartheta)\mathrm{d}\vartheta = 1, \quad \lim_{n\to\infty} w_n(\vartheta) = f_\delta(\vartheta + \tau) \, , \tag{4.4}$$

where f_δ is the Dirac distribution. Figure 4.1 shows the weight functions for parameters $n = 2, 10, 50, 100$ and $\tau = 1$. It can be seen, that the greater n is, the more correct the approximation is. Fargue (1973) proved that equation (4.2) converges to $x(t - \tau)$ as n tends to infinity, i.e.

$$\lim_{n\to\infty} \int_{-\infty}^{0} w_n(\vartheta)x(t + \vartheta)\mathrm{d}\vartheta = x(t - \tau) \, . \tag{4.5}$$

Consequently, n can be called as approximation parameter.

Application of approximation (4.2) with a fixed finite n in equation (4.1) results the periodic RFDE

$$\ddot{x}(t) + b_0\dot{x}(t) + c_0(t)x(t) = c_1(t) \int_{-\infty}^{0} w_n(\vartheta)x(t + \vartheta)\mathrm{d}\vartheta \, , \quad c_{0,1}(t + T) = c_{0,1}(t) \, . \tag{4.6}$$

Now, introduce the new variables $y_1, y_2, \dots, y_{n+3}$ in several steps in the following way:

$$y_1(t) = x(t) \, , \tag{4.7}$$

$$y_2(t) = \dot{x}(t) \, , \tag{4.8}$$

$$y_3(t) = \int_{-\infty}^{0} w_n(\vartheta)x(t + \vartheta)\mathrm{d}\vartheta \approx x(t - \tau) \, . \tag{4.9}$$

Since

$$\frac{\mathrm{d}}{\mathrm{d}t}x(t+\vartheta) = \frac{\mathrm{d}}{\mathrm{d}\vartheta}x(t+\vartheta) = \dot{x}(t+\vartheta)\,, \tag{4.10}$$

the derivative of $y_3(t)$ with respect to the time t can be calculated via integration by parts as follows

$$
\begin{aligned}
\dot{y}_3(t) &= \int_{-\infty}^{0}(-1)^n\frac{n^{n+1}}{\tau^{n+1}n!}\vartheta^n\,\mathrm{e}^{n\vartheta/\tau}\dot{x}(t+\vartheta)\mathrm{d}\vartheta\\
&= \left[(-1)^n\frac{n^{n+1}}{\tau^{n+1}n!}\vartheta^n\,\mathrm{e}^{n\vartheta/\tau}x(t+\vartheta)\right]_{-\infty}^{0}\\
&\qquad - \int_{-\infty}^{0}x(t+\vartheta)\frac{\mathrm{d}}{\mathrm{d}\vartheta}\left((-1)^n\frac{n^{n+1}}{\tau^{n+1}n!}\vartheta^n\,\mathrm{e}^{n\vartheta/\tau}\right)\mathrm{d}\vartheta\\
&= 0 - \frac{n}{\tau}\int_{-\infty}^{0}x(t+\vartheta)(-1)^n\frac{n^{n+1}}{\tau^{n+1}n!}\vartheta^n\,\mathrm{e}^{n\vartheta/\tau}\mathrm{d}\vartheta\\
&\qquad - \int_{-\infty}^{0}x(t+\vartheta)(-1)^n\frac{n^{n+1}}{\tau^{n+1}(n-1)!}\vartheta^{n-1}\,\mathrm{e}^{n\vartheta/\tau}\mathrm{d}\vartheta\\
&= -\frac{n}{\tau}y_3(t) - \int_{-\infty}^{0}(-1)^n\frac{n^{n+1}}{\tau^{n+1}(n-1)!}\vartheta^{n-1}\,\mathrm{e}^{n\vartheta/\tau}x(t+\vartheta)\mathrm{d}\vartheta\,.
\end{aligned}
\tag{4.11}
$$

This time, the second term in equation (4.11) is defined as the subsequent new variable

$$y_4(t) = \int_{-\infty}^{0}(-1)^n\frac{n^{n+1}}{\tau^{n+1}(n-1)!}\vartheta^{n-1}\,\mathrm{e}^{n\vartheta/\tau}x(t+\vartheta)\mathrm{d}\vartheta\,. \tag{4.12}$$

Similar calculation results

$$\dot{y}_4(t) = -\frac{n}{\tau}y_4(t) - \int_{-\infty}^{0}(-1)^n\frac{n^{n+1}}{\tau^{n+1}(n-2)!}\vartheta^{n-2}\,\mathrm{e}^{n\vartheta/\tau}x(t+\vartheta)\mathrm{d}\vartheta\,, \tag{4.13}$$

where the second term defines a new variable, again,

$$y_5(t) = \int_{-\infty}^{0}(-1)^n\frac{n^{n+1}}{\tau^{n+1}(n-2)!}\vartheta^{n-2}\,\mathrm{e}^{n\vartheta/\tau}x(t+\vartheta)\mathrm{d}\vartheta\,. \tag{4.14}$$

After the introduction of all the new variables in the same way, and calculating their time derivatives via integration by parts, the degree of ϑ decreases each time by 1. The $(n+2)$nd new variable and its derivative read

$$y_{n+2}(t) = \int_{-\infty}^{0}(-1)^n\frac{n^{n+1}}{\tau^{n+1}1!}\vartheta\,\mathrm{e}^{n\vartheta/\tau}x(t+\vartheta)\mathrm{d}\vartheta\,, \tag{4.15}$$

$$\dot{y}_{n+2}(t) = -\frac{n}{\tau}y_{n+2}(t) - \int_{-\infty}^{0}(-1)^n\frac{n^{n+1}}{\tau^{n+1}}\,\mathrm{e}^{n\vartheta/\tau}x(t+\vartheta)\mathrm{d}\vartheta\,, \tag{4.16}$$

where the last new variable is defined as

$$y_{n+3}(t) = \int_{-\infty}^{0}(-1)^n\frac{n^{n+1}}{\tau^{n+1}}\,\mathrm{e}^{n\vartheta/\tau}x(t+\vartheta)\mathrm{d}\vartheta\,. \tag{4.17}$$

The derivative of $y_{n+3}(t)$ reads

$$
\begin{aligned}
\dot{y}_{n+3}(t) &= -\frac{n}{\tau}y_{n+3}(t) - \int_{-\infty}^{0}(-1)^n\frac{n^{n+1}}{\tau^{n+1}}\,\mathrm{e}^{n\vartheta/\tau}x(t+\vartheta)\mathrm{d}\vartheta \\
&= -\frac{n}{\tau}y_{n+3}(t) - (-1)^n\frac{n^{n+1}}{\tau^{n+1}}x(t)\,.
\end{aligned}
\tag{4.18}
$$

Equations (4.11)-(4.17) define the recursion

$$
\dot{y}_j(t) = -\frac{n}{\tau}y_j(t) - y_{j+1}(t)\,, \quad j = 3, 4, \ldots, n+2\,, \tag{4.19}
$$

while equation (4.18) forms a connection with $y_1(t) = x(t)$. Together with the equations (4.6)-(4.9), a finite $(n+3)$ dimensional system of ODEs with a τ-periodic coefficient matrix can be defined:

$$
\dot{\mathbf{y}}(t) = \mathbf{A}(t)\mathbf{y}(t)\,, \tag{4.20}
$$

where $\mathbf{y} = \mathrm{col}(y_1\ y_2\ \ldots\ y_{n+3})$ and

$$
\mathbf{A}(t) = \begin{pmatrix}
0 & 1 & 0 & 0 & \cdots & 0 \\
-c_0(t) & -b_0 & c_1(t) & 0 & \cdots & 0 \\
0 & 0 & -n/\tau & -1 & \cdots & 0 \\
\vdots & \vdots & \vdots & \ddots & \ddots & \vdots \\
0 & 0 & 0 & \cdots & -n/\tau & -1 \\
(-1)^n\,(-n/\tau)^{n+1} & 0 & 0 & \cdots & 0 & -n/\tau
\end{pmatrix}\,. \tag{4.21}
$$

As it was shown by Fargue (1973), equation (4.6) is equivalent to equation (4.20). Thus, the stability of equation (4.20) gives the stability of equation (4.6), i.e. if equation (4.6) is stable, then equation (4.20) is stable too, and vice versa.

System (4.20) is asymptotically stable, if and only if all the characteristic multipliers denoted by μ_j, $j = 1, 2, \ldots, n+3$, are in modulus less than one. As mentioned in Section 2.2, there are no general methods to calculate the characteristic multipliers of system (4.20) in an algebraic form, but there are various types of approximation methods. Here, we will use the piecewise constant approximation of the coefficient matrix $\mathbf{A}(t)$.

Construct the time intervals $[t_{i-1}, t_i]$ of length Δt_i, $i = 1, 2, \ldots, k$, so that the principal period can be expressed as $T = \sum_{i=1}^{k}\Delta t_i$. The functions $c_0(t)$ and $c_1(t)$ are approximated with constant (say average) values

$$
c_{0\,i} = \frac{1}{\Delta t_i}\int_{t_{i-1}}^{t_i}c_0(t)\mathrm{d}t \approx c_0(t_i - \Delta t_i/2)\,, \quad i = 1, 2, \ldots, k\,, \tag{4.22}
$$

$$
c_{1\,i} = \frac{1}{\Delta t_i}\int_{t_{i-1}}^{t_i}c_1(t)\mathrm{d}t \approx c_1(t_i - \Delta t_i/2)\,, \quad i = 1, 2, \ldots, k \tag{4.23}
$$

in each time interval. Correspondingly, the piecewise constant approximation of the coefficient matrix is

$$
\mathbf{A}_i = \begin{pmatrix}
0 & 1 & 0 & 0 & \cdots & 0 \\
-c_{0\,i} & -b_0 & c_{1\,i} & 0 & \cdots & 0 \\
0 & 0 & -n/\tau & -1 & \cdots & 0 \\
\vdots & \vdots & \vdots & \ddots & \ddots & \vdots \\
0 & 0 & 0 & \cdots & -n/\tau & -1 \\
(-1)^n\,(-n/\tau)^{n+1} & 0 & 0 & \cdots & 0 & -n/\tau
\end{pmatrix}, \qquad (4.24)
$$

for $t \in [t_{i-1}, t_i]$, $i = 1, 2, \ldots, k$.

The Floquet transition matrix of the system can be given by coupling the solutions for each interval:

$$
\mathbf{\Phi}(T) = \exp(\mathbf{A}_k \Delta t_k)\exp(\mathbf{A}_{k-1}\Delta t_{k-1})\cdots\exp(\mathbf{A}_1 \Delta t_1)\,. \qquad (4.25)
$$

This matrix is a finite dimensional approximation of the monodromy operator $\mathbf{U}(T)$ of system (4.1). At this point, several numerical methods can be used to determine the critical eigenvalue, that is the greatest in modulus.

4.2 Time scale transformation

A numerical problem arises in the Fargue-type approximation. The bottom left element of the piecewise constant matrix (4.24) increases in modulus exponentially with the approximation parameter. It means, that for large n, the matrix (4.24) is not well conditioned, and the computation of the matrix exponential in equation (4.25) needs high CPU capacity and may still result numerical errors.

For example, if $n = 20$ and $\tau = 1$, then $(-1)^n\,(-n/\tau)^{n+1} \approx 2.0972 \times 10^{27}$, i.e. the norm of the matrix is at least 2.0972×10^{27}. Thus, the norm of the exponential matrix is about $10^{9.108 \times 10^{26}}$. This order of magnitude of numbers leads to numerical difficulties during the evaluation of the Floquet transition matrix $\mathbf{\Phi}(T)$.

A solution for this problem is to introduce the new dimensionless time $\tilde{t} = (n/\tau)t$. The derivatives w.r.t. $\tilde{t}$ are denoted by comma, and defined by

$$
\frac{\mathrm{d}}{\mathrm{d}t} = \frac{n}{\tau}\frac{\mathrm{d}}{\mathrm{d}\tilde{t}} \qquad (4.26)
$$

For this time scale, the equation (4.1) has the form

$$
x''\left(\tilde{t}\right) + \left(\frac{\tau}{n}\right)b_0 x'\left(\tilde{t}\right) + \left(\frac{\tau}{n}\right)^2 c_0\left(\tilde{t}\right)x\left(\tilde{t}\right) = \left(\frac{\tau}{n}\right)^2 c_1\left(\tilde{t}\right)x\left(\tilde{t} - n\right)\,, \qquad (4.27)
$$

$$
c_{0,1}\left(\tilde{t} + \left(\frac{n}{\tau}\right)T\right) = c_{0,1}\left(\tilde{t}\right)\,.
$$

The point is, that in equation (4.27), the time delay is just equal to the approximation parameter, and the approximated coefficient matrix resulted by the Fargue-type approximation is well conditioned now:

$$
\mathbf{A}_i = \begin{pmatrix}
0 & 1 & 0 & 0 & \cdots & 0 \\
-\left(\frac{\tau}{n}\right)^2 c_{0\,i} & -\left(\frac{\tau}{n}\right) b_0 & \left(\frac{\tau}{n}\right)^2 c_{1\,i} & 0 & \cdots & 0 \\
0 & 0 & -1 & -1 & \cdots & 0 \\
\vdots & \vdots & \vdots & \ddots & \ddots & \vdots \\
0 & 0 & 0 & \cdots & -1 & -1 \\
(-1)^n & 0 & 0 & \cdots & 0 & -1
\end{pmatrix} . \tag{4.28}
$$

The norm of this matrix is about 2 (it also depends on the parameters b_0, $c_{0\,i}$, $c_{1\,i}$, n, τ, of course), and the numerical problems mentioned before do not arise. Approximation parameter $n = 100$ can be used with a reasonable CPU capacity to determine the Floquet transition matrix

$$
\mathbf{\Phi}\left(\frac{n}{\tau}T\right) = \exp\left(\mathbf{A}_k \frac{n}{\tau}\Delta t_k\right) \exp\left(\mathbf{A}_{k-1} \frac{n}{\tau}\Delta t_{k-1}\right) \cdots \exp\left(\mathbf{A}_1 \frac{n}{\tau}\Delta t_1\right) . \tag{4.29}
$$

The comparison of the CPU times for evaluating characteristic multipliers of Floquet transition matrices with and without time scale transformation can be seen in Figure 4.2. The figure shows the CPU time for evaluating eigenvalues of matrices (4.25) and (4.29), respectively, for various approximation parameters n and for interval number $k = 10$. It can be seen, that the CPU time is higher for computations without time scale transformation. For higher approximation parameter, the difference between the two method increases exponentially. Furthermore, for $n > 25$, the accumulated numerical errors become too large during the calculation without time scale transformation. That is, without time scale transformation, the method can only be used for $n < 25$. With time scale transformation, the method can be used for higher approximation parameters as well.

4.3 Example: the damped delayed Mathieu equation

The special case of equation (4.1)

$$
\ddot{x}(t) + b_0\dot{x}(t) + c_0(t)x(t) = c_1 x(t - \tau), \quad c_0(t) = c_{0\,\delta} + c_{0\,\varepsilon}\cos(2\pi t/T). \tag{4.30}
$$

is investigated. The case $c_1 = 0$ with $\tau = 2\pi$ and the case $c_{0\,\varepsilon} = 0$ give the equations (2.11) and (2.27), respectively. The boundary curves for these cases were determined in Chapter 2 (see Figures 2.3 and 2.4). The case $b_0 = 0$, $T = \tau = 2\pi$ gives the delayed Mathieu equation (3.3), for which, the closed form stability chart was constructed in Chapter 3.
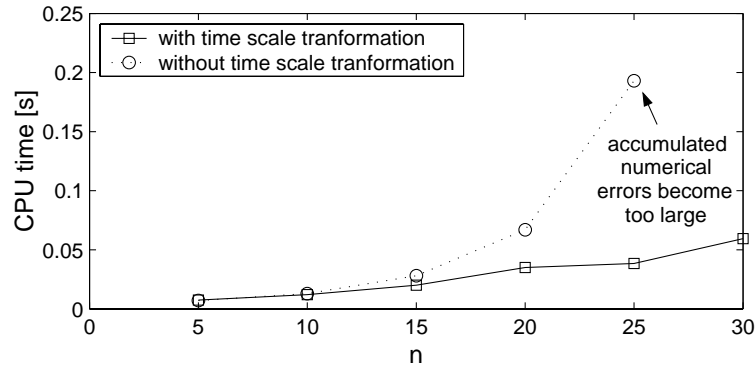
Figure 4.2: Comparison of Fargue-type approximations with and without time scale transformation

Equation (4.30) is approximated by the RFDE

$$\ddot{x}(t) + b_0 \dot{x}(t) + c_0(t)x(t) = c_1 \int_{-\infty}^{0} w_n(\vartheta)x(t+\vartheta)\mathrm{d}\vartheta, \qquad (4.31)$$

$$c_0(t) = c_{0\,\delta} + c_{0\,\varepsilon}\cos(2\pi t/T),$$

with the weight function $w_n(\vartheta)$ defined by (4.3). The approximated stability charts for the general cases ($b_0 \neq 0$, $c_1 \neq 0$ and $c_{0\,\varepsilon} \neq 0$) will be constructed here.

For the undamped autonomous case ($b_0 = 0$ and $c_{0\,\varepsilon} = 0$), the stability charts for various approximation parameters ($n = 2, 5, 10, 20, 50, 100$) are shown in Figure 4.3. Grey colored parameter domains refer to asymptotically stable systems. It can be followed, how the stability charts converge to the exact chart of equation (2.27) that is shown by dotted lines on the $n = 100$ chart. In the $0 < c_{0\,\delta} < 1$, $-0.5 < c_1 < 0.5$ parameter domain, $n = 100$ gives a satisfactory approximation with errors less than 1%. This means a 103 dimensional approximation of the infinite dimensional state space of equation (4.30).

Although, the $n \to \infty$ limit case gives the Dirac distribution and results a discrete time delay in the equation, this type of weight function can effectively be used for approximating systems including distributed delays. The charts in Figure 4.3 also show, that for lower approximation parameter, i.e., for more distributed time delay, the stable domains are more extended, especially for large c_0 parameter. This means, that the distribution of the time delay has a kind of stabilizing effect.

Figure 4.4 shows the stability charts for equation (4.31) with $\tau = T = 2\pi$ and $n = 100$, that is, the approximated stability charts for equation (4.30) with $\tau = T = 2\pi$. For the special case $c_{0\,\varepsilon} = 0$, the boundary curves were determined in Section 2.3 (see Figure 2.3). For the case $b_0 = 0$, the closed form stability chart was constructed in Chapter 3. For these limit cases, the accurate boundary curves are shown by dotted
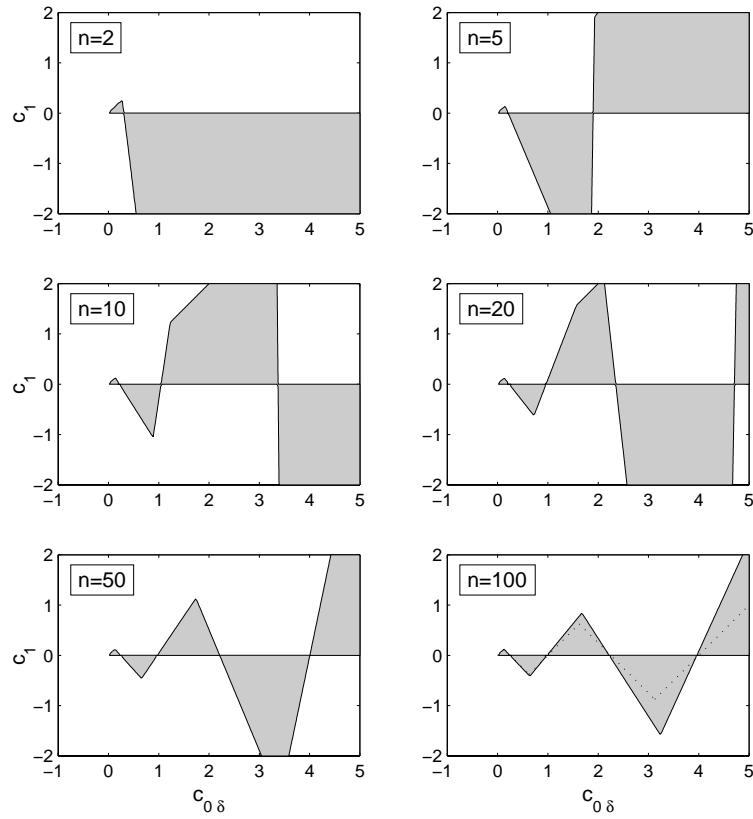
Figure 4.3: Stability charts for equation (4.31) with $b_0 = 0$ and $c_{0\,\varepsilon} = 0$

lines again in Figure 4.4. This helps to estimate the accuracy of the approximation.

It was shown in Chapter 3, that the period one and period two boundary curves are linear also in the case $b_0 \neq 0$. In the charts $[c_{0\,\varepsilon} = 1\,, b_0 = 0.1]$, $[c_{0\,\varepsilon} = 2\,, b_0 = 0.1]$ and $[c_{0\,\varepsilon} = 2\,, b_0 = 0.2]$, these linear boundaries occur. In the chart $[c_{0\,\varepsilon} = 1\,, b_0 = 0.2]$, this extra boundary curve is not a straight line. This is due to the fact, that equation (4.31) is only an approximation of equation (4.30). For higher approximation parameter, this boundary curves converge to two parallel lines.

The stability charts for equation (4.31) with $n = 100$, $\tau = 2\pi$, $T = \pi$ and $T = 4\pi$ can be seen in Figures 4.5 and 4.6, respectively. For the case $T = \pi$, the linear boundaries are still present and the stability charts have a clear structure. For the case $T = 4\pi$, the structures of the charts are not so clear, and also disjunct stable parameter domains arise.

In Chapter 5, the stability charts shown in the Figures 4.4, 4.5 and 4.6 are also determined by the semi-discretization method. Thus, the two numerical methods will also be compared later.
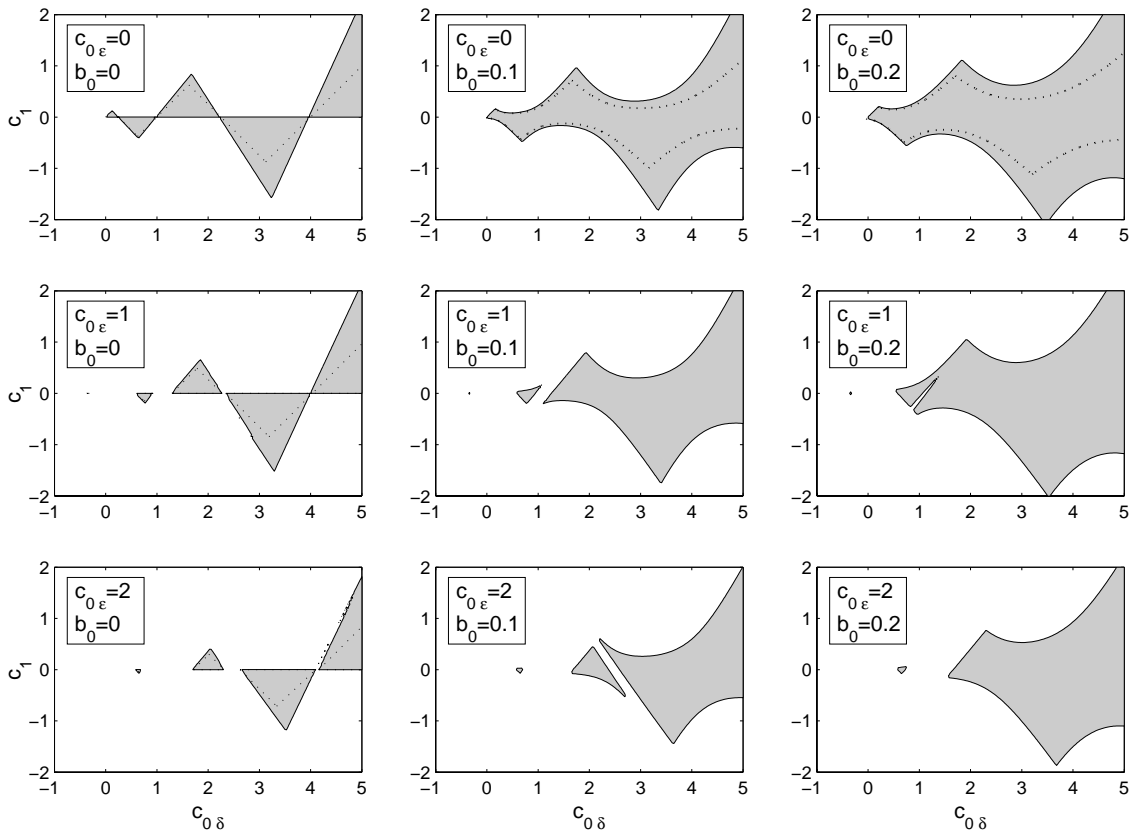
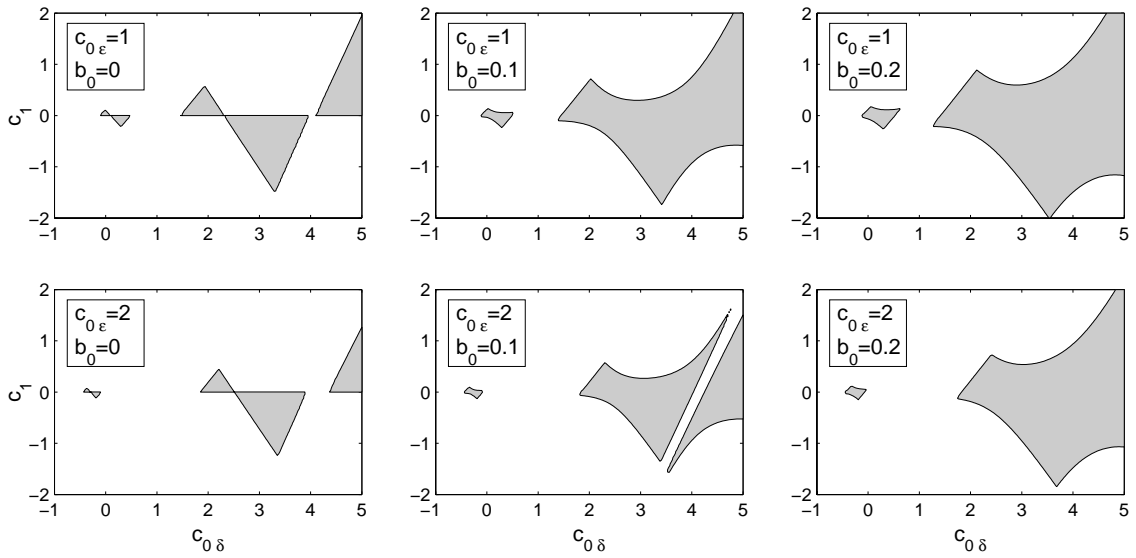Figure 4.4: Stability charts for equation (4.31) with $n = 100$, $\tau = 2\pi$ and $T = 2\pi$

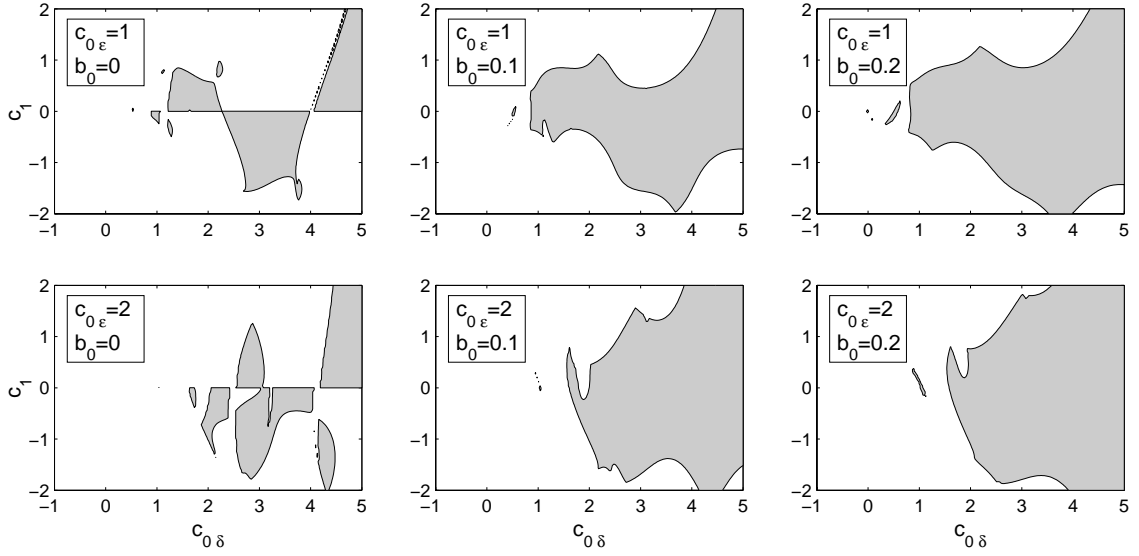Figure 4.5: Stability charts for equation (4.31) with $n = 100$, $\tau = 2\pi$ and $T = \pi$

Figure 4.6: Stability charts for equation (4.31) with $n = 100$, $\tau = 2\pi$ and $T = 4\pi$

4.4 New results

Thesis 2 *Fargue's theorem (1973) was applied to transform the linear periodic RFDE*

$$\ddot{x}(t) + b_0\dot{x}(t) + c_0(t)x(t) = c_1(t)\int_{-\infty}^{0} w_n(\vartheta)x(t+\vartheta)\mathrm{d}\vartheta\,, \quad c_{0,1}(t+T) = c_{0,1}(t)$$

with the weight function

$$w_n(\vartheta) = (-1)^n \frac{n^{n+1}}{\tau^{n+1}n!}\,\vartheta^n\,\mathrm{e}^{n\vartheta/\tau}$$

into the $(n+3)$ dimensional ODE of the form

$$\dot{\mathbf{y}}(t) = \mathbf{A}(t)\mathbf{y}(t)\,.$$

The Floquet transition matrix was determined by piecewise constant approximation of the coefficient matrix $\mathbf{A}(t)$. The method was used for approximating RDDEs with finite dimensional ODEs. A time scale transformation was introduced, that make the approximation numerically more effective.

Approximate stability charts for the periodic RDDE (the damped delayed Mathieu equation)

$$\ddot{x}(t) + b_0\dot{x}(t) + c_0(t)x(t) = c_1x(t-\tau)\,, \quad c_0(t) = c_{0\,\delta} + c_{0\,\varepsilon}\cos(2\pi t/T)$$

were constructed.

Chapter 5

Semi-discretization

Discretization techniques are important for differential equations for which the solution cannot be given in closed forms. Approximation with discrete systems has become more important by the development of computer technology. Nowadays, the numerical dynamics is a very active and rapidly evolving field of research. Since any discretization is a parameterized family of small perturbations (with the stepsize as parameter), the classical theory of perturbations can be adapted to discretizations, see, e.g., Arnold (1978), Stuart and Humphries (1996), Garay (1996, 1998), Garay and Hilger (2001). Generally, one may say that, for a sufficiently small stepsize, the solutions of the original differential equations persist under discretization.

The semi-discretization method presented in this chapter is an efficient numerical method for the stability analysis of linear delayed systems. The method is based on a special kind of discretization technique with respect to the past effect only. Mathematically, this discretization corresponds to a delay perturbation (see Győri and Turi, 1991, Cooke *et al.*, 1991 and Győri *et al.*, 1995, 1996). The resulting approximate system is delayed and also time periodic, but still, it can be transformed analytically into a high dimensional linear discrete system. The method is applied to determine the stability charts of the Mathieu equation also with distributed time delay.

5.1   Preliminaries

In this Section, the basic idea of semi-discretization is shown for a simple case. Let us consider the one dimensional, second order autonomous RFDE with a discrete time delay (the undamped delayed oscillator)

$$\ddot{x}(t) + c_0 x(t) = c_1 x(t - \tau) \,. \tag{5.1}$$

Equation (5.1) was already investigated in Section 2.3, and its stability chart was also constructed (see Figures 2.4 or 3.2). Here, the semi-discretization method will be
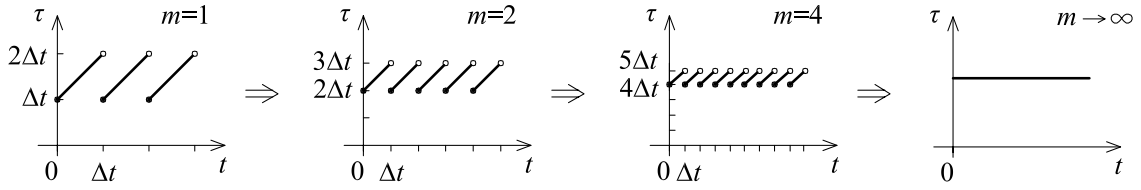
Figure 5.1: Time dependent delay

introduced first for equation (5.1).

5.1.1   Basic idea of semi-discretization

Consider the intervals $[t_i, t_{i+1})$ where $t_{i+1} - t_i = \Delta t$, $i = 0, 1, \ldots$, and the RFDE

$$\ddot{x}(t) + c_0 x(t) = c_1 x(t_{i-m}), \quad t \in [t_i, t_{i+1}), \quad m \in \mathbb{Z}, \quad i = 0, 1, \ldots. \qquad (5.2)$$

This equation for the case $m = 1$ often comes up in control problems modeling the sampling effect (see, for example, Stépán, 1991, 2001a, or Kovács and Stépán, 2002). In opposite to equation (5.1), the time delay in equation (5.2) is not constant, it is a piecewise linear periodic function with period Δt, as it is shown in Figure 5.1. As the parameter m tends to infinity, the time delay tends to the constant value τ if $\Delta t = \tau/(m + 1/2)$, and equation (5.2) approximates equation (5.1).

Although equation (5.2) is a non-autonomous RFDE with infinite dimensional phase space, its Poincaré map has a simple finite dimensional representation since it can be solved in each time interval as an ODE (details will be explained in Section 5.2). The stability chart defined for various values of m can be seen in Figure 5.2 (stable parameter domains are denoted by grey color). It shows, how the stability chart of equation (5.2) approximates the chart of equation (5.1) for increasing parameter m. For $m = 10$, the stability chart approximates the chart in Figure 3.2 with errors less than 1%. For the charts in Figure 5.2, $\tau = 2\pi$, consequently, $\Delta t = 2\pi/(m + 1/2)$.

For the case $m = 1$, the necessary and sufficient criteria for asymptotic stability can be given after a lengthy algebraic work (see Appendix A) as

$$c_1 < c_0, \quad c_0 \neq \frac{k^2 \pi^2}{\Delta t^2}, \quad k = 0, 1, \ldots \qquad (5.3)$$

and

$$0 < c_1 < \frac{1 + 2\cos\left(\sqrt{c_0}\Delta t\right)}{1 - \cos\left(\sqrt{c_0}\Delta t\right)} c_0 \quad \text{or} \quad 0 > c_1 > \frac{1 + 2\cos\left(\sqrt{c_0}\Delta t\right)}{1 - \cos\left(\sqrt{c_0}\Delta t\right)} c_0, \qquad (5.4)$$

where $\Delta t = 4\pi/3$. The formulae are more and more complicated for $m \geq 2$.

The point of the semi-discretization method is that, while the actual time domain terms are left in the original form, the delayed terms are approximated by piecewise
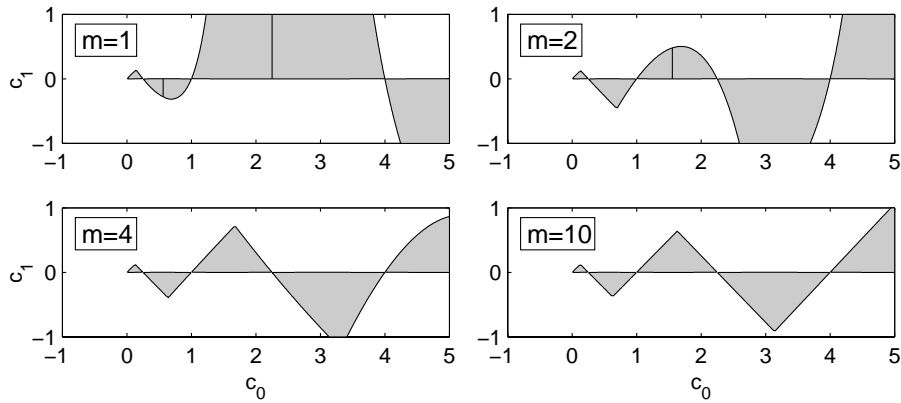
Figure 5.2: Stability charts for equation (5.2) with $\tau = 2\pi$

constant values, and are treated as constant excitations in ODEs. In Section 5.2, the generalization of the above introduced method will be shown. Before that, the full-discretization is compared to the semi-discretization.

5.1.2 Full discretization

The following question arises naturally: why do not we discretize all the actual time domain terms? The use of the interval division shown in Section 5.1.1 leads to the approximated derivatives of $x(t)$

$$\dot{x}(t) \approx \frac{x_{i+1} - x_i}{\Delta t} \,, \tag{5.5}$$

$$\ddot{x}(t) \approx \frac{x_{i+2} - 2x_{i+1} + x_i}{\Delta t^2} \,, \tag{5.6}$$

where $x_i = x(t_i)$. Substitution into equation (5.2) yields the recursive formula

$$x_{i+2} = \alpha_1 x_{i+1} + \alpha_2 x_i + \alpha_3 x_{i-m} \,, \tag{5.7}$$

where $\alpha_1 = 2$, $\alpha_2 = -1 - c_0 \Delta t^2$ and $\alpha_3 = c_1 \Delta t^2$. This connection is described by the discrete map

$$\mathbf{y}_{i+1} = \mathbf{B} \mathbf{y}_i \,, \tag{5.8}$$

where the $m + 2$ dimensional state vector is

$$\mathbf{y}_i = \mathrm{col}\big(x_{i+1} \;\; x_i \;\; x_{i-1} \;\; \dots \;\; x_{i-m}\big) \,, \tag{5.9}$$
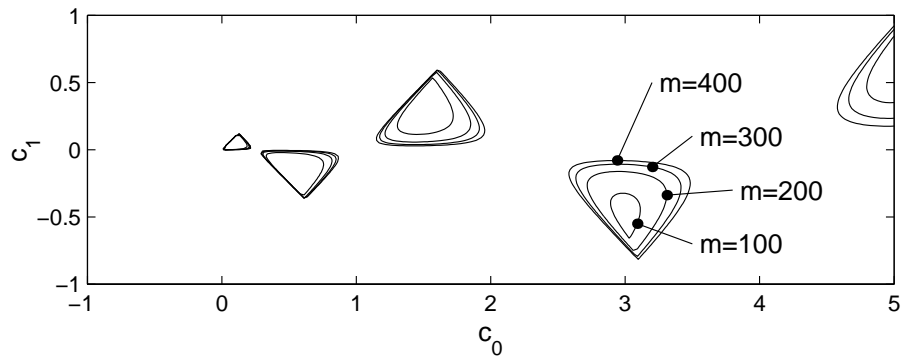
Figure 5.3: Stability boundaries for equation (5.1) constructed by full discretization

and the coefficient matrix has the form

$$
\mathbf{B} = \begin{pmatrix} \alpha_1 & \alpha_2 & 0 & \ldots & 0 & \alpha_3 \\ 1 & 0 & 0 & \ldots & 0 & 0 \\ 0 & 1 & 0 & \ldots & 0 & 0 \\ \vdots & \vdots & \vdots & \ddots & \vdots & \vdots \\ 0 & 0 & 0 & \ldots & 0 & 0 \\ 0 & 0 & 0 & \ldots & 1 & 0 \end{pmatrix} .
\tag{5.10}
$$

The stability chart constructed by full discretization can be seen in Figure 5.3 for various approximation parameter values. Comparison of the charts in Figure 5.2 and in Figure 5.3 shows, that the semi-discretization method is much more effective.

5.2   Semi-discretization method

The so-called semi-discretization is a well known technique used for example, in the finite element analysis of solid bodies, or in computational fluid mechanics. The basic idea is, that the corresponding partial differential equation (PDE) is discretized along the spatial coordinates only, while the time coordinates are unchanged. From a dynamical systems viewpoint, the PDE has an infinite dimensional state space, which is approximated by the finite dimensional state space of a high dimensional ODE.

The same idea can be used for any RFDE, but its implementation is not trivial. The infinite dimensional nature of the RFDE is due to the presence of past effects, described by functions embedded also in the time domain, above the past interval $[t - \sigma, t]$, where σ denotes the length of the delay effect.

In this section, we will investigate the n dimensional RFDE

$$
\dot{\mathbf{x}}(t) = \int_{-\sigma}^{0} \mathrm{d}_\vartheta \boldsymbol{\eta}(\vartheta, t) \mathbf{x}(t + \vartheta), \quad \boldsymbol{\eta}(\vartheta, t + T) = \boldsymbol{\eta}(\vartheta, t) ,
\tag{5.11}
$$

where the lower limit σ can also be infinity and the condition (2.41) holds.

The integral in equation (5.11) is a Stieltes one, i.e. it may contain discrete and continuous time delays like

$$\int_{-\sigma}^{0} \mathrm{d}_\vartheta \boldsymbol{\eta}(\vartheta, t)\mathbf{x}(t+\vartheta) = \sum_{j=1}^{r} \mathbf{R}_j(t)\mathbf{x}(t-\tau_j) + \int_{-\sigma}^{0} \mathbf{W}(\vartheta, t)\mathbf{x}(t+\vartheta)\mathrm{d}\vartheta\,, \qquad (5.12)$$

where the number r of discrete time delays can also be infinity. Nevertheless, the discrete time delay can also be defined as

$$\mathbf{x}(t-\tau_j) = \int_{-\sigma}^{0} w_j(\vartheta)\mathbf{x}(t+\vartheta)\mathrm{d}\vartheta\,, \qquad (5.13)$$

where the weight function is the Dirac distribution at $-\tau_j$:

$$w_j(\vartheta) = f_\delta(\vartheta+\tau_j)\,, \qquad (5.14)$$

and $\tau_j < \sigma$. This makes it possible to consider the discrete time delay as a special case of the continuous one. Thus, we will investigate the RFDE of the form

$$\dot{\mathbf{x}}(t) = \mathbf{A}(t)\mathbf{x}(t) + \int_{-\sigma}^{0} \mathbf{W}(\vartheta, t)\mathbf{x}(t+\vartheta)\mathrm{d}\vartheta\,, \qquad (5.15)$$

$$\mathbf{A}(t+T) = \mathbf{A}(t), \quad \mathbf{W}(\vartheta, t+T) = \mathbf{W}(\vartheta, t)\,,$$

where $\mathbf{W}(\vartheta, t)$ is now a weight distribution including such breaks like Dirac distribution, and the dependence on the present state of $\mathbf{x}(t)$ is determined by the matrix $\mathbf{A}(t)$. According to equation (2.41), the condition for $\mathbf{W}(\vartheta, t)$ reads

$$\int_{-\infty}^{0} \mathrm{e}^{-\nu\vartheta}\,|W_{jk}(\vartheta, t)|\,\mathrm{d}\vartheta < \infty, \quad j,k = 1, 2, \ldots, n, \quad \nu > 0, \quad t \in \mathbb{R}. \qquad (5.16)$$

Because of this condition, in approximations, the value of σ in equation (5.15) can be considered as any large, but still finite value.

5.2.1 Structure of semi-discretization

One of the main steps of semi-discretization is the construction of the time intervals $[t_i, t_{i+1})$ of length Δt, $i = 0, 1, \ldots$, so that the principal period can be expressed as $T = k\Delta t$, $k \in \mathbb{Z}$.

There are three steps of approximations of the distribution matrix $\mathbf{W}(\vartheta, t)$ in equation (5.15).

1. Consider equation (5.15) in the time intervals $t \in [t_i, t_{i+1})$, $i = 0, 1, \ldots$. The time dependent matrices $\mathbf{A}(t)$ and $\mathbf{W}(\vartheta, t)$ can be approximated with constant

matrices

$$\mathbf{A}_i = \frac{1}{\Delta t} \int_{t_i}^{t_{i+1}} \mathbf{A}(t)\mathrm{d}t\,, \tag{5.17}$$

$$\mathbf{W}_i(\vartheta) = \frac{1}{\Delta t} \int_{t_i}^{t_{i+1}} \mathbf{W}(\vartheta, t)\mathrm{d}t \tag{5.18}$$

for each discretization interval, that is $\mathbf{A}_i$ and $\mathbf{W}_i(\vartheta)$ are not time dependent any more. This step is equivalent to the piecewise autonomous approximation of non-autonomous systems.

2. The continuous distribution matrix $\mathbf{W}_i(\vartheta)$ can be approximated as a sum of shifted Dirac distributions

$$\tilde{\mathbf{W}}_i(\vartheta) = \sum_{j=1}^{m} f_\delta(\vartheta + (j - \tfrac{1}{2})\Delta t)\mathbf{W}_{i,j}\,, \tag{5.19}$$

where the weights of the terms are

$$\mathbf{W}_{i,j} = \int_{-j\Delta t}^{(1-j)\Delta t} \mathbf{W}_i(\vartheta)\mathrm{d}\vartheta\,, \tag{5.20}$$

and m can also be infinity, similarly to σ. This step leads to a kind of piecewise constant approximation of the delayed term.

3. Finally, $\tilde{\mathbf{W}}_i(\vartheta)$ can be approximated with a time dependent distribution for $t \in [t_i, t_{i+1})$

$$\tilde{\tilde{\mathbf{W}}}_i(\vartheta, t) = \tilde{\mathbf{W}}_i(\vartheta - \tfrac{1}{2}\Delta t + t) = \sum_{j=1}^{m} f_\delta(\vartheta + (j - 1)\Delta t + t)\mathbf{W}_{i,j}\,. \tag{5.21}$$

This is a generalization of the approximation of discrete time delays shown in Figure 5.1.

The geometrical visualization of the approximation process can be seen in Figure 5.4.

The application of these approximations in equation (5.15) results in a non-autonomous RFDE which seems to be more complicated than the original RFDE. However, the integral expression in equation (5.15) can be approximated by a summation as follows

$$\int_{-\sigma}^{0} \mathbf{W}(\vartheta, t)\mathbf{x}(t + \vartheta)\mathrm{d}\vartheta \approx \int_{-\sigma}^{0} \tilde{\tilde{\mathbf{W}}}(\vartheta, t)\mathbf{x}(t + \vartheta)\mathrm{d}\vartheta = \sum_{j=1}^{m} \mathbf{W}_{i,j}\mathbf{x}_{i-j+1}\,, \tag{5.22}$$

where

$$\mathbf{x}_{i-j+1} = \mathbf{x}(t_i - (j - 1)\Delta t), \quad i = 0, 1, \ldots, \quad j = 0, 1, \ldots, m\,. \tag{5.23}$$
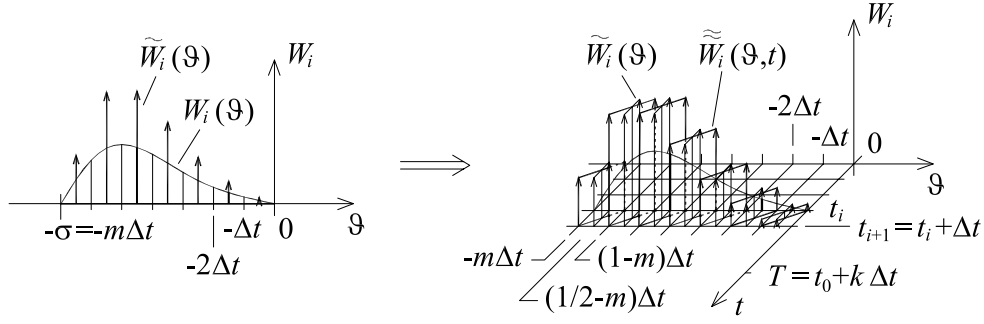
Figure 5.4: Approximation of the weight function

In spite of the fact, that the approximated system is a non-autonomous RFDE, it can be defined as a series of autonomous ODEs with constant excitations in each discretization interval

$$\dot{\mathbf{x}}(t) = \mathbf{A}_i \mathbf{x}(t) + \sum_{j=1}^{m} \mathbf{W}_{i,j} \mathbf{x}_{i-j+1}, \quad t \in [t_i, t_{i+1}), \quad i = 0, 1, \ldots. \tag{5.24}$$

In other words, equation (5.15) is approximated now with a series of piecewise autonomous ODEs.

Let us assume, that the matrix $\mathbf{A}_i$ is invertible for all i. Then, the solution of equation (5.24) assumes the form

$$\mathbf{x}(t) = \exp\left(\mathbf{A}_i(t - t_i)\right) \mathbf{K}_i - \sum_{j=1}^{m} \mathbf{A}_i^{-1} \mathbf{W}_{i,j} \mathbf{x}_{i-j+1}, \tag{5.25}$$

where the constant vector $\mathbf{K}_i$ depends on the initial value $\mathbf{x}(t_i) = \mathbf{x}_i$:

$$\mathbf{K}_i = \mathbf{x}_i + \sum_{j=1}^{m} \mathbf{A}_i^{-1} \mathbf{W}_{i,j} \mathbf{x}_{i+1-j}. \tag{5.26}$$

If the matrix $\mathbf{A}_i$ is not invertible, then the solution can still be expressed in a more complicated form, and the semi-discretization method can also be applied.

Substitution of equation (5.26) into equation (5.25) and $t = t_{i+1}$ yield

$$\mathbf{x}_{i+1} = \mathbf{M}_{i,0} \mathbf{x}_i + \sum_{j=1}^{m-1} \mathbf{M}_{i,j} \mathbf{x}_{i-j}, \tag{5.27}$$

where the coefficient matrices are

$$\mathbf{M}_{i,0} = \exp(\mathbf{A}_i \Delta t) + (\exp(\mathbf{A}_i \Delta t) - \mathbf{I}) \mathbf{A}_i^{-1} \mathbf{W}_{i,1}, \tag{5.28}$$

$$\mathbf{M}_{i,j} = (\exp(\mathbf{A}_i \Delta t) - \mathbf{I}) \mathbf{A}_i^{-1} \mathbf{W}_{i,j+1}. \tag{5.29}$$

Equation (5.27) gives the connection between the states of the system at time instants t_i and t_{i+1}. This connection can be presented as a discrete map

$$\mathbf{y}_{i+1} = \mathbf{B}_i \mathbf{y}_i, \tag{5.30}$$

where the mn dimensional state vector is

$$\mathbf{y}_i = \mathrm{col}(\mathbf{x}_i \ \ \mathbf{x}_{i-1} \ \ \dots \ \ \mathbf{x}_{i-m+1}) \,, \tag{5.31}$$

and the coefficient matrix is a hypermatrix of the form

$$\mathbf{B}_i = \begin{pmatrix} \mathbf{M}_{i,0} & \mathbf{M}_{i,1} & \mathbf{M}_{i,2} & \dots & \mathbf{M}_{i,m-2} & \mathbf{M}_{i,m-1} \\ \mathbf{I} & \mathbf{0} & \mathbf{0} & \dots & \mathbf{0} & \mathbf{0} \\ \mathbf{0} & \mathbf{I} & \mathbf{0} & \dots & \mathbf{0} & \mathbf{0} \\ \vdots & \vdots & \vdots & \ddots & \vdots & \vdots \\ \mathbf{0} & \mathbf{0} & \mathbf{0} & \dots & \mathbf{0} & \mathbf{0} \\ \mathbf{0} & \mathbf{0} & \mathbf{0} & \dots & \mathbf{I} & \mathbf{0} \end{pmatrix} \,. \tag{5.32}$$

The next step is to determine the transition matrix $\mathbf{\Phi}$ over the principal period $T = k\Delta t$. This serves a finite dimensional approximation of the monodromy operator in the infinite dimensional version of the Floquet Theory. The transition matrix gives the connection between $\mathbf{y}_0$ and $\mathbf{y}_k$ in the form

$$\mathbf{y}_k = \mathbf{\Phi}\mathbf{y}_0 \,, \tag{5.33}$$

where $\mathbf{\Phi}$ is given by coupling the solutions

$$\mathbf{\Phi} = \mathbf{B}_{k-1}\mathbf{B}_{k-2}\dots\mathbf{B}_1\mathbf{B}_0 \,. \tag{5.34}$$

This transition matrix is a finite dimensional approximation of the monodromy operator $\mathbf{U}(T)$ of system (5.15). Here, the notation $\mathbf{\Phi}$ is used instead of $\mathbf{\Phi}(T)$ in order to emphasize that it is a transition matrix for the discrete system (5.30), and not for a continuous one.

Now, the stability investigation of equation (5.24) is reduced to the problem, whether the eigenvalues of $\mathbf{\Phi}$ are in modulus less than 1 (see Lakshmikantham and Trigiante, 1988). Any standard or advanced numerical algorithm can be used for this last step.

5.2.2   Convergence of semi-discretization

The convergence of the method can be seen by refining the interval division, e.g. by decreasing Δt and increasing m. The approximation defined by equation (5.22) satisfies

$$\lim_{\Delta t \to 0} \int_{-\sigma}^{0} \tilde{\tilde{\mathbf{W}}}(\vartheta, t)\mathbf{x}(t+\vartheta)\mathrm{d}\vartheta = \lim_{\Delta t \to 0} \sum_{j=1}^{m} \mathbf{W}_{i,j}\mathbf{x}_{i-j+1} = \int_{-\sigma}^{0} \mathbf{W}(\vartheta, t)\mathbf{x}(t+\vartheta)\mathrm{d}\vartheta \,, \tag{5.35}$$

since it is a rectangular sum approximation of integral expressions according to the classical definition of the Riemann integral.
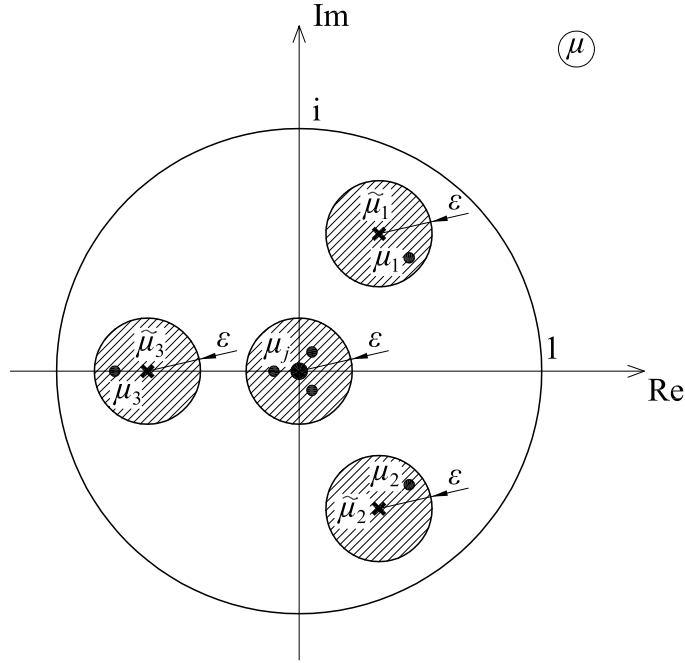
Figure 5.5: Eigenvalue localization

Let us denote the characteristic multipliers of the original equation (5.15) by μ_j, $j = 1, 2, \ldots$, and the characteristic multipliers of the approximating equation (5.33) by $\tilde{\mu}_j$, $j = 1, 2, \ldots, mn$.

For any small $\varepsilon > 0$, there exists an integer $M(\varepsilon)$, so that for every $m > M(\varepsilon)$, the set $\bigcup\limits_{j=1}^{mn} S_{\tilde{\mu}_j, \varepsilon}$ contains exactly mn number of characteristic multipliers μ_j of equation (5.11), and all the other characteristic multipliers of equation (5.11) are in modulus less than ε.

Thus, if all the characteristic multipliers of equation (5.33) are in modulus less than 1, then choosing $\varepsilon = \frac{1}{2}\left(1 - \max_j |\tilde{\mu}_j|\right)$, the finite approximation number $M(\varepsilon)$ exists, and if $m > M(\varepsilon)$ fulfils, then the discretized and the original system has the same stability properties (see Figure 5.5 with $nm = 3$). A rigorous proof of the above statement can be constructed with the methods presented by Farkas and Stépán (1992) which use the continuous dependence of the eigenvalues on the system parameters.

Clearly, the semi-discretization does not preserve the solutions of the original system. It preserves, however, their exponential stability if the semi-discretization is fine enough in the sense presented above.

5.3   Example: the damped delayed Mathieu equation

One dimensional, higher order systems can be investigated by transforming the system into the form of equation (5.15) according to the Cauchy transformation, and then using the semi-discretization method. In some special cases of higher order systems, the direct semi-discretization leads to a lower dimensional approximation than the semi-discretization of the Cauchy-transformed systems. This is the case, for example, when the damped delayed Mathieu equation

$$\ddot{x}(t) + b_0 \dot{x}(t) + c_0(t)x(t) = c_1 x(t - \tau)\,, \quad c_0(t) = c_{0\,\delta} + c_{0\,\varepsilon} \cos(2\pi t/T)\,. \qquad (5.36)$$

is investigated.

Let the time interval division be defined as in Section 5.2.1. In the interval $t \in [t_i, t_{i+1})$ of length Δt, $i = 0, 1, \ldots$, equation (5.36) can be approximated as

$$\ddot{x}(t) + b_0 \dot{x}(t) + c_{0\,i}x(t) = c_1 x_{i-m}\,, \qquad (5.37)$$

where

$$c_{0\,i} = \frac{1}{\Delta t} \int_{t_i}^{t_{i+1}} c_0(t)\mathrm{d}t \approx c_0(t_i + \Delta t/2)\,, \qquad (5.38)$$

and $\tau = (m + 1/2)\Delta t$ as it was shown in Section 5.1.1.

For the initial conditions $x(t_i) = x_i$, $\dot{x}(t_i) = \dot{x}_i$, the solution and its derivative at each time instant t_{i+1} can be determined:

$$x_{i+1} = x(t_{i+1}) = a_{0\,0}x_i + a_{0\,1}\dot{x}_i + b_{0\,m}x_{i-m}\,, \qquad (5.39)$$

$$\dot{x}_{i+1} = \dot{x}(t_{i+1}) = a_{1\,0}x_i + a_{1\,1}\dot{x}_i + b_{1\,m}x_{i-m}\,, \qquad (5.40)$$

where

$$a_{0\,0} = \kappa_{1\,0} \exp(\lambda_1 \Delta t) + \kappa_{2\,0} \exp(\lambda_2 \Delta t)\,,$$

$$a_{0\,1} = \kappa_{1\,1} \exp(\lambda_1 \Delta t) + \kappa_{2\,1} \exp(\lambda_2 \Delta t)\,,$$

$$a_{1\,0} = \kappa_{1\,0}\lambda_1 \exp(\lambda_1 \Delta t) + \kappa_{2\,0}\lambda_2 \exp(\lambda_2 \Delta t)\,,$$

$$a_{1\,1} = \kappa_{1\,1}\lambda_1 \exp(\lambda_1 \Delta t) + \kappa_{2\,1}\lambda_2 \exp(\lambda_2 \Delta t)\,,$$

$$b_{0\,m} = \sigma_1 \exp(\lambda_1 \Delta t) + \sigma_2 \exp(\lambda_2 \Delta t) + c_1/c_{0\,i}\,,$$

$$b_{1\,m} = \sigma_1\lambda_1 \exp(\lambda_1 \Delta t) + \sigma_2\lambda_2 \exp(\lambda_2 \Delta t)\,,$$

and

$$\lambda_{1,2} = \frac{-b_0 \pm \sqrt{b_0^2 - 4c_{0\,i}}}{2}\,,$$

$$\kappa_{1\,0} = \frac{\lambda_2}{\lambda_2 - \lambda_1}\,, \qquad \kappa_{1\,1} = \frac{-1}{\lambda_2 - \lambda_1}\,, \qquad \sigma_1 = \frac{-\lambda_2}{\lambda_2 - \lambda_1}\frac{c_1}{c_{0\,i}}\,,$$

$$\kappa_{2\,0} = \frac{-\lambda_1}{\lambda_2 - \lambda_1}\,, \qquad \kappa_{2\,1} = \frac{1}{\lambda_2 - \lambda_1}\,, \qquad \sigma_2 = \frac{\lambda_1}{\lambda_2 - \lambda_1}\frac{c_1}{c_{0\,i}}\,.$$

Equations (5.39) and (5.40) define the discrete map

$$\mathbf{y}_{i+1} = \mathbf{B}_i \mathbf{y}_i \,, \tag{5.41}$$

where the $m + 2$ dimensional state vector is

$$\mathbf{y}_i = \text{col}(\dot{x}_i \ \ x_i \ \ x_{i-1} \ \ \ldots \ \ x_{i-m}) \,, \tag{5.42}$$

and the coefficient matrix has the form

$$\mathbf{B}_i = \begin{pmatrix} a_{1\,1} & a_{1\,0} & 0 & \ldots & 0 & b_{1\,m} \\ a_{0\,1} & a_{0\,0} & 0 & \ldots & 0 & b_{0\,m} \\ 0 & 1 & 0 & \ldots & 0 & 0 \\ \vdots & \vdots & \vdots & \ddots & \vdots & \vdots \\ 0 & 0 & 0 & \ldots & 0 & 0 \\ 0 & 0 & 0 & \ldots & 1 & 0 \end{pmatrix} \,. \tag{5.43}$$

Consider the case $\tau = T$. For this case, there are no integers k, m that satisfies both equations $\tau = (m + 1/2)\Delta t$ and $T = k\Delta t$. This problem can be handled by increasing the approximation parameter m, but this may result high computation time. A more efficient solution is that we consider the double principal period $2T = 2k\Delta t$. With $2k = 2m + 1$, both $2k$ and $2m + 1$ are integers. Now, the transition matrix over the double principal period, that is, the square of the transition matrix over the principal period, can be determined as

$$\mathbf{\Phi}^2 = \mathbf{B}_{2k-1}\mathbf{B}_{2k-2}\ldots\mathbf{B}_0 \,. \tag{5.44}$$

The eigenvalues of $\mathbf{\Phi}^2$ are the square of the eigenvalues of $\mathbf{\Phi}$. Since $|\mu| < 1$ if and only if $|\mu^2| < 1$, the stability can be determined according the eigenvalues of $\mathbf{\Phi}^2$, too.

Stability analysis of equation (5.36) is done by using the semi-discretization method with approximation parameter $m = 20$. The stability charts for equation (5.36) with time delay $\tau = 2\pi$ and principal period $T = 2\pi$, $T = \pi$ and $T = 4\pi$ can be seen in Figures 5.6, 5.7 and 5.8, respectively. These charts can be compared with the charts shown in Figures 4.4, 4.5 and 4.6.

With the semi-discretization method, the approximation errors are less than 1% in the presented parameter domain ($-1 < c_{0\,\delta} < 5$ and $-2 < c_1 < 2$). Also, the linear boundary curves of the damped delayed Mathieu equation (see Chapter 3) show up without error. These stability charts were determined by a 22×22 sized discrete map model opposite to the 103×103 sized Fargue-type approximation. This shows, that the semi-discretization method is more effective than the Fargue-type approximation.

Similarly to the charts given by the Fargue-type approximation, the cases $T = \pi$ and $T = 2\pi$ show linear stability boundaries, while the case $T = 4\pi$ gives the intriguing stability charts with disjunct stable domains.
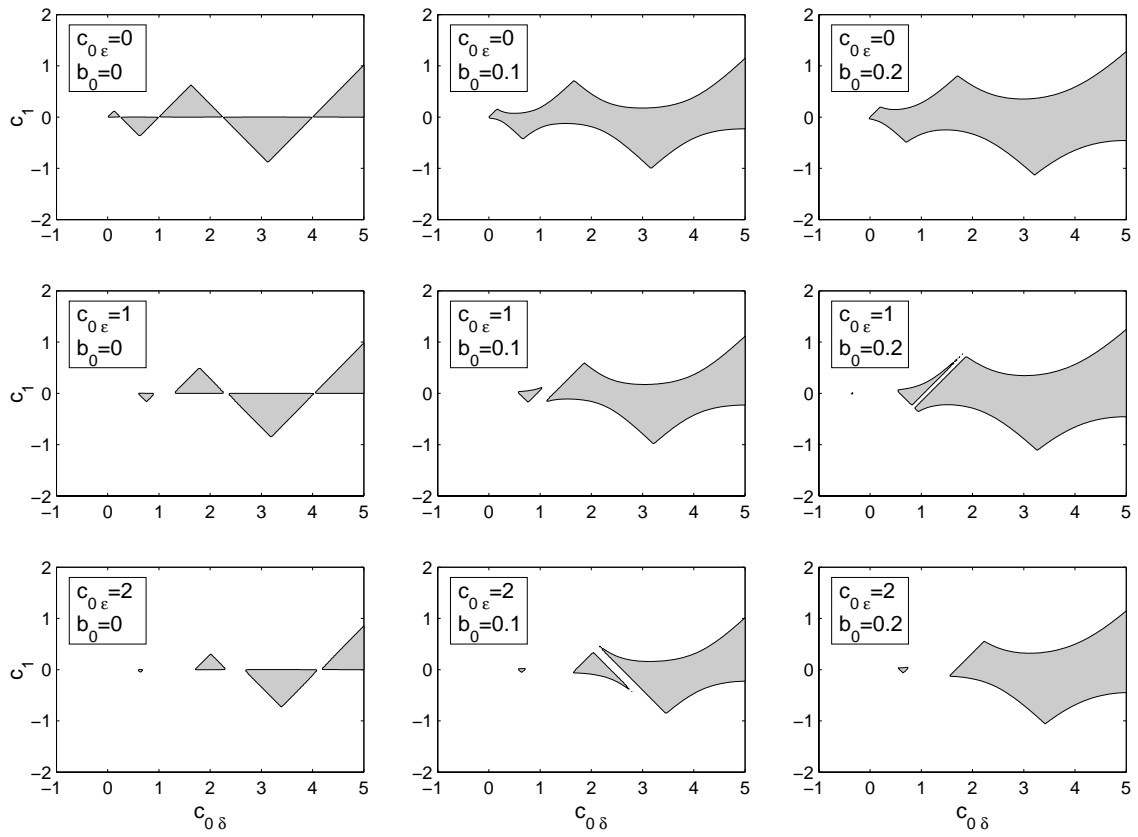
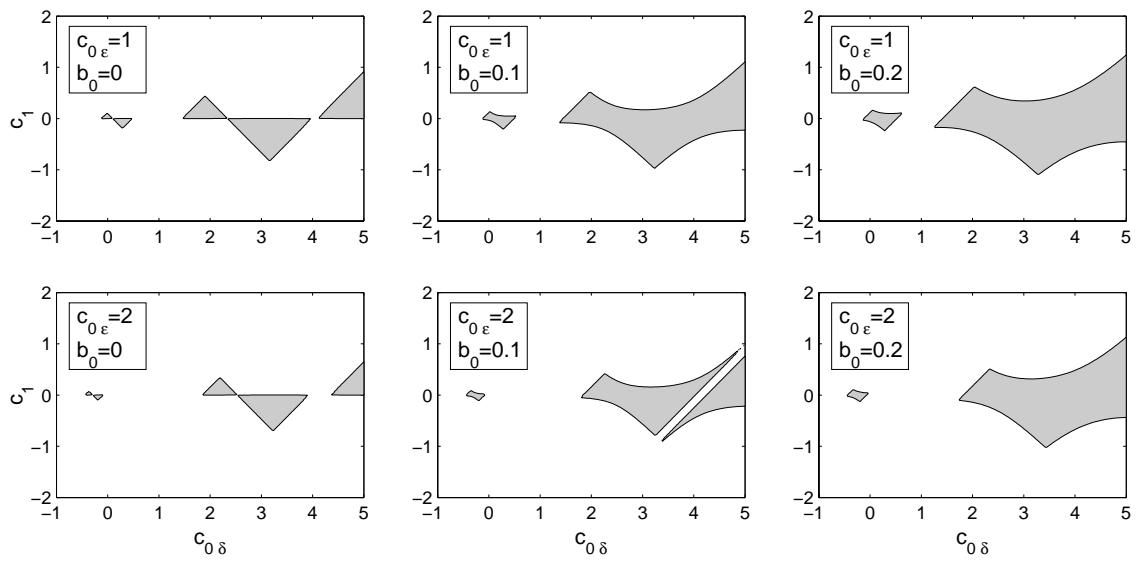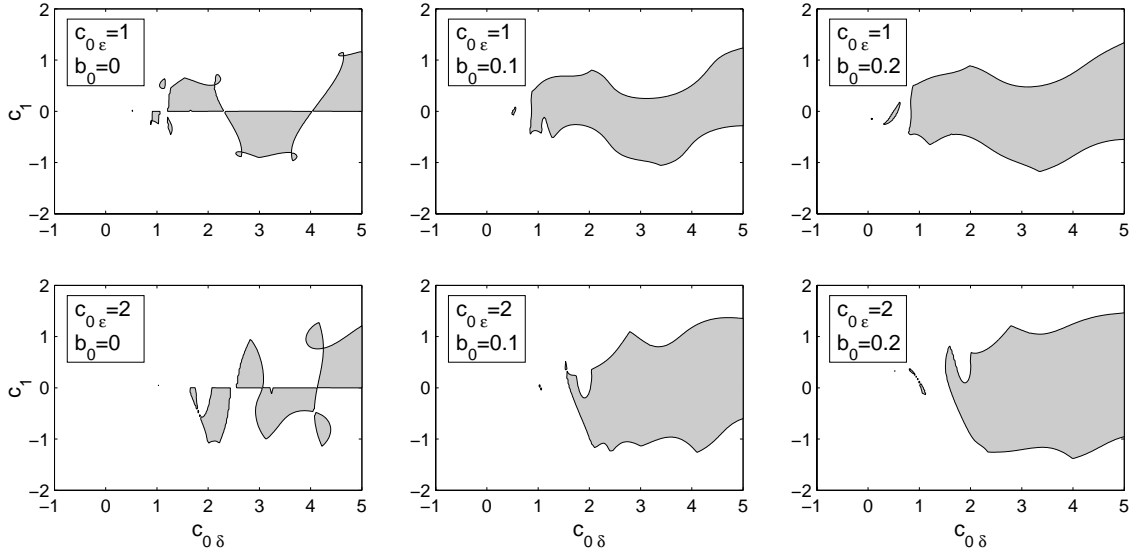Figure 5.6: Stability charts for equation (5.36) with $\tau = 2\pi$ and $T = 2\pi$

Figure 5.7: Stability charts for equation (5.36) with $\tau = 2\pi$ and $T = \pi$

Figure 5.8: Stability charts for equation (5.36) with $\tau = 2\pi$ and $T = 4\pi$

5.4   Example: the delayed oscillator with distributed time delay

Consider now the damped Mathieu equation with distributed time delay of maximum length 1

$$\ddot{x}(t) + b_0 \dot{x}(t) + c_0(t)x(t) = c_1 \int_{-1}^{0} w(\vartheta)x(t+\vartheta)\mathrm{d}\vartheta, \quad c_0(t) = c_{0\,\delta} + c_{0\,\varepsilon}\cos(2\pi t/T). \quad (5.45)$$

Such equations can still arise in machine tool vibration models (see Stépán, 1998).

Define the time interval division as in Section 5.2.1. In the interval $t \in [t_i, t_{i+1})$ of length Δt, $i = 0, 1, \ldots$, equation (5.45) can be approximated as

$$\ddot{x}(t) + b_0 \dot{x}(t) + c_{0\,i}x(t) = c_1 \sum_{j=1}^{m} w_j x_{i-j+1}, \quad (5.46)$$

where

$$c_{0\,i} = \frac{1}{\Delta t}\int_{t_i}^{t_{i+1}} c_0(t)\mathrm{d}t \approx c_0(t_i + \Delta t/2), \quad (5.47)$$

$$w_j = \int_{-j\Delta t}^{(1-j)\Delta t} w(\vartheta)\mathrm{d}\vartheta \approx \Delta t\, w((1/2 - j)\Delta t). \quad (5.48)$$

The initial conditions $x(t_i) = x_i$, $\dot{x}(t_i) = \dot{x}_i$ defines the solution and its derivative at time t_{i+1} in the form

$$x_{i+1} = x(t_{i+1}) = a_{0\,0}x_i + a_{0\,1}\dot{x}_i + \sum_{h=1}^{m-1} b_{0\,h}x_{i-h}, \quad (5.49)$$

$$\dot{x}_{i+1} = \dot{x}(t_{i+1}) = a_{1\,0}x_i + a_{1\,1}\dot{x}_i + \sum_{h=1}^{m-1} b_{1\,h}x_{i-h}, \quad (5.50)$$

where

$$a_{0\,0} = \kappa_{1\,0}\exp(\lambda_1\Delta t) + \kappa_{2\,0}\exp(\lambda_2\Delta t) + c_1 w_1/c_{0\,i}\,,$$

$$a_{0\,1} = \kappa_{1\,1}\exp(\lambda_1\Delta t) + \kappa_{2\,1}\exp(\lambda_2\Delta t)\,,$$

$$a_{1\,0} = \kappa_{1\,0}\lambda_1\exp(\lambda_1\Delta t) + \kappa_{2\,0}\lambda_2\exp(\lambda_2\Delta t)\,,$$

$$a_{1\,1} = \kappa_{1\,1}\lambda_1\exp(\lambda_1\Delta t) + \kappa_{2\,1}\lambda_2\exp(\lambda_2\Delta t)\,,$$

$$b_{0\,h} = \sigma_{1\,h}\exp(\lambda_1\Delta t) + \sigma_{2\,h}\exp(\lambda_2\Delta t) + c_1 w_{h+1}/c_{0\,i}\,, \qquad h = 1, 2, \ldots, m-1\,,$$

$$b_{1\,h} = \sigma_{1\,h}\lambda_1\exp(\lambda_1\Delta t) + \sigma_{2\,h}\lambda_2\exp(\lambda_2\Delta t)\,, \qquad h = 1, 2, \ldots, m-1\,,$$

and

$$\lambda_{1,2} = \frac{-b_0 \pm \sqrt{b_0^2 - 4c_{0\,i}}}{2}\,,$$

$$\kappa_{1\,0} = \frac{\lambda_2(1 - c_1 w_1/c_{0\,i})}{\lambda_2 - \lambda_1}\,, \qquad \kappa_{1\,1} = \frac{-1}{\lambda_2 - \lambda_1}\,, \qquad \sigma_{1\,j} = \frac{-\lambda_2 c_1 w_{j+1}/c_{0\,i}}{\lambda_2 - \lambda_1}\,,$$

$$\kappa_{2\,0} = \frac{-\lambda_1(1 - c_1 w_1/c_{0\,i})}{\lambda_2 - \lambda_1}\,, \qquad \kappa_{2\,1} = \frac{1}{\lambda_2 - \lambda_1}\,, \qquad \sigma_{2\,j} = \frac{\lambda_1 c_1 w_{j+1}/c_{0\,i}}{\lambda_2 - \lambda_1}\,.$$

Equations (5.49) and (5.50) define the discrete map

$$\mathbf{y}_{i+1} = \mathbf{B}_i \mathbf{y}_i\,, \tag{5.51}$$

where the $m + 1$ dimensional state vector is

$$\mathbf{y}_i = \mathrm{col}(\dot{x}_i \ \ x_i \ \ x_{i-1} \ \ \ldots \ \ x_{i-m+1})\,, \tag{5.52}$$

and the coefficient matrix has the form

$$\mathbf{B}_i = \begin{pmatrix} a_{1\,1} & a_{1\,0} & b_{1\,1} & b_{1\,2} & \ldots & b_{1\,m-2} & b_{1\,m-1} \\ a_{0\,1} & a_{0\,0} & b_{0\,1} & b_{0\,2} & \ldots & b_{0\,m-2} & b_{0\,m-1} \\ 0 & 1 & 0 & 0 & \ldots & 0 & 0 \\ 0 & 0 & 1 & 0 & \ldots & 0 & 0 \\ \vdots & \vdots & \vdots & \vdots & \ddots & \vdots & \vdots \\ 0 & 0 & 0 & 0 & \ldots & 0 & 0 \\ 0 & 0 & 0 & 0 & \ldots & 1 & 0 \end{pmatrix}\,. \tag{5.53}$$

Now, the transition matrix can be given according to equation (5.34), and the stability can be determined by simple eigenvalue analysis.

Three types of weight functions are considered, all of them are taken from the book of Stépán (1989). The stability charts are shown in Figures 5.9, 5.10 and 5.11 for principal period $T = 1/2$ and coefficients $b_0 = 0$, $c_{0\,\varepsilon} = 0, 20, 40, 60$. The charts for the autonomous case, when $c_{0\,\varepsilon} = 0$, were constructed in closed form in the book of Stépán (1989). These cases can be used for checking the accuracy of the method. The
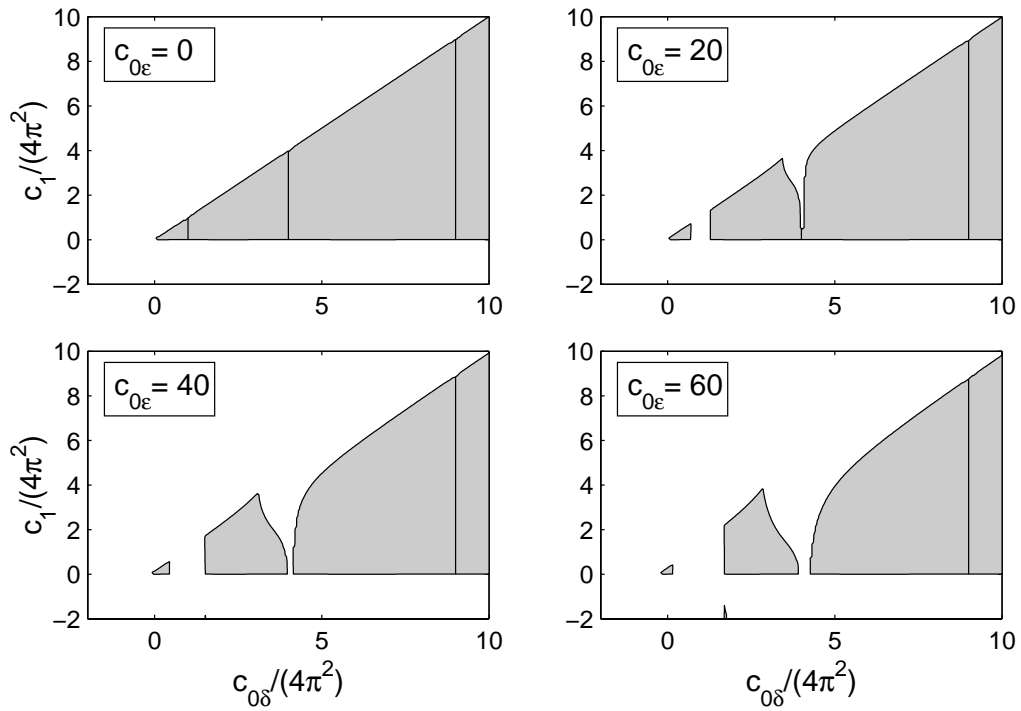
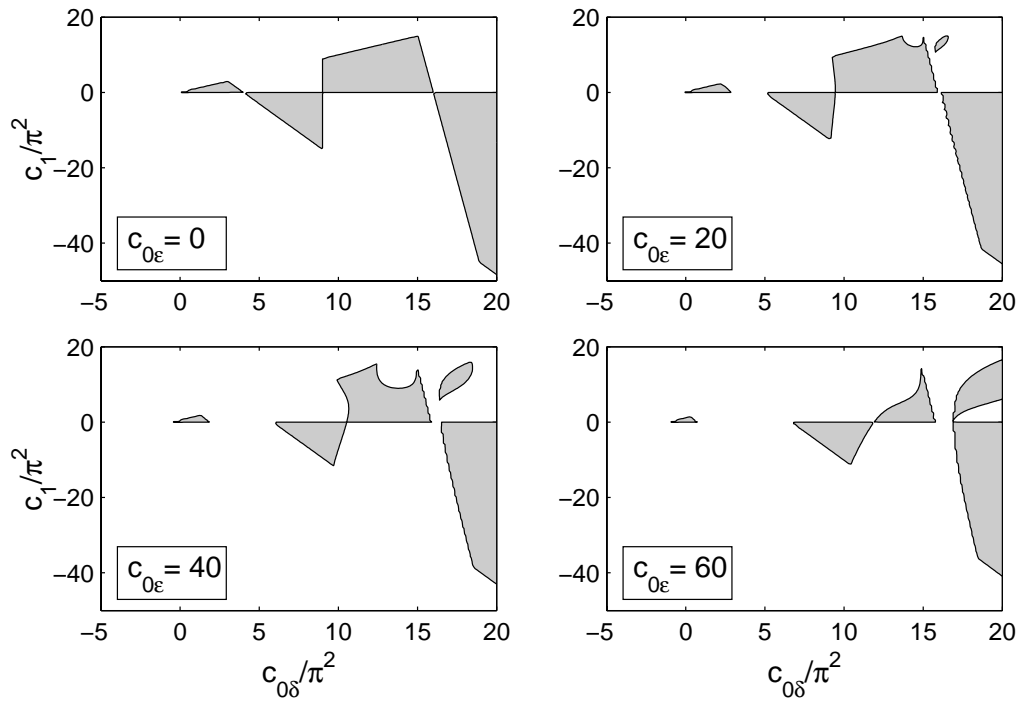Figure 5.9: Stability charts for equation (5.45) with $w(\vartheta) \equiv 1$, $b_0 = 0$ and $T = 1/2$

Figure 5.10: Stability charts for equation (5.45) with $w(\vartheta) = -\dfrac{\pi}{2}\sin(\pi\vartheta)$, $b_0 = 0$ and $T = 1/2$
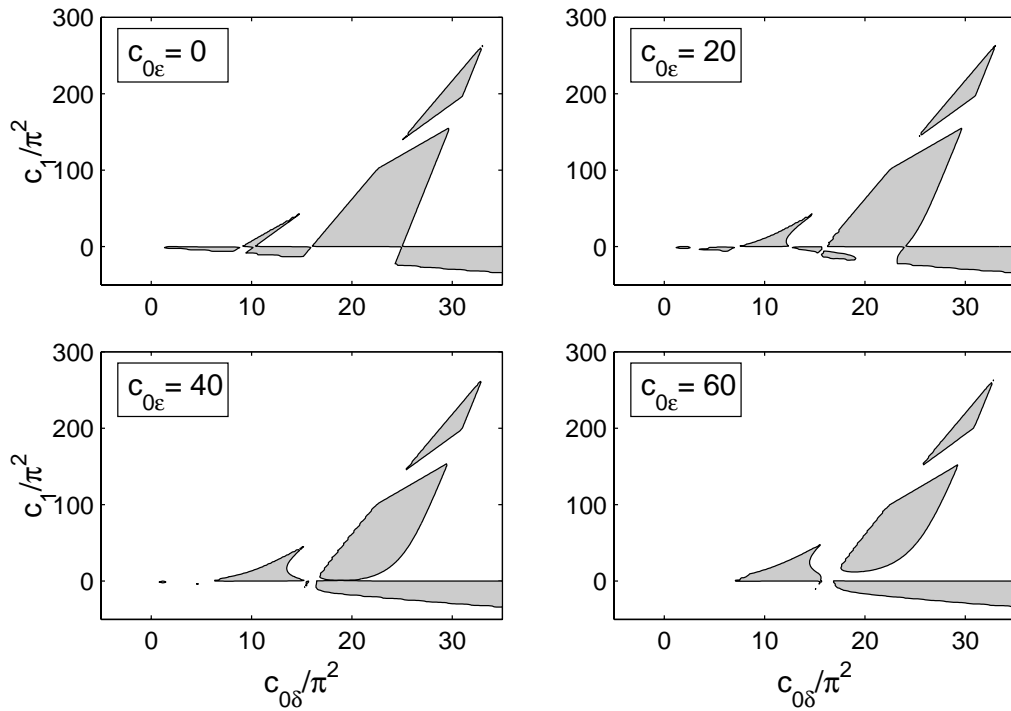
Figure 5.11: Stability charts for equation (5.45) with $w(\vartheta) = \dfrac{\pi}{2}\sin(\pi\vartheta) + \dfrac{13}{77}\,\pi\sin(2\pi\vartheta)$, $b_0 = 0$ and $T = 1/2$

approximation number $m = 20$, that is a 21 dimensional discrete map approximation of the infinite dimensional equation (5.45) results stability boundaries with errors less than 1% in the parameter domain considered here.

As an even more complex problem, study the equation

$$\ddot{x}(t) + (6 + c_{0\,\varepsilon}\cos(2\pi t/T))x(t) = x(t - \tau_1) + x(t - \tau_2)\,. \qquad (5.54)$$

This is a special case of equation (5.45) with $b_0 = 0$, $c_{0\,\delta} = 6$, $c_1 = 1$ and $w(\vartheta) = f_\delta(\vartheta + \tau_1) + f_\delta(\vartheta + \tau_2)$, where f_δ is the Dirac distribution. Although the two discrete time delays seem to be an extreme case, these types of systems arise in several practical application, like in the modeling of grinding processes (Thopmson, 1986a, 1986b), or in the modeling of turning operation with a tool head of two multiple-tool rows (Gouskov et al., 2001).

The analysis of the case $c_{0\,\varepsilon} = 0$ can also be found in Stépán's book (1989). For this autonomous two-delay system, the stability chart in the plane of the two delay parameters τ_1 and τ_2 can be seen in Figure 5.12.

For the cases $c_{0\,\varepsilon} = 6$ and $T = 1, 2, 5, 10$, the stability charts in the plane (τ_1, τ_2) can be seen in Figure 5.13.
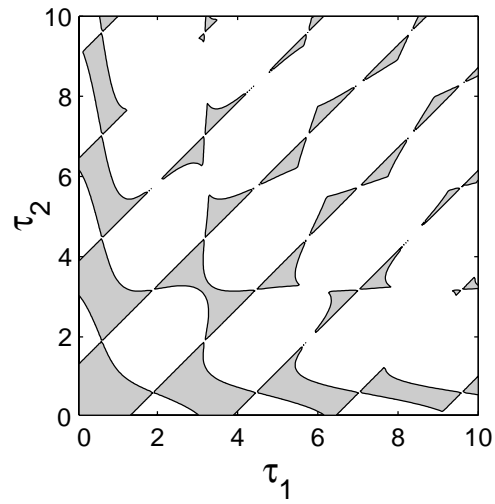
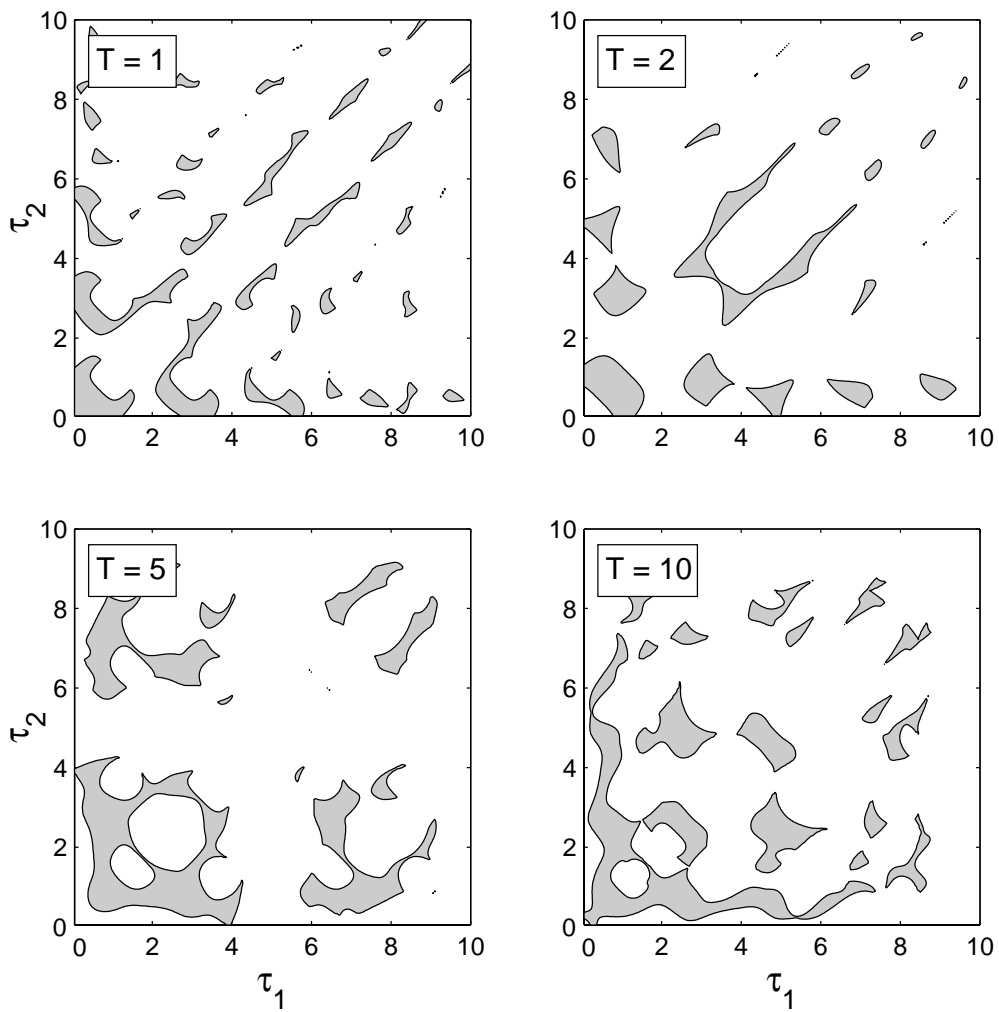Figure 5.12: Stability chart for equation (5.54) with $c_{0\,\varepsilon} = 0$

Figure 5.13: Stability charts for equation (5.54) with $c_{0\,\varepsilon} = 6$

5.5 New results

Thesis 3 *An efficient new method was introduced for the stability investigation of general linear periodic delay-differential equations of the form*

$$\dot{\mathbf{x}}(t) = \int_{-\sigma}^{0} \mathrm{d}_{\vartheta} \boldsymbol{\eta}(\vartheta, t) \mathbf{x}(t + \vartheta), \quad \boldsymbol{\eta}(\vartheta, t + T) = \boldsymbol{\eta}(\vartheta, t).$$

The efficiency of this so-called semi-discretization method was compared to that of full discretization in the time domain. The main steps of the method were listed, an algorithm was presented and also a proof for the convergence was given. The method was applied for the delayed Mathieu equation with various distributed and discrete delays. A range of intriguing stability charts were plotted for parametrically excited delayed oscillators. It was shown by examples, that the semi-discretization method is also more effective than the Fargue-type approximation.

Chapter 6

Chatter analysis in milling processes

In this chapter, the stability of the milling process and the relating time periodic delay-differential equation is investigated by the semi-discretization method introduced in Chapter 5.

6.1 Literature review on machine tool dynamics

The history of machine tool chatter goes back to almost 100 years in the past, when Taylor (1907) described machine tool chatter as the "most obscure and delicate of all problems facing the machinist". After the extensive work of Tlusty *et al.* (1962), Tobias (1965) and Kudinov (1955, 1967), the so-called regenerative effect has become the most commonly accepted explanation for machine tool chatter (see, e.g., Moon, 1998, Tlusty, 2000). This effect is related to the cutting force variation due to the wavy workpiece surface cut one revolution ago. The corresponding mathematical models are delay-differential equations (DDEs). Stability properties can be predicted through the investigation of these DDEs (see Stépán, 1989, 1998).

For several decades, machine tool chatter research has had only very limited influence on manufacturing industry, it often had an academic nature. Vibration monitoring systems or adaptive control on machine tools were predicted to have much more industrial success. This was partly caused by the complexity of the models involved in the description of chatter, partly by the unreliable parameter identification of the machine tool structure and the cutting force itself. The improved experimental modal testing, the more sophisticated mechanical models, the latest mathematical results in nonlinear dynamics, and the use of computer algebra have made the latest research efforts more accessible for industrial applications during the last decade. This is true for industrial applications from the conventional turning (see Kondo *et al.*, 1992), to the advanced high-speed milling (see Halley *et al.*, 1999, Esterling *et al.*, 2002).

The identification of the arising vibrations can effectively be supported by frequency analysis of the chatter signal (Gradišek *et al.*, 1998a, 1998b, Schmitz *et al.*, 2001, Sitz *et al.*, 2001). The stability charts published in the specialist literature are almost always accompanied by frequency diagrams that represent the chatter frequencies at the loss of stability. The reason of this custom is that these frequencies can precisely be identified experimentally and so this is a direct way to verify theoretical models and predictions.

6.1.1   Turning

For the simplest model of turning, the governing equation of motion is an autonomous DDE with a corresponding infinite dimensional state space. This fact results infinite number of characteristic roots, most of them having negative real parts referring to damped components of the vibration signals. There may be some finite number of characteristic roots that have positive real parts. Each of those roots which are just pure imaginary correspond to a single well defined vibration frequency. For turning, these critical chatter frequencies are usually about 0–15% above the first natural frequency of the tool (see Stépán, 1989) .

The theory of nonlinear regenerative cutting processes was developed by Hanna and Tobias (1974). The study of nonlinear phenomena in the cutting process showed that the chatter frequencies are related to unstable periodic motions about the stable stationary cutting, i.e. a so-called subcritical Hopf bifurcation occurs, as it was proved experimentally by Shi and Tobias (1984) and later analytically by Stépán and Kalmár-Nagy (1997). As a consequence, the vibrations usually increase till the tool starts leaving the material of the workpiece. In these cases, the system has sudden switches between the infinite dimensional dynamics of regenerative cutting and the finite dimensional one of a damped oscillator as the tool enters and leaves the workpiece (see Stépán, 2001b). These vibrations lead to a different kind of system often called as interrupted cutting. The resulting vibrations can be calculated by simulation (see Kalmár-Nagy *et al.*, 1999) but there also exist analytical methods to estimate their amplitude as shown by Metallidis and Natsiavas (2000). Based on different nonlinear models, other types of bifurcation were analyzed by Nayfeh *et al.* (1997) and by Fofana and Bukkapatnam (2001). The main sources of nonlinearities in the cutting process are also summarized by Wiercigroch and Budak (2001).

Prevention of chatter is a primary problem for the machinist. The idea that parametric excitation effects may suppress vibrations during the cutting process comes from the famous problem of stabilizing inverted pendulums by parametric excitation (see, for example, Insperger and Horváth, 2000). The governing equation of motion of the turning process with parametric excitation is a time periodic DDE (see Section 2.4).

In the seventies, it was in the focus of researchers' work, that continuous variation of the spindle speed can be used for suppressing chatter (see Inamura and Sata, 1974, Takemura *et al.*, 1974, Hosho *et al.*, 1977, Sexton *et al.*, 1977, Sexton and Stone, 1978). The corresponding mathematical model is a DDE with time varying delay. Inamura and Sata, (1974) and Sexton *et al.* (1977) approximated the quasi-periodic solutions of the time periodic DDE by periodic ones and applied the harmonic balance method to derive stability boundaries. They predicted improvements in stability properties by a factor of 10 for properly chosen parameter values. In spite of some reports on successful experiments, the stability investigations of cutting with time varying spindle speeds were not reliable enough to present a breakthrough in this field.

With their novel approach, Jayaram *et al.* (2000) created stability charts for turning with varying spindle speed. They used quasi-periodic trial solutions for the periodic DDE, and combined the Fourier expansion with an expansion with respect to Bessel function series, and determined stability boundaries by harmonic balance method.

As it is shown in Chapter 7, the semi-discretization method introduced in Chapter 5 can also be used to predict stability charts for operations with varying spindle speed (see Insperger *et al.*, 2001).

Another method for chatter suppression has been recently suggested by Seagalmann and Butcher (2000). They investigated the turning process where the system stiffness was varied periodically. The frequency of the modulation was half of the spindle frequency. They investigated the resulted periodic DDE by the harmonic balance method, and found some improvements in the stability properties.

A tool head with two multiple-tool rows was considered by Gouskov *et al.* (2001) as another possible way of chatter suppression. They analyzed the mathematical model with two delays with respect to the possible cutting discontinuities and showed the influence of technological parameters on the stability.

6.1.2   Milling

The modeling of the milling process is more difficult than that of the turning process, since the tooth pass excitation effect results a parametric excitation in the system. Accordingly, the governing equation of motion is a time periodic DDE. These systems can be investigated by the extended Floquet Theory of DDEs (see Section 2.4). Most of the infinite number of characteristic multipliers are located within the open unit disc of the complex plane referring to damped oscillation components, and only a finite number of multipliers can have a magnitude greater than 1. The critical multipliers are located on the unit circle and each of them refers to an infinite series of vibration frequencies (see Insperger *et al.*, 2002).

However, the resultant cutting force varies with the number of active teeth. If this number is great, this may show only a small periodic component. For these cases, the conventional time-averaging was used in the classical literature (see Tobias, 1965) and so the stability results were similar to those of turning. From mathematical viewpoint, this averaging can hardly be justified since significant errors (even qualitative ones) can occur due to the time-dependent parameters in the model.

For smaller tooth number, the tooth pass excitation effect becomes more and more dominant, and the time-averaging methods cannot be used even as approximations. For a single tooth miller, the process may look like an interrupted cutting. The milling of thin-walled structures is a limit case, since the ratio of time spent cutting to not cutting becomes infinitesimal. Here, the moment of cutting can be considered as an impact, and the process can be modeled by a discrete system (see Davies and Balachandran, 2000). For analytical investigation of highly interrupted cutting, Davies *et al.* (2001) developed a special discrete map model as opposed to the conventional DDE approach. Interrupted cutting can also be a desired way of machining as shown by Batzer *et al.* (1999) for vibratory drilling.

The modeling of the milling process is somewhere between the two extreme models: the autonomous DDE for turning and the discrete map model of highly interrupted cutting. For a precise mathematical analysis, the parametric excitation effect cannot be neglected in the modeling.

As mentioned in Section 2.4, no closed form stability criteria can be given for periodic DDEs. However, there exist several approximation methods. The harmonic balance method was used by Minis and Yanushevsky (1993). They used the first harmonics of the time-periodic parameters and showed slight deviations in the stability of milling relative to the results with the time-averaging method. Altintas and Budak (1995) used 3rd order harmonic balance in the milling problem. They also generalized their method (Budak and Altintas, 1998a, 1998b), and applied for different operations like helical end milling (Altintas and Lee, 1996), ball end milling (Altintas and Lee, 1998, Altintas *et al.*, 1999b) and variable pitch cutters (Altintas *et al.*, 1999a). The harmonic balance method with some new numerical techniques was used by Corpus and Endres (2000) and by Tian and Hutton (2001).

The Fargue-type approximation introduced in Chapter 4 was used by Insperger and Stépán (2000b). With this method, they constructed stability charts for the high-speed parameter domain. The application of semi-discretization method introduced in Chapter 5 results reliable stability charts even for low spindle speeds (see Insperger *et al.*, 2001, Insperger and Stépán, 2001c).

The finite element analysis (FEA) in time was developed by Bayly *et al.*, (2001a). This is a kind of generalization of the discrete map model of highly interrupted cut-

ting, but this method can also be used for general milling processes (see Bayly *et al.*, 2002). The point of the FEA method in time is that the solution of the periodic DDE is assumed as a combination of some trial functions, and after substitution into the governing equation, the weighted residual method is applied. The resulted system is a finite dimensional discrete map, for that the stability investigation can be done with appropriate numerical methods.

Sophisticated milling models can be built up via the extended analysis of the cutting process. These result complex mathematical models, that are generally analyzed by numerical simulation (see, e.g. Smith and Tlusty, 1991, 1993, Balachandran and Zhao, 2000, Balachandran, 2001, Zhao and Balachandran, 2001).

In the past decade, essential developments have been done in the field of manufacturing that resulted the rapid commercialization of reliable high-speed machining systems (see, e.g., Davies *et al.*, 1999). The main components that have enabled this development include: spindles capable of speeds exceeding 40,000 rpm while delivering 30 kW of power to the cutting zone, low-mass machine tool structures and high-speed sideways with speed 1 m/s and acceleration 10 m/s^2. The spread of high-speed technology is also due to the decreasing number of parts and joints of products, and the consequent economical benefits. These changes require the thorough analysis of the high-speed machining dynamics (see Tlusty, 1986). Generally, high-speed machine tools are long slender end millers with relatively low natural frequency, that rise up the possibilities of undesired vibrations (see Tlusty *et al.*, 1996, or Davies *et al.*, 1998).

The extended investigation of the milling process and the corresponding periodic DDE lead to the realization of a new bifurcation phenomena. In addition to Hopf bifurcation, period doubling bifurcation is also a typical way of stability loss in milling processes, as it was shown analytically by Davies *et al.* (2002), Insperger and Stépán (2000c), Corpus and Endres (2000), Bayly *et al.* (2001a), experimentally by Davies *et al.* (2002), Bayly *et al.* (2001a) and via numerical simulation by Zhao and Balachandran (2001). The nonlinear analysis of Stépán and Szalai (2001) showed that this period doubling bifurcation is subcritical.

6.1.3 Other cutting operations

Regenerative effects also arise in other types of operations. The dynamics of drilling operation is similar to the dynamics of the milling process. In drilling processes, one of the basic problems is the formation of lobed holes caused by the bending vibration of the tool (Bayly *et al.*, 2001b, Whitehead *et al.*, 2001). Although reaming is often performed to increase the precision and roundness of drilled holes, these bending vibrations may also arise in the finishing reaming operations (Bayly *et al.*, 2001d). In

contrast to chatter observed in milling and turning, chatter in drilling often involves large-amplitude torsional vibration (Bayly *et al.*, 2001c).

Chatter arising in grinding operations can also be explained by the regenerative effect. Although, the wear of the wheel is necessary to expose new abrasive grits, it is also a source of the regenerative instabilities. General grinding operations involve a driven motion of both the tool and the workpiece. The modeling of the dynamic variation in the shape of both the workpiece and the grinding wheel results two time delay in the equation of motion of the system. Since most of the practical grinding processes are unstable, dynamic investigations should be extended after the onset of instability. Thopmson (1986a, 1986b) developed a linear model to describe the double regenerative effect, and derived stability charts. These charts have similar structure as the one in Figure 5.12, but they show the exponential growth rate of chatter instead of pure stability or instability. This growth rate characterizes dynamic behavior of the grinding process and determines how often the grinding wheel must be dressed during machining. More sophisticated models of the tool-workpiece system lead to the thorough understanding of the grinding process dynamics (Thompson, 1992, Davies, 1998).

6.2   Stability analysis of the turning process

The mechanical model of the turning process in case of orthogonal cutting can be seen in Figure 6.1. The mass m of the tool, the damping coefficient c, and the spring stiffness k can be determined via modal analysis of the machine tool that has a well-separated first (lowest) natural frequency. The structure is assumed to be flexible in the x direction only. This reduces the model to 1 degree of freedom. Assume the prescribed feed motion to be uniform with a constant speed v of the tool. The angular speed of the workpiece is denoted by Ω. According to Newton's law, the equation of motion reads

$$m\ddot{x}(t) = -F_x + k(vt - x(t)) + c(v - \dot{x}(t)) \,. \tag{6.1}$$

The cutting force F_x reads

$$F_x = Kwf^{x_F} \,. \tag{6.2}$$

where K is the cutting coefficient, w is the depth of cut, f is the feed and the exponent x_F is a small constant, $x_F = 0.8$ or $3/4$ are typical values for this parameter (Tlusty, 2000). The feed is equal to the difference of the present and the delayed position of the tool, i.e., $f = x(t) - x(t - \tau)$, where $\tau = 60/\Omega$ [s] is the rotation period if Ω is given in rpm. Obviously, in the ideal case, $f = v\tau$. Now, the equation of motion is the
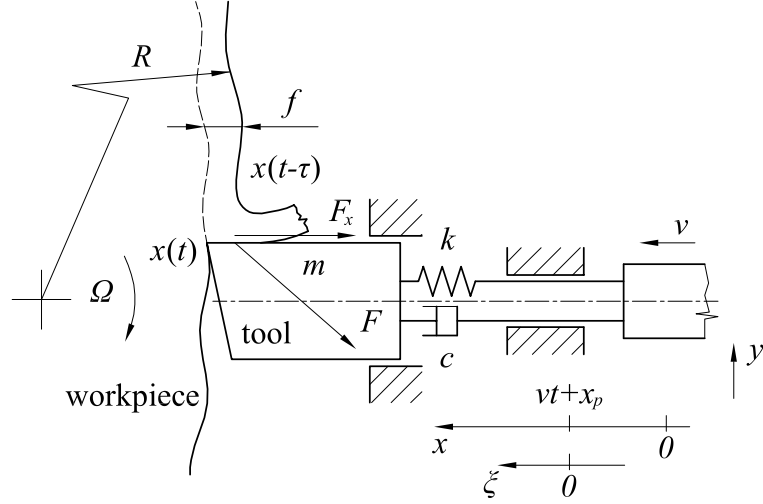
Figure 6.1: Mechanical model of turning processes

following DDE

$$m\ddot{x}(t) + c\dot{x}(t) + kx(t) = -Kw(x(t) - x(t - \tau))^{x_F} + kvt + cv . \qquad (6.3)$$

Assume the tool motion in the form

$$x(t) = vt + x_p + \xi(t) , \qquad (6.4)$$

where vt is the linear feed motion, x_p is a particular part related to the static compression of the spring, and $\xi(t)$ is the perturbation (see Figure 6.1). Substitution of equation (6.4) into equation (6.3) yields

$$kx_p + m\ddot{\xi}(t) + c\dot{\xi}(t) + k\xi(t) = -Kw\left(v\tau + \xi(t) - \xi(t - \tau)\right)^{x_F} . \qquad (6.5)$$

The ideal case $\xi(t) \equiv 0$ associated with the tool motion $x(t) = vt + x_p$ gives an equation for the static spring compression x_p :

$$kx_p = -Kw(v\tau)^{x_F} \quad \Rightarrow \quad x_p = -\frac{Kw(v\tau)^{x_F}}{k} . \qquad (6.6)$$

For linear stability analysis, we determine the variational system of equation (6.3) about the linear motion $x_p + vt$. Expand the nonlinear term in equation (6.5) into Taylor series with respect to ξ and neglect the higher order terms:

$$kx_p + m\ddot{\xi}(t) + c\dot{\xi}(t) + k\xi(t) = -Kw(v\tau)^{x_F} - Kwx_F(v\tau)^{x_F-1}\left(\xi(t) - \xi(t - \tau)\right) . \qquad (6.7)$$

Then, with equations (6.7) and (6.6), a linear autonomous DDE is obtained for ξ

$$m\ddot{\xi}(t) + c\dot{\xi}(t) + k\xi(t) = -wh\left(\xi(t) - \xi(t - \tau)\right) , \qquad (6.8)$$

where $h = K x_F (v\tau)^{x_F - 1}$ is the specific cutting force variation.

Using the modal parameters, equation (6.8) reads

$$\ddot{\xi}(t) + 2\zeta\omega_n\dot{\xi}(t) + \omega_n^2\xi(t) = -\frac{wh}{m}\left(\xi(t) - \xi(t - \tau)\right), \qquad (6.9)$$

where $\omega_n = \sqrt{k/m}$ is the natural angular frequency and $\zeta = c/(2m\omega_n)$ is the relative damping factor of the tool. Machine tools usually have low damping, generally, $\zeta \approx 0.005 - 0.02$. Equation (6.9) is the standard linear DDE model of the turning process.

Equation (6.9) can be even further simplified. Introduce the dimensionless time $\tilde{t}$ by $\tilde{t} = t\omega_n$, and by abuse of notation, drop the tilde immediately. This gives the dimensionless equation of motion

$$\ddot{\xi}(t) + 2\zeta\dot{\xi}(t) + \xi(t) = -\frac{wh}{m\omega_n^2}\left(\xi(t) - \xi(t - \omega_n\tau)\right). \qquad (6.10)$$

The stability chart of turning process gives those technological parameters where no chatter arises. Usually, these parameters are the spindle speed Ω [rpm] and the depth of cut w [mm]. The stability analysis of equation (6.9) can be carried out in the way as it was shown for equation (2.27) in Chapter 2. The stability boundaries obtained by the D-subdivision method read

$$\Omega = \frac{30\omega}{j\pi - \mathrm{atan}\left(\dfrac{\omega^2 - \omega_n^2}{2\zeta\omega_n\omega}\right)}, \quad j = 1, 2, \ldots, \qquad (6.11)$$

$$w = \frac{m}{2h}\frac{\left(\omega^2 - \omega_n^2\right)^2 + 4\zeta^2\omega_n^2\omega^2}{\omega^2 - \omega_n^2}, \qquad (6.12)$$

where the parameter ω is the frequency of the arising vibrations. In the literature, these boundary curves are called stability lobes. In Figure 6.2, these lobes are plotted in the plane of the dimensionless spindle speed $\Omega/(60f_n)$ and dimensionless depth of cut $\tilde{w} = (wh)/(m\omega_n^2)$. Here, $f_n = \omega_n/2\pi$ [Hz] is the natural frequency of the tool, and the spindle speed Ω is given in rpm. The only parameter is the relative damping ζ of the tool, it is chosen for 0.02. This stability chart is a kind of transformation of the chart of equation (2.27) in Figure 2.4 (see Stépán, 1989). The numbers in some domains denote the number of characteristic roots with positive real parts. Since, for turning process, only Hopf bifurcation occurs, these numbers change by 2 on the stability boundaries corresponding to the complex conjugate characteristic roots crossing the imaginary axis. The number 0 refers to asymptotic stability. In Figure 6.2, only the $j = 1, 2, \ldots, 10$ lobes are shown. For each number j, there is a pair of lobes, one in the $\tilde{w} > 0$ domain, the other in the $\tilde{w} < 0$ domain. The first pair of lobes $(j = 1)$ has vertical asymptote at $\Omega/(60f_n) = 1$, the second $(j = 2)$ has an asymptote at $\Omega/(60f_n) = 1/2$, etc. For the lobes in the domain $\tilde{w} > 0$, the frequency parameter ω
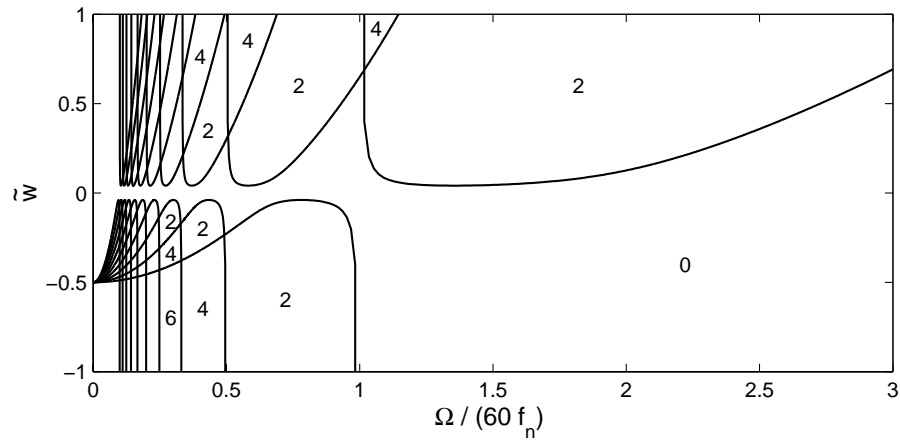
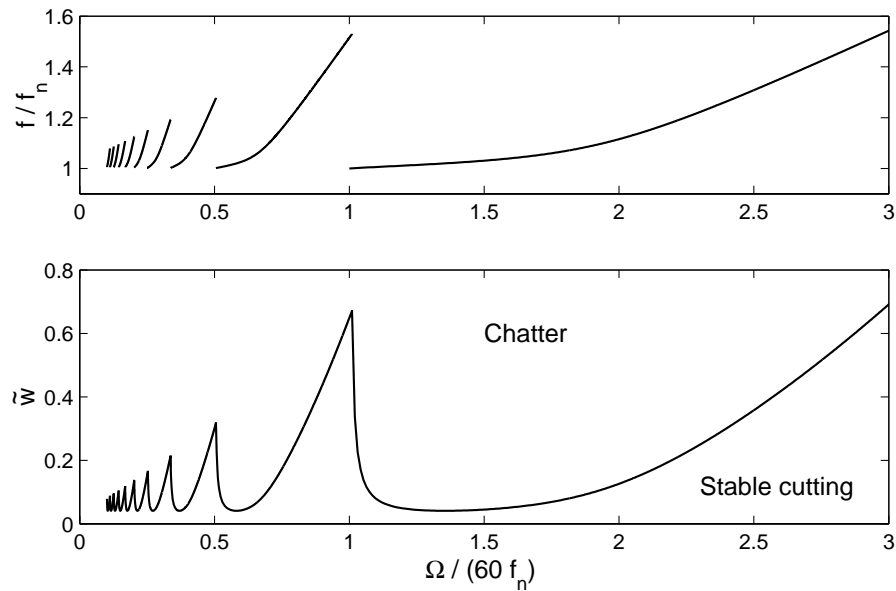Figure 6.2: Stability boundaries for equation (6.9) with $\zeta = 0.02$

Figure 6.3: Stability chart and chatter frequencies for turning processes with $\zeta = 0.02$

is greater than the angular natural frequency ω_n of the tool, while for the lobes in the domain $\tilde{w} < 0$, ω is between 0 and ω_n. The parameters $\omega < 0$ result boundary curves in the negative spindle speed domain.

In a turning process, of course, there are only positive depth of cuts. In Figure 6.3, the stability chart and the frequency diagram are given for this positive domain. The frequency diagram shows the frequency ratio $\omega/\omega_n = f/f_n$ of the arising vibrations and the natural frequency of the tool. Here, $f = \omega/2\pi$ [Hz] is the chatter frequency. As it was mentioned in the introductory part of the chapter, these chatter frequencies are somewhat above the natural frequency f_n of the tool. The vertical asymptotes

at $\Omega/(60f_n) = 1, 1/2, 1/3, \ldots$ have important role, since the lobe numbers can be identified by them. The first lobe $(j = 1)$ is in the domain $\Omega/(60f_n) > 1$, the second lobe $(j = 2)$ is about in the domain $1/2 \lesssim \Omega/(60f_n) \lesssim 1$, the third $(j = 3)$ in $1/3 \lesssim \Omega/(60f_n) \lesssim 1/2$, etc.

The domain of the first few lobes is called high-speed domain, since here, the spindle speed is commensurable to the natural frequency of the tool.

Although, the negative depth of cut has no physical meaning in turning processes, the lobes in the domain $\tilde{w} < 0$ can play important role in milling processes, where the direction of the resultant cutting force is changing, and its x component may be also negative, for example in the case of down-milling. Similar phenomenon may occur in case of drilling (Bayly *et al.*, 2001c), where the chatter frequency is usually below the natural frequency.

6.3 Mechanical model of the milling process

Figure 6.4 shows the 1 degree of freedom mechanical model of the milling process with parameters: mass m of the tool, damping coefficient c, spring stiffness k, feed speed v, and spindle speed Ω of the tool.

According to Newton's law, the equation of motion reads

$$m\ddot{x}(t) = -F_x(t) + k(vt - x(t)) + c(v - \dot{x}(t)) .\tag{6.13}$$

To determine the x component $F_x(t)$ of the the cutting force, further analysis of the cutting process is needed. Let the number of the teeth be z, and each tooth be indexed by $j = 1, \ldots, z$. The angular position of the tooth j can be given in the form

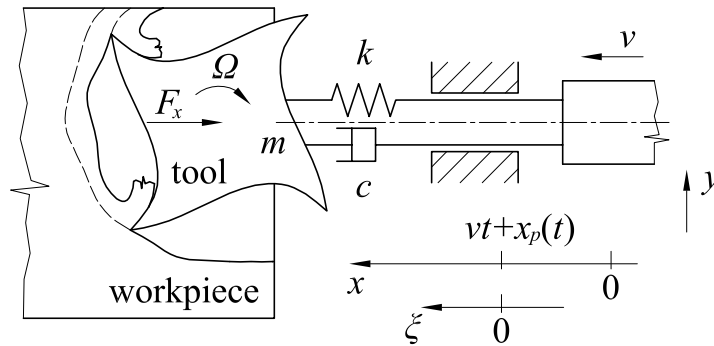$$\varphi_j(t) = (2\pi\Omega/60)t + j\,2\pi/z ,\tag{6.14}$$

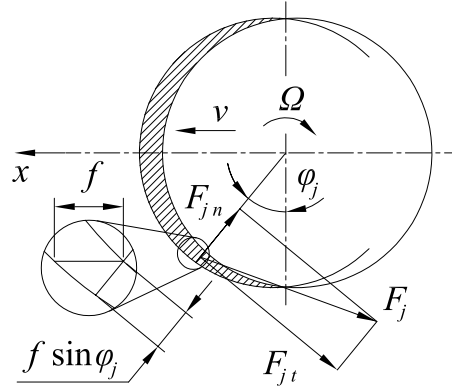Figure 6.4: Mechanical model of milling processes

Figure 6.5: Cutting force components in milling processes

where Ω is the spindle speed of the tool given in rpm. The tangential component of the cutting force acting on the active tooth j can be determined according to

$$F_{j\,t}(t) = K w (f \sin \varphi_j(t))^{x_F} \,, \qquad (6.15)$$

where K is the cutting coefficient, w is the depth of cut, f is the feed per tooth and the exponent is a constant, generally, $x_f = 0.8$ or $3/4$. According to the literature (Bálint, 1967, Bali, 1988, Tlusty, 2000), the normal component of the cutting force is usually estimated as

$$F_{j\,n}(t) = 0.3 \, F_{j\,t}(t) \,. \qquad (6.16)$$

The x component of the cutting force depends on the angular position of the tool as it can be seen in Figure 6.5:

$$F_{j\,x}(t) = g_j(t) \left(F_{j\,t}(t) \cos \varphi_j(t) + F_{j\,n}(t) \sin \varphi_j(t) \right) \,. \qquad (6.17)$$

Here, $g_j(t)$ is a screen function (see Laczik, 1986), it is equal to 1, if the jth tooth is active and 0 if it is not working. This screen function is determined by the disposition of the tool-workpiece system. The tooth j works only if its angular position fulfil the condition

$$\varphi_s < \varphi_j(t) < \varphi_f \,, \qquad (6.18)$$

where the angles φ_s and φ_f are the locations of entering and leaving the workpiece, respectively, defined as

$$\cos \varphi_s = \frac{B + 2e}{D}, \qquad \cos \varphi_f = \frac{B - 2e}{D} \,, \qquad (6.19)$$

and B is the width of the workpiece, e is the distance between the center lines of the tool and the workpiece, and D is the diameter of the tool (see Figure 6.6). Then, the screen function reads

$$g_j(t) = \frac{1}{2} \left(1 + \mathrm{sgn} \left(\sin \left(\varphi_j(t) - \psi \right) - p \right) \right) = \begin{cases} 1 & \text{if } \varphi_s < \varphi_j(t) < \varphi_f \\ 0 & \text{otherwise} \end{cases} \,, \qquad (6.20)$$
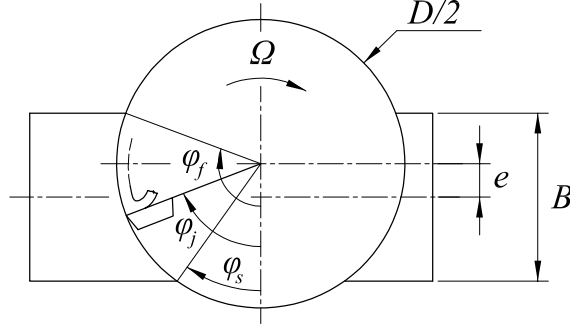
Figure 6.6: Tool-workpiece disposition in milling processes

where the constants ψ and p are defined as

$$\tan \psi = \frac{\sin \varphi_s - \sin \varphi_f}{\cos \varphi_s - \cos \varphi_f}, \qquad p = \sin(\varphi_s - \psi). \tag{6.21}$$

The feed is just equal to the difference of the present and the delayed position of the tool, i.e., $f = x(t) - x(t - \tau)$. If the spindle speed Ω of the tool is given in [rpm], than the time delay is $\tau = 60/(z\Omega)$ [s]. The x component of the cutting force acting on the tool is given by the sum of $F_{j\,x}(t)$ (see equation (6.17)) for all j. Introducing the τ-periodic function $q(t)$, the excitation force in equation (6.13) reads

$$F_x(t) = wq(t)\left(x(t) - x(t - \tau)\right)^{x_F}, \tag{6.22}$$

where

$$q(t) = K \left(\sum_{j=1}^{z} g_j(t) \sin^{x_F} \varphi_j(t) \left(\cos \varphi_j(t) + 0.3 \sin \varphi_j(t)\right) \right). \tag{6.23}$$

Thus, the equation of motion is the following nonautonomous nonlinear DDE

$$m\ddot{x}(t) + c\dot{x}(t) + kx(t) = -wq(t)\left(x(t) - x(t - \tau)\right)^{x_F} + kvt + cv. \tag{6.24}$$

Note that the time period of $q(t)$ is equal to the time delay τ.

As a base for the linarization of equation (6.24), assume the tool motion in the form

$$x(t) = vt + x_p(t) + \xi(t), \tag{6.25}$$

where vt is the linear feed motion, the particular part $x_p(t) = x_p(t + \tau)$ is a τ-periodic motion that can also be considered as the unperturbed, or ideal tool motion when no self-excited vibrations arise, and $\xi(t)$ is the perturbation (see Figure 6.4). Substitute equation (6.25) into equation (6.24):

$$m\ddot{x}_p(t) + c\dot{x}_p(t) + kx_p(t) + m\ddot{\xi}(t) + c\dot{\xi}(t) + k\xi(t)$$
$$= -wq(t)\left(v\tau + \xi(t) - \xi(t - \tau)\right)^{x_F}. \tag{6.26}$$

In the ideal case, $\xi(t) \equiv 0$ and the tool moves according to $x(t) = vt + x_p(t)$. This case gives an ordinary differential equation for x_p

$$m\ddot{x}_p(t) + c\dot{x}_p(t) + kx_p(t) = -w(v\tau)^{x_F}q(t) . \tag{6.27}$$

Since this is a linear differential equation with τ-periodic excitation, it has a τ periodic solution, namely, the particular one. This proves the existence of the τ-periodic function $x_p(t)$ and verifies equation (6.25). Furthermore, we can state that $x_p(t)$ has the same harmonics as the excitation $q(t)$. In general, this means that all the higher harmonics of the basic frequency $2\pi/\tau$ appear in $x_p(t)$.

For linear stability analysis, we determine the variational system of equation (6.24) about the combined linear and periodic motion $vt + x_p(t)$. Expand the nonlinear term in equation (6.26) into Taylor series with respect to ξ and neglect the higher order terms:

$$m\ddot{x}_p(t) + c\dot{x}_p(t) + kx_p(t) + m\ddot{\xi}(t) + c\dot{\xi}(t) + k\xi(t)$$
$$= -w(v\tau)^{x_F}q(t) - wx_F(v\tau)^{x_F-1}q(t)\left(\xi(t) - \xi(t-\tau)\right) . \tag{6.28}$$

Using equations (6.27) and (6.28), a linear time periodic DDE is obtained for ξ

$$m\ddot{\xi}(t) + c\dot{\xi}(t) + k\xi(t) = -wh(t)\left(\xi(t) - \xi(t-\tau)\right) , \tag{6.29}$$

where $h(t) = x_F(v\tau)^{x_F-1}q(t)$ is now a time dependent specific force variation.

Similarly to the equation of motion of the turning process, equation (6.29) can also be given in the modal form

$$\ddot{\xi}(t) + 2\zeta\omega_n\dot{\xi}(t) + \omega_n^2\xi(t) = -\frac{wh(t)}{m}\left(\xi(t) - \xi(t-\tau)\right) , \tag{6.30}$$

or in the dimensionless modal form

$$\ddot{\xi}(t) + 2\zeta\dot{\xi}(t) + \xi(t) = -\frac{wh(t)}{m\omega_n^2}\left(\xi(t) - \xi(t-\omega_n\tau)\right) , \tag{6.31}$$

where $\omega_n = \sqrt{k/m}$ is the natural angular frequency, $\zeta = c/(2m\omega_n)$ is the relative damping of the tool. Equation (6.30) is considered as a standard linear DDE model of the milling process. Note, that equation (6.9) of the turning process is the special case of equation (6.30) with $h(t) \equiv h$.

The relation of feed and tool rotation directions defines two types of partial immersion milling operation: the up-milling and the down-milling (see Figure 6.7). Concerning the end product, both types of operations give the same result, but the dynamics and, consequently, the stability properties alter from each other. Partial immersion milling operations are characterized by the number z of teeth and the radial immersion ratio a/D, where a is the radial depth of cut, D is the diameter of the tool. In the subsequent section, the stability charts for different milling processes are determined.
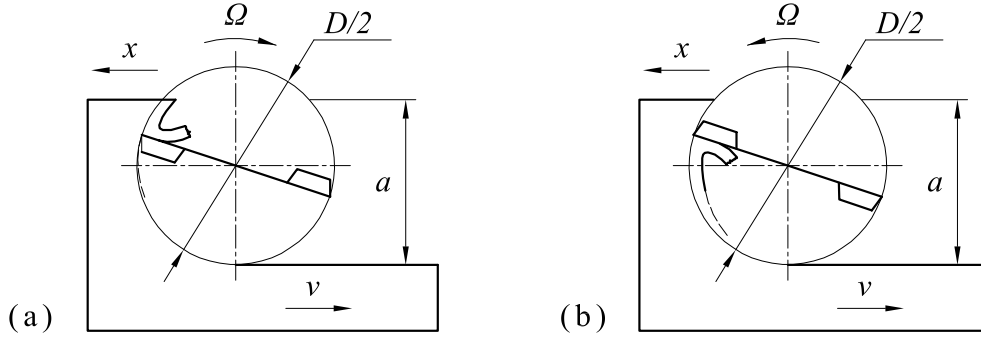
Figure 6.7: Up-milling (a) and down-milling (b) operations

6.4   Stability charts for high-speed milling processes

The stability analysis of equation (6.30) is carried out in the same way as it was done for equation (5.36) in Section 5.3. Since, the time delay is equal to the principal period, $\mathbf{\Phi}^2$ (the transition matrix over the double principal period) is calculated instead of $\mathbf{\Phi}$.

Stability charts are plotted in the dimensionless parameter plane as in Figure 6.3, but the dimensionless spindle speed is given in the form $z\Omega/(60 f_n)$, so that the milling operations with different tooth numbers can be compared. The turning process can be considered as the special case when $h(t) \equiv h$ with $z = 1$.

Here, only the high-speed domain of the first and the second lobes is investigated $(0.5 < z\Omega/(60 f_n) < 3)$. The number z of teeth, the radial immersion ratio a/D, and the cases of either up- or down-milling are presented besides the charts. The only parameter is the relative damping ζ which is chosen for 0.01 for all the charts.

The transition between the autonomous model for turning and the discrete map model of highly interrupted cutting is shown in Figure 6.8. The intermediate cases are partial immersion up-milling processes. Each chart is accompanied by the graph of function $h(t)$, so that it can be followed, how the $h(t) \equiv h$ case of turning changes into the highly interrupted, low immersion milling.

As it can be seen, a new series of extra stability lobes arise in addition to the Hopf lobes of turning. The numerical calculation of the relevant characteristic multipliers shows a new kind of bifurcation phenomena: these extra lobes are related to *period two* or *flip* bifurcation (see the chart (d) in Figure 6.8). A schematic picture of the framed part of chart (c) in Figure 6.8 and the wandering of the relevant characteristic multipliers can be seen in Figure 6.9. Through the parameter points $1-2-3$, the critical pair of characteristic multipliers moves into the unit circle presenting a Hopf bifurcation at point 2. Through points $3 - 4 - 5$, the complex pair of characteristic multipliers becomes real, then through $5 - 6 - 7$, one of them moves out of the unit circle at -1 presenting a flip bifurcation at point 6. Through $7-8-9$, the relevant real characteristic
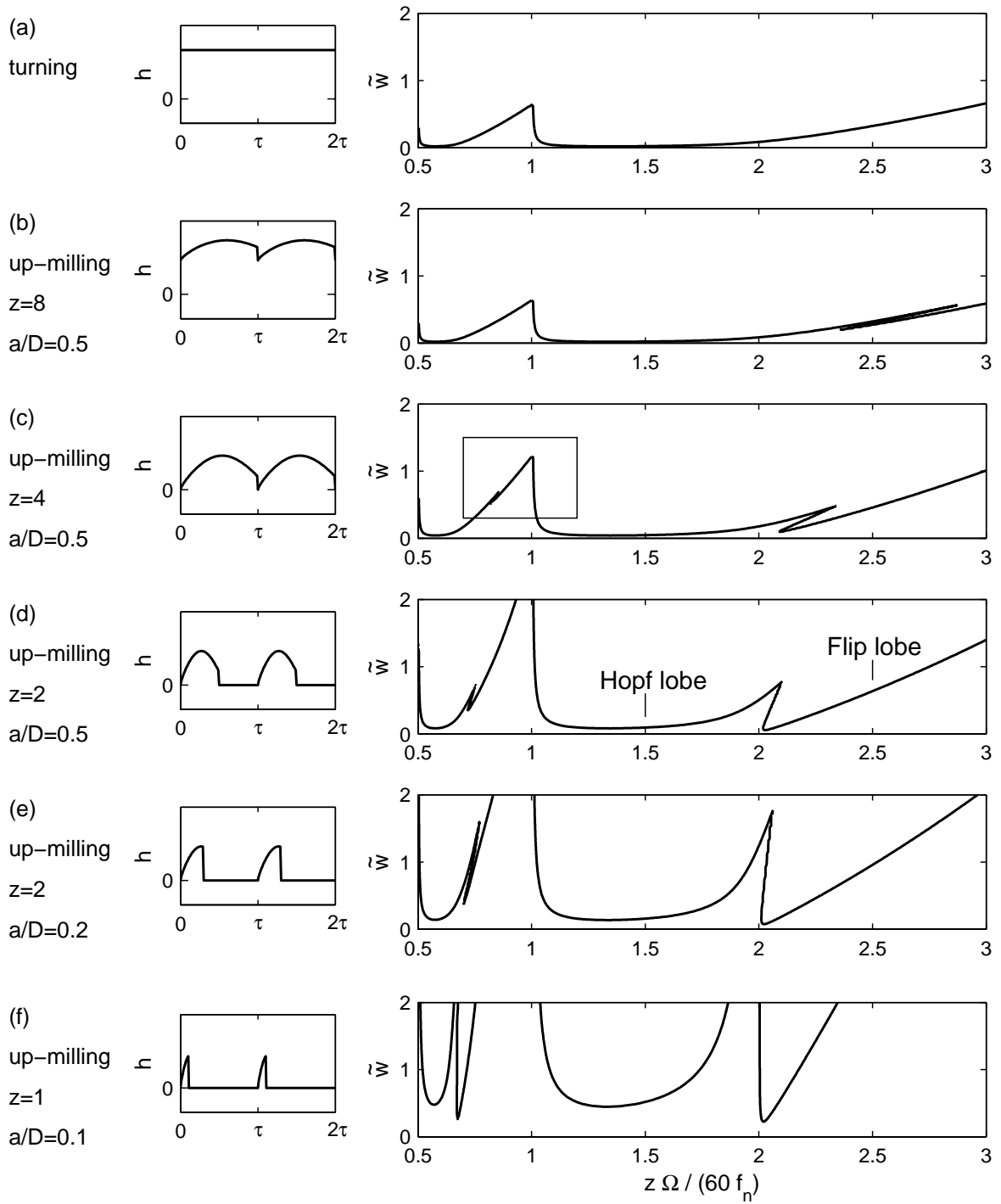
Figure 6.8: Transition between turning and low immersion milling
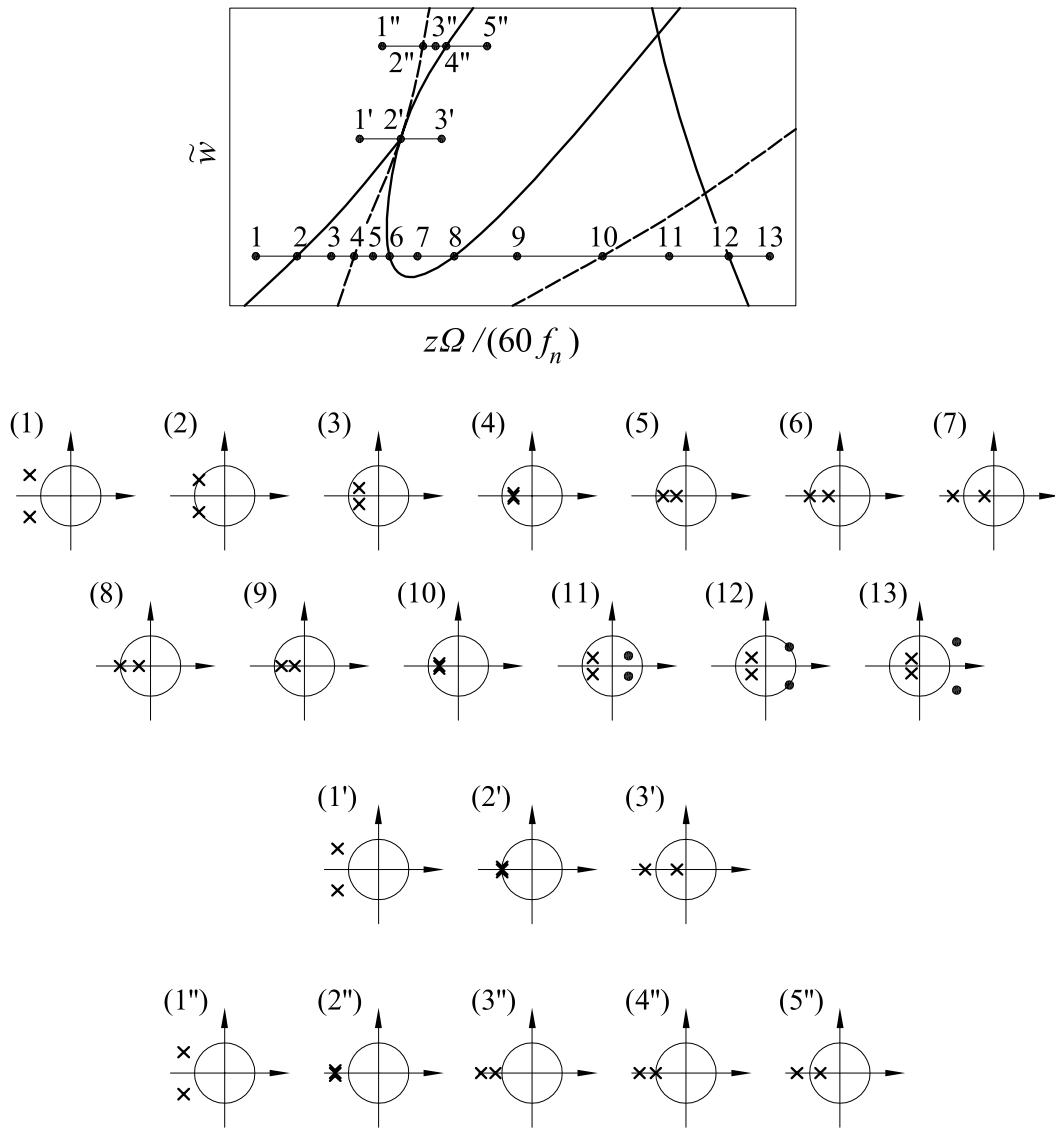
Figure 6.9: Position of the relevant characteristic multipliers for different cutting parameters

multiplier moves back into the unit circle presenting another flip bifurcation at point 8. Through $9 - 10 - 11$, the two relevant real characteristic multipliers become a pair of complex conjugate roots again, and they decrease in modulus, while through $11 - 12 - 13$, another complex pair of characteristic multipliers moves out of the unit circle in the positive half of the complex plane presenting another Hopf bifurcation at point 12.

The dashed curve in the chart of Figure 6.9 presents the parameters where real characteristic multiplier occurs with multiplicity 2. This curve crosses the intersection of the two kinds of stability limits at $2'$ presenting a degenerate (co-dimension 2) flip-Hopf bifurcation (see points $1' - 2' - 3'$), and proceeds in the unstable domain (see points $1'' - 2'' - 3'' - 4'' - 5''$).

In Figure 6.10, stability charts are presented for both up- and down-milling cases with various a/D ratio and also for full immersion milling. For all charts, the number of teeth is $z = 2$. For various radial immersion ratio, the stability charts are different. While for some fixed parameter pairs $(z\Omega/(60 f_n), \tilde{w})$, the up-milling operation is unstable, the down-milling operation might be stable and vice-versa. This may have a great importance in industrial applications, since unstable processes can be stabilized by changing the direction of tool rotation. In practice, it means the application of a mirror workpiece/tool configuration, while the sense of the tool rotation is the same. The reason for this is the backward cutting effect of down-milling. The transition from up-milling to down-milling is detailed in Figure 6.11. The numbers denote the number of unstable characteristic roots. The number 0 refers to asymptotically stable systems. On the boundary curves, where this number changes by 2, there is secondary Hopf bifurcation, where it changes by 1, there is flip bifurcation and where it is not changing, there are double real characteristic multipliers just becoming a complex pair. As the ratio a/D increases for up-milling cases, a new Hopf lobe emerges, and sinks slowly, while the original boundary curve rises. The intersections of these lobes creates the intriguing stability chart of the full immersion milling. As the ratio a/D decreases for down-milling cases, the original boundary curve lifts up, and the new lobe takes over its role.

The new Hopf lobe can be associated to the lobes belonging to negative depth of cut in Figure 6.2, since for these milling operations, the x component of the resultant cutting force may also be negative, as it is shown by the function $h(t)$ at the charts. It can also be seen, that the negative part of the function $h(t)$ becomes more and more dominant as we come along from charts (a) to (f). This effect is often called as backward cutting effect.

Experimental verification of the differences between up- and down-milling can be seen in Figure 6.13. The measurments were carried out in the Laboratory of the De-
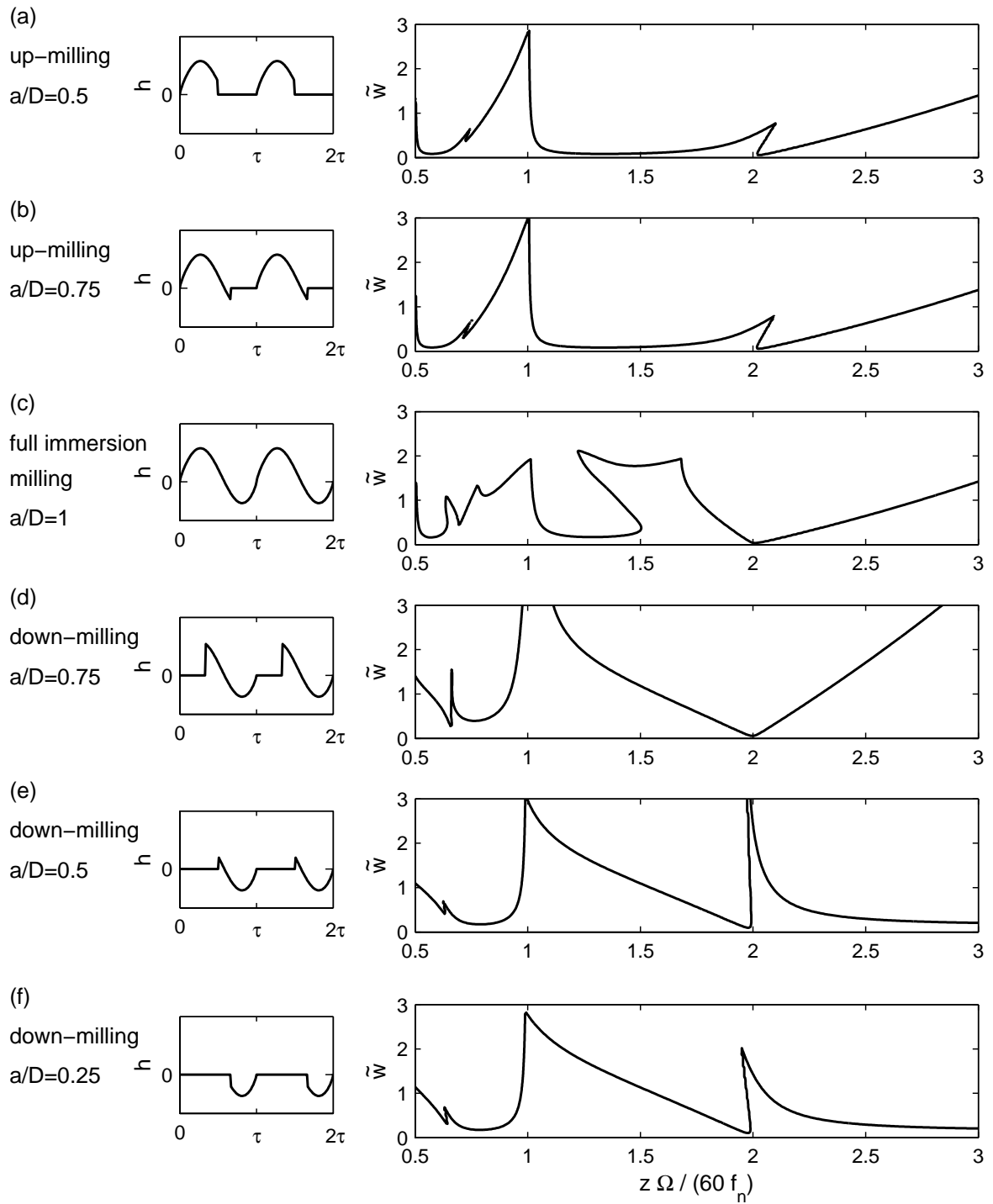
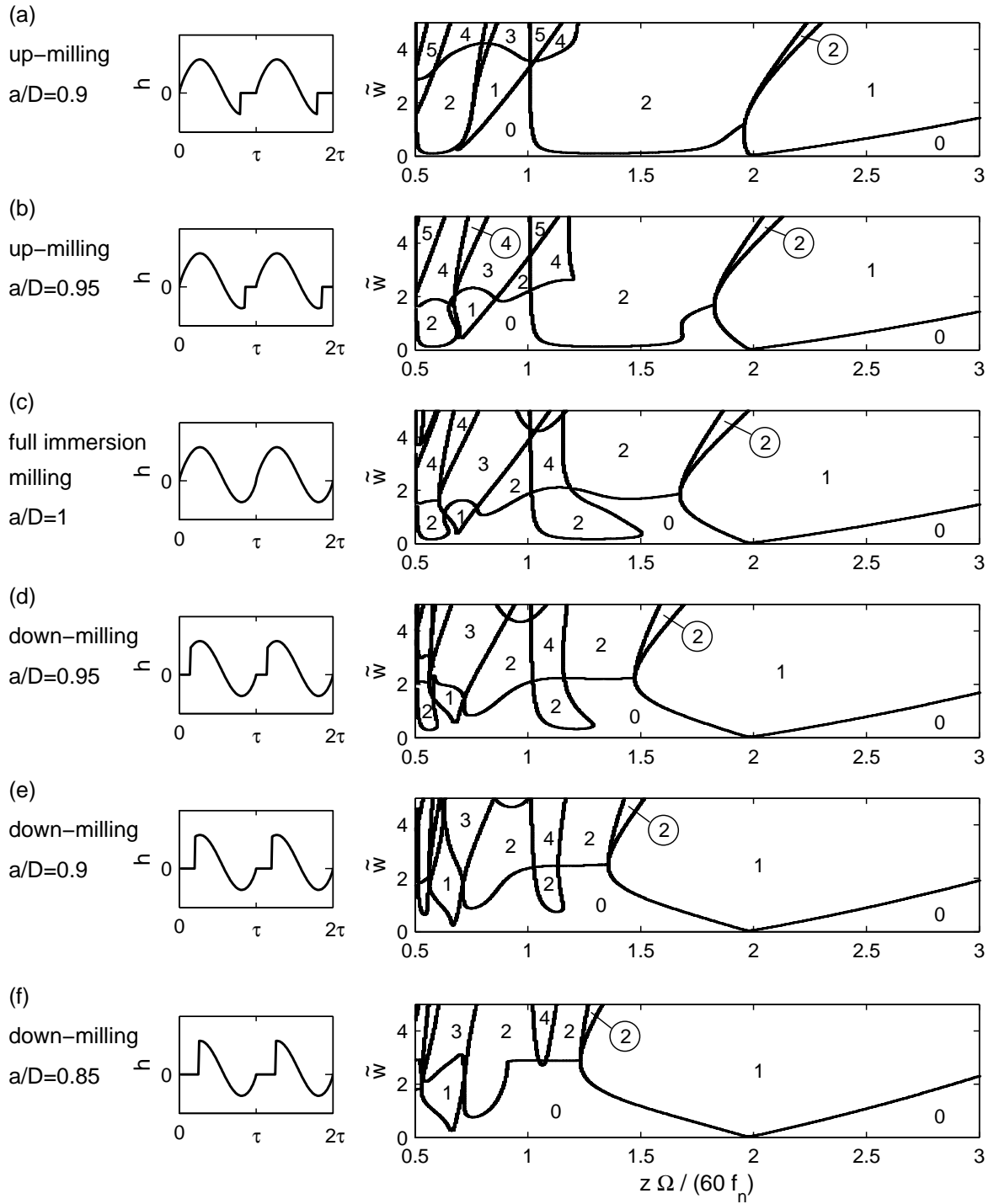Figure 6.10: Stability charts for up-, down- and full immersion milling

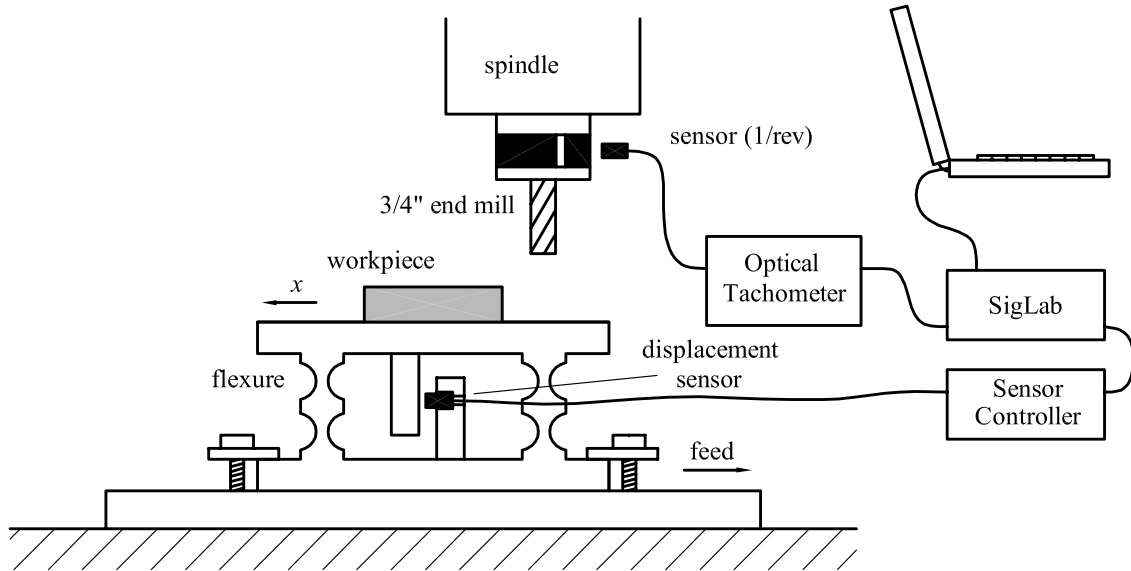Figure 6.11: Boundary curves for up-, down- and full immersion milling

Figure 6.12: Scheme of the experiment

partment of Mechanical Engineering at Washington University in St. Louis, Missouri, USA, in collaboration with Dr. Philip V. Bayly, Brian P. Mann (Department of Mechanical Engineering, Washington University, St. Louis, Missouri, USA) and Jeremiah E. Halley (The Boeing Company, St. Louis, Missouri, USA).

Milling tests were performed with an experimental flexure designed to mimic the 1-DOF system described above (Mann, 2001, Bayly *et al.*, 2002). A monolithic, unidirectional flexure was machined from aluminum and instrumented with a single non-contact, eddy current displacement transducer as shown in Figure 6.12. A radial immersion of 4.515 mm was used to up-mill and down-mill aluminum (7075-T6) test samples of width 1/4 inch (6.35 mm) over a specified range of spindle speeds Ω and axial depths of cut w. A 0.750-inch (19.05 mm) diameter carbide end mill with a single flute ($z = 1$) was used, the second flute was ground off to remove any effects due to asymmetry or runout. Consequently, the radial immersion ratio was $a/D = 0.237$. Feed was held constant: $v\tau = 0.004$ in $= 0.1016$ mm.

The stiffness of the flexure to deflections in the x-direction was measured to be $k = 2.18 \times 10^6$ N/m. The natural frequency was experimentally determined to be $f_n = 146.5$ Hz, and the damping ratio was $\zeta = 0.0032$, which corresponds to very light damping. In comparison, the values of stiffness in the perpendicular y- and z-directions were more than 20 times greater, than that in the x-direction.

The displacement transducer output was anti-alias filtered and sampled (16-bit precision, 12800 samples/sec) with SigLab 20-22a data acquisition hardware connected to a Toshiba Tecra 520 laptop computer. A periodic 1/rev pulse was obtained with the
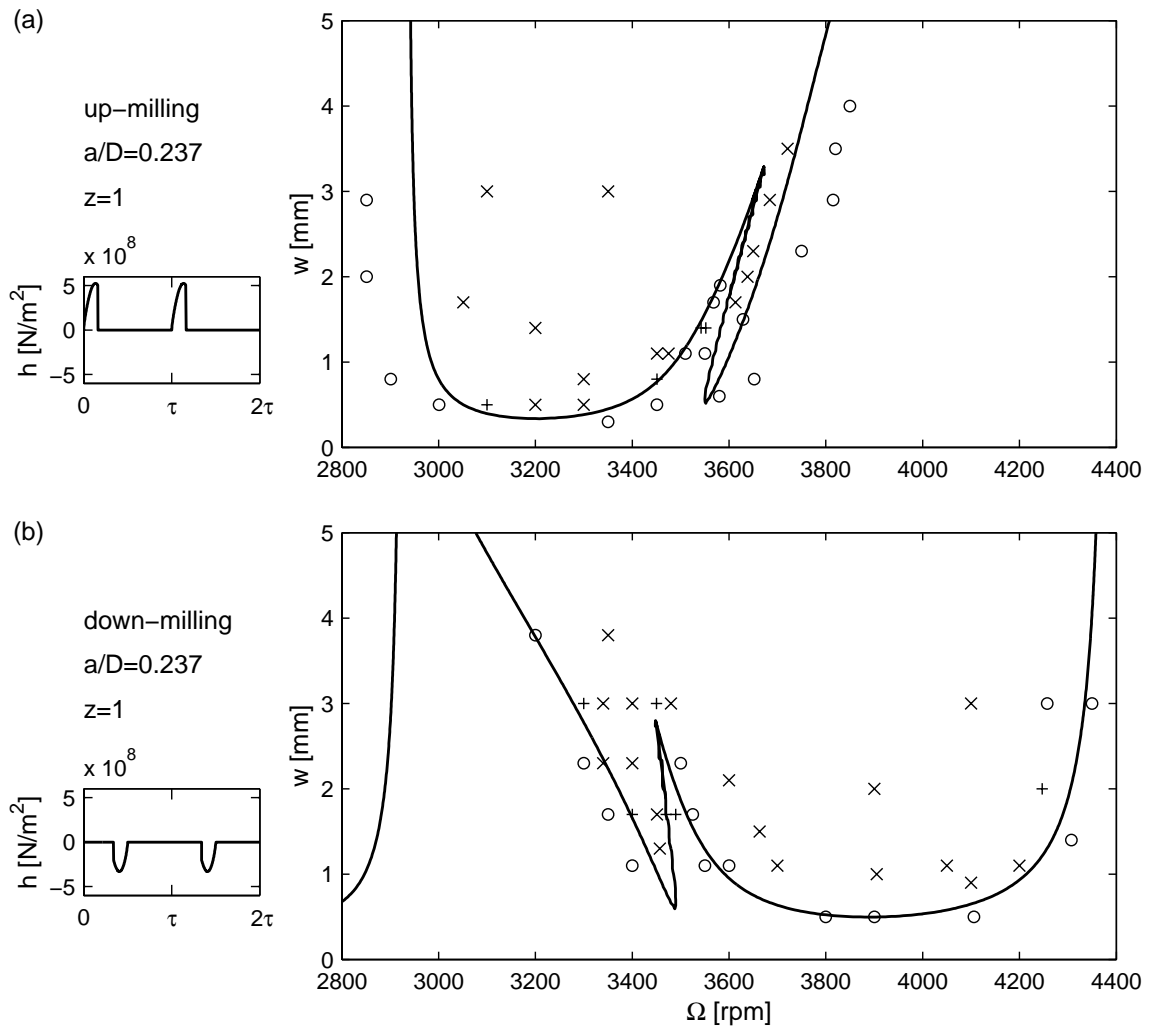
Figure 6.13: Theoretical boundary curves and experimental data (stable cutting: ∘, boundary: +, unstable cutting: ×)

use of a laser tachometer to sense a black-white transition on the rotating tool holder.

The theoretical boundary curves were determined through the investigation of the characteristic multipliers calculated by the semi-discretization method. For the calculations, the following experimentally identified parameters were used: $m = 2.573$ kg, $\zeta = 0.0032$, $\omega_n = 920.5$ rad/s. Based on the experimental results of Halley (1999), the cutting coefficient was chosen to the reasonable value $K = 1 \times 10^8$ N/m$^{1+x_F}$, where $x_F = 0.8$.

The presented lobes in Figure 6.12 are of number 3, since $f_n/3 < z\Omega/60 < f_n/2$. The experimental data correlate well with the theoretical predictions. The flip lobes lean to the right for up-milling, and to the left for down-milling.

6.5 Vibration frequencies during milling operation

Opposite to the turning process, the identification of the chatter frequencies in milling processes is not a trivial task either experimentally or theoretically. The power spectrum of the signals show several peaks of complicated structure. Some of them refer to the tooth pass excitation effect, others refer to the regenerative effect, and the natural frequency of the tool also appears. In this section, a clear picture is given about these frequencies arising in the chatter during the milling process.

Chatter arises if the linear equation (6.30) loses stability. As explained in the Section 2.4 about the extended Floquet Theory of DDEs, the stability properties are determined by the (infinite number) of characteristic multipliers. If $\mu = \mathrm{e}^{\lambda \tau}$ is a characteristic multiplier of equation (6.30), then there exists a solution in the form

$$\xi(t) = p(t)\,\mathrm{e}^{\lambda t} + \bar{p}(t)\,\mathrm{e}^{\bar{\lambda} t}\,, \tag{6.32}$$

where $p(t) = p(t + \tau)$ is a τ-periodic function, λ is the characteristic exponent and bar denotes complex conjugates. Equation (6.30) is asymptotically stable, if and only if, all the characteristic multipliers are in modulus less than one, in other words, all characteristic exponents have negative real part. The semi-discretization method provides a finite number of approximate multipliers. The vibration frequencies corresponding to the relevant characteristic multiplier can be determined in the following way.

If equation (6.30) is at the border of stability, then there is at least one characteristic multiplier (either one real, or one complex conjugate pair) in modulus just equal to one. All the other infinite number of characteristic multipliers are in modulus less than one, so they are not important for chatter frequency analysis.

The critical characteristic multipliers can be located in three typical ways as introduced in Section 2.2. The corresponding bifurcations are secondary Hopf (Im $\mu \neq 0$ and $|\mu| = 1$), period one ($\mu = 1$) and period two ($\mu = -1$) bifurcations.

It can easily be seen that the $\mu = 1$ case cannot arise in equation (6.30). To prove this, assume the characteristic multiplier $\mu = 1$. Since $\xi(t + \tau) = \mu\,\xi(t)$ in the critical subspace, the substitution of $\xi(t - \tau) = \xi(t)$ into the equation (6.30) results the damped oscillator

$$\ddot{\xi}(t) + 2\zeta\omega_n\dot{\xi}(t) + \omega_n^2\xi(t) = 0\,. \tag{6.33}$$

Since the damping is positive, equation (6.33) is asymptotically stable. This prove that the period one bifurcation is excluded for equation (6.30).

For a given $|\mu| = 1$, $\lambda = \mathrm{i}\omega$ is pure imaginary, where $\omega = \mathrm{Im}\,(\ln\mu)/\tau$. Essentially, the chatter angular frequencies are denoted by ω. Since the complex exponential function is periodic, the logarithmic function is not unique in the plane of complex

numbers. This raises the possibility of multiple chatter frequencies. To give a clear view of the resulting frequencies, equation (6.32) must be analyzed.

For secondary Hopf case, the relevant characteristic exponents form complex pairs. Substitute $\lambda = \mathrm{i}\,\omega$ into equation (6.32), expand $p(t)$ into Fourier series and use trigonometrical transformations. Then equation (6.32) can be written in the form

$$\xi(t) = \sum_{n=-\infty}^{\infty} \left(C_n \, \mathrm{e}^{\mathrm{i}\,(\omega + n2\pi/\tau)t} + \bar{C}_n \, \mathrm{e}^{\mathrm{i}\,(-\omega + n2\pi/\tau)t} \right), \tag{6.34}$$

where C_n's are complex coefficients. This shows that the arising frequencies in the signal $\xi(t)$ are

$$f_H = \left\{ \pm\omega + n\frac{2\pi}{\tau} \right\} \ [\mathrm{rad/s}] = \left\{ \pm\frac{\omega}{2\pi} + n\frac{z\Omega}{60} \right\} \ [\mathrm{Hz}], \quad n = \dots, -1, 0, 1, \dots, \tag{6.35}$$

where τ is given in s, Ω in rpm. The index of f_H refers to the secondary Hopf bifurcation. There are infinite number of frequencies with amplitudes corresponding to the coefficients C_n's. This is in accordance with the periodic property of the complex exponential function mentioned before. Of course, only the positive values of f_H have physical meaning.

For the period doubling case ($\mu = -1$), the characteristic exponent is $\lambda = (\ln(-1))/\tau$ and the frequencies can be written in the simple form of

$$f_{PD} = \left\{ \frac{\pi}{\tau} + n\frac{2\pi}{\tau} \right\} \ [\mathrm{rad/s}] = \left\{ \frac{z\Omega}{30} + n\frac{z\Omega}{60} \right\} \ [\mathrm{Hz}], \quad n = \dots, -1, 0, 1, \dots, \tag{6.36}$$

where the index of f_{PD} refers to the period doubling bifurcation.

Either the frequency set f_H or f_{PD} shows up during chatter. If equation (6.29) is stable, then these frequencies do not arise.

The arising frequencies during the milling operation are related to all components of $x(t)$ defined by equation (6.25). The term vt is the linear feed motion, and it does not contain any periodicity, but the periodic motion $x_p(t)$ contains the following frequencies

$$f_{TPE} = \left\{ \frac{nz\Omega}{60} \right\} \ [\mathrm{Hz}], \quad n = 1, 2, \dots, \tag{6.37}$$

as it was shown by equation (6.27). The index of f_{TPE} refers to the tooth pass excitation effect.

Since the damping of machine tools is small, the transient phenomena ease slowly. This results another peak in the spectrum at the damped natural frequency $f_d = \omega_n \sqrt{1 - \zeta^2}/(2\pi)$ of the tool.

The frequencies f_{TPE} and f_d are present in the vibration signal both for stable and unstable cutting.
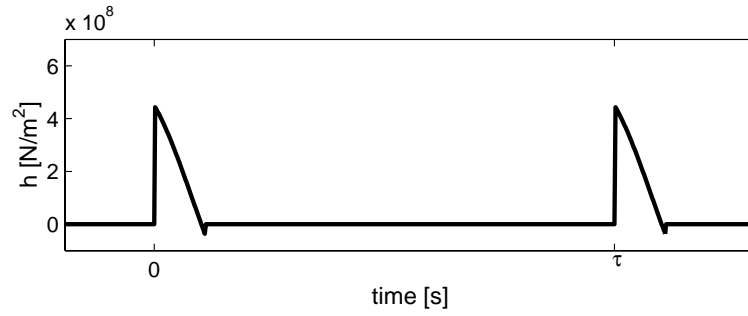
Figure 6.14: The specific force variation

For experimental verification, aluminum (7075-T6) test samples of width 1/4 inch (6.35 mm) were centrally milled by a 3/4 inch (19.05 mm) diameter carbide end mill with a single flute (Mann, 2001, Insperger *et al.*, 2002). The scheme of the experiment is shown in Figure 6.12. The stiffness of the flexure was measured to be $k = 2.18 \times 10^6$ N/m. The natural frequency was experimentally determined to be $f_n = 146.8$ Hz, and the damping ratio was $\zeta = 0.0038$. Feed was held constant: $v\tau = 0.004$ in = 0.1016 mm.

Theoretical stability charts and the chatter frequencies were determined through the investigation of the characteristic multipliers calculated by the semi-discretization method. For the calculations, the following experimentally identified parameters were used: $m = 2.586$ kg, $\zeta = 0.0038$, $\omega_n = 922.4$ rad/s in accordance with the above measured values. The cutting coefficient was chosen to the reasonable value $K = 1.5 \times 10^8$ N/m$^{1+x_F}$, with $x_F = 0.8$. The damped natural frequency of the flexure was $f_d = \sqrt{1 - \zeta^2} f_n \approx 146.8$ Hz.

The relative position of the tool and the workpiece defines the specific force variation $h(t)$ shown in Figure 6.14.

The theoretical stability chart and the corresponding chatter frequencies can be seen in Figure 6.15. Solid lines denote the chatter frequencies f_H and f_{PD}. Dashed lines refer to the frequencies f_{TPE} caused by the tooth pass excitation effect, and a dotted line denotes the damped natural frequency f_d of the flexure.

Experiments were made at a constant depth of cut $w = 2$ mm and three different spindle speeds $\Omega = 3300$, 3500 and 3590 rpm denoted by A, B and C in Figure 6.16, respectively. As the stability chart shows, point A is in an unstable parameter domain of Hopf type, point B is in a stable domain, and point C is in an unstable domain of period doubling type.

The vertical lines raised from the corresponding parameter points of the chart intersect the frequency lines in the frequency diagram above the chart and assign the frequency sets belonging to the corresponding vibration signal of the machine tool.
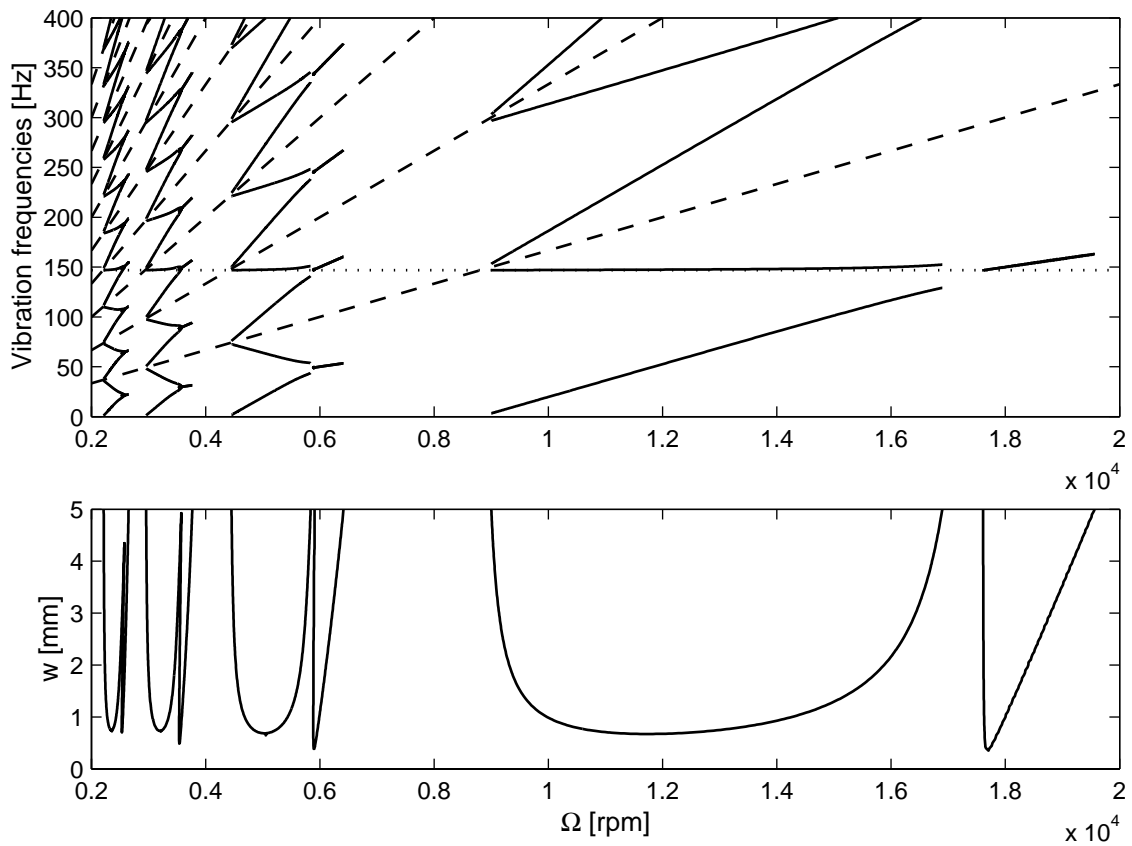
Figure 6.15: Theoretical stability chart and vibration frequencies

The symbols $\circ$, $\triangle$, $\square$ and $\bullet$ refer to the four different classes of frequency sets f_H, f_{PD}, f_{TPE} and f_d, respectively. The same symbols also show up in Figure 6.18. The three power spectra are calculated from the three vibration signals presented in Figure 6.17 in three different forms, each: time history, sampled time history, and Poincaré (or stroboscopic) map. In the power spectra of Figure 6.18, the dashed lines denote the theoretical tooth pass excitation frequency and its higher harmonics. The symbols mentioned above help to identify all the various frequency sets.

For parameter point A, the theory shows that the relevant characteristic multiplier is a complex pair. The experiment confirms the theoretical expectation: the most dominant peaks in the power spectrum show up at the frequencies f_H, f_{TPE} and f_d.

Cutting defined by parameter point B is stable, so only frequencies f_{TPE} and f_d are expected. This is also confirmed by the measurement result.

Parameter point C defines an unstable, period doubling cutting process. In this case, the most dominant peaks in the power spectrum are at the frequencies f_{PD}, f_{TPE} and f_d, and clearly, it is also confirmed by the experiments.

The transition between the secondary Hopf and the period doubling case can be
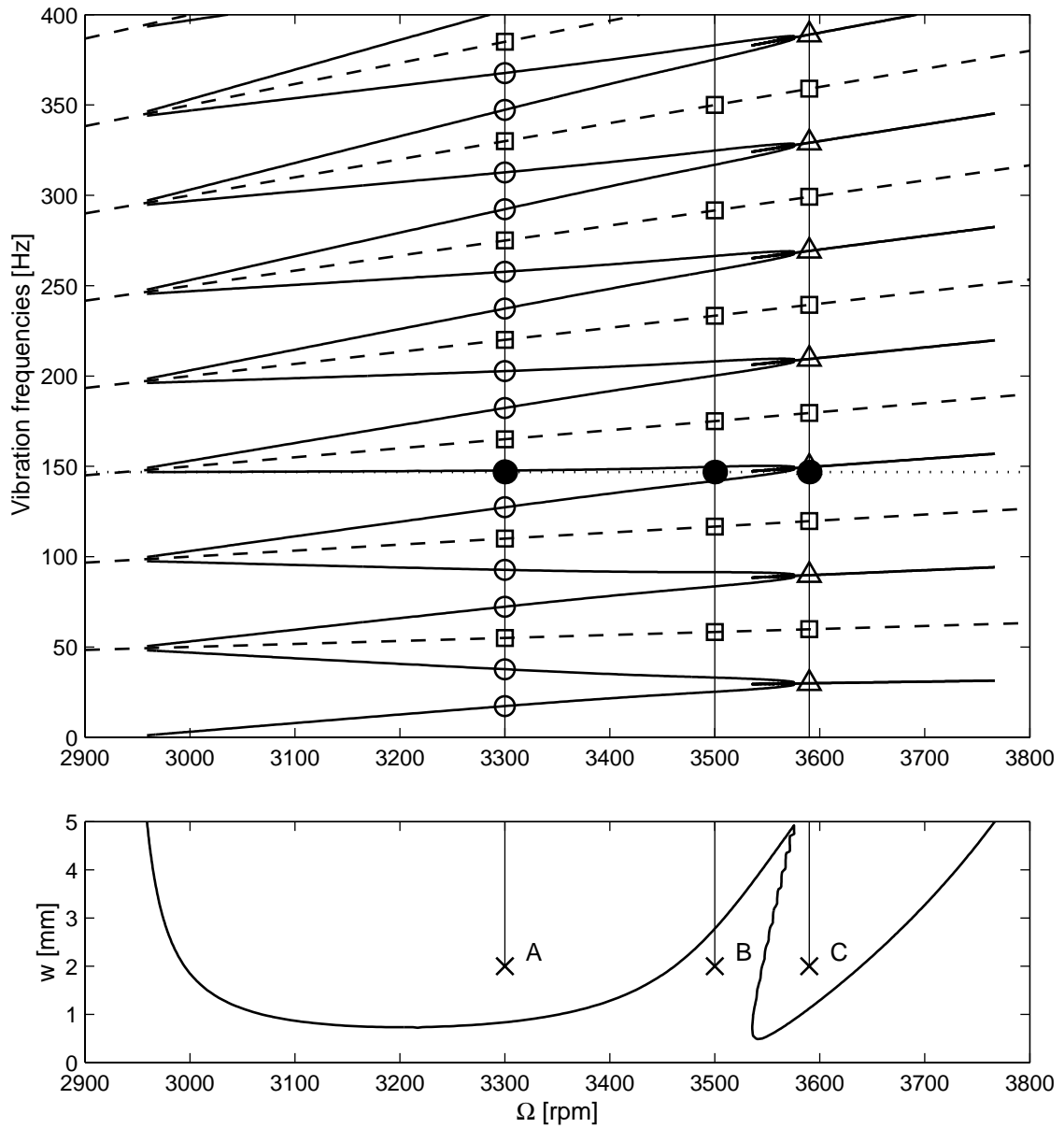
Figure 6.16: Theoretical vibration frequencies (continuous $-$ f_H and f_{PD}, dashed $-$ f_{TPE}, dotted $-$ f_d) and experimental ones
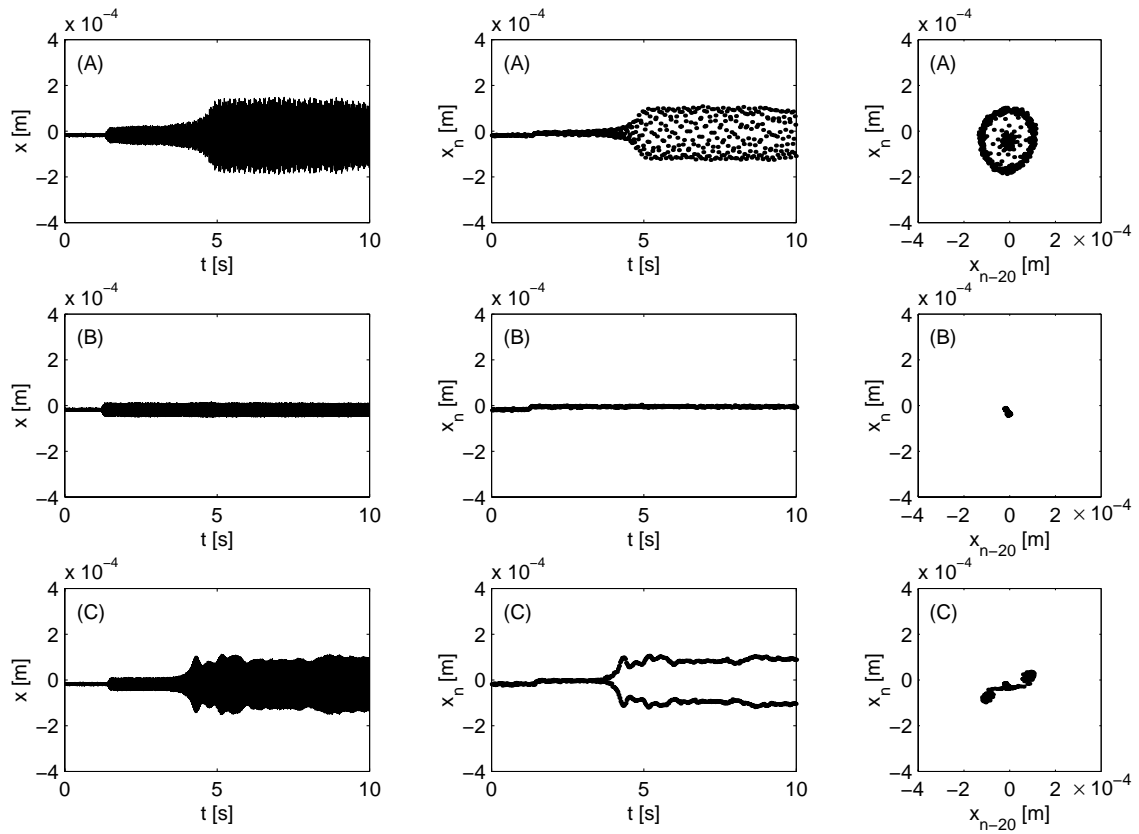
Figure 6.17: Continuous time histories, 1/rev sampled signals, and Poincaré sections for parameter points A, B and C

followed in the chatter frequency plots of Figures 6.15 and 6.16. For a secondary Hopf type chatter, there are two f_H-frequencies in the neighbor of each f_{TPE}-frequencies, one below, and one above of that. As we increase the spindle speed, the f_H-frequencies move away from the f_{TPE}-frequencies until they meet the f_H-frequencies belonging to the neighborhood of the other nearby f_{TPE}-frequencies, and they meet right at the middle of two f_{TPE}-frequencies. Above this spindle speed, the bifurcation is period doubling, that is, the f_{PD}-frequencies are located just in the middle between two nearby f_{TPE}-frequencies.

Figure 6.18: Power spectra for parameter points A, B and C ($\circ$ $-$ f_H, $\triangle$ $-$ f_{PD}, $\square$ $-$ f_{TPE}, $\bullet$ $-$ f_d)

6.6 New results

Thesis 4 *The dynamic behavior of milling process was investigated. A range of stability charts were constructed that shows the transition between turning and highly interrupted milling through partial immersion milling operations as in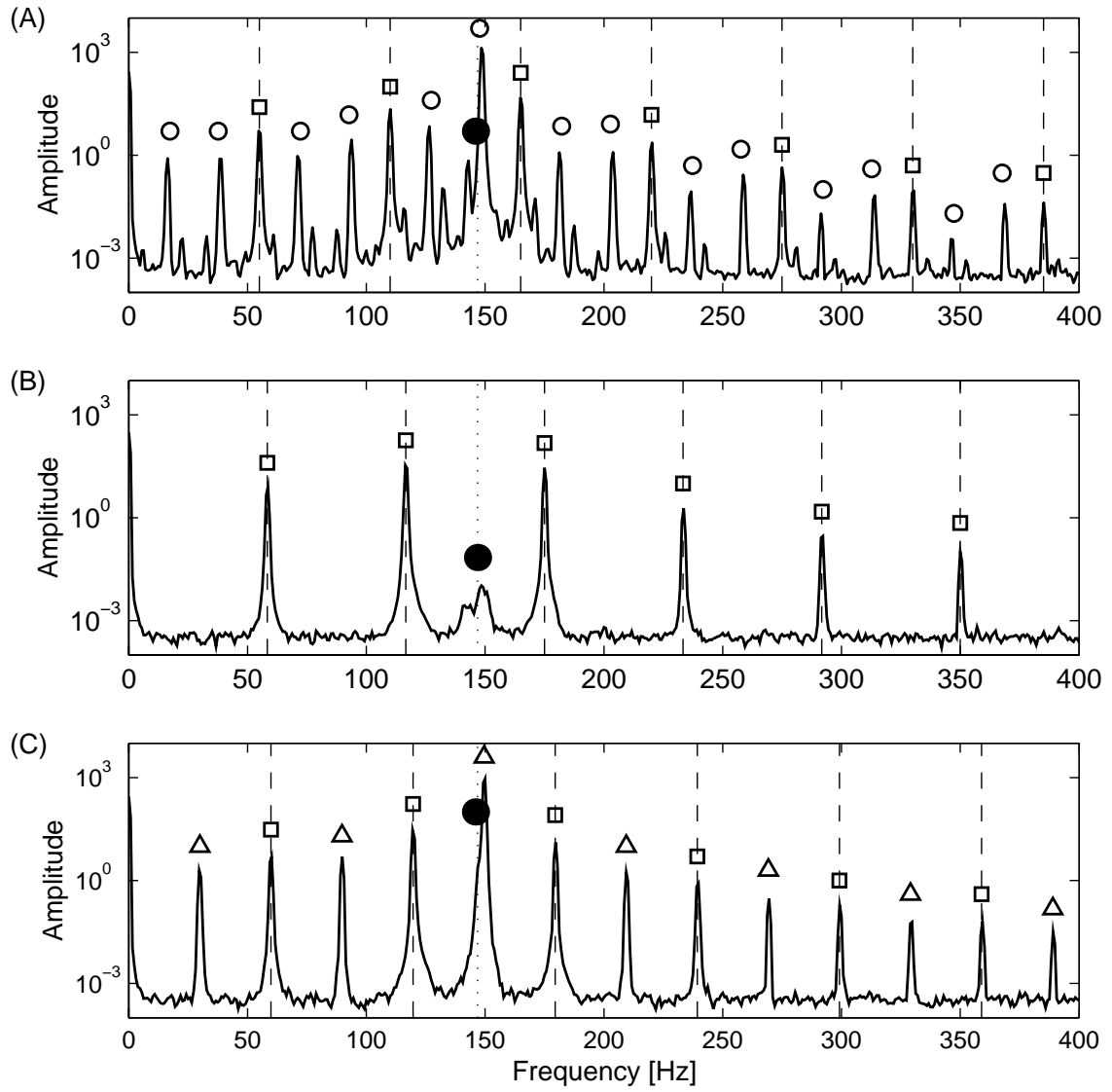termediate levels. Via localization of the relevant characteristic multipliers, the bifurcation types were identified. It was shown, that in addition to secondary Hopf bifurcation, period two bifurcation is also a typical way of stability loss.*

The transition between up-milling, full immersion milling and down-milling was investigated. It was shown, that up-milling operations have different stability properties than the down-milling operations with the same immersion. The effect of backward cutting was detected as an explanation for the intriguing stability lobes of the full immersion milling. The results were experimentally verified.

The vibration frequencies during milling operation were identified. In addition to the two types of chatter frequencies (the Hopf type frequencies or the period two type frequencies), the frequencies caused by the tooth pass excitation effect and the natural frequency of the tool were explained according to the theoretical model and also identified experimentally in the corresponding vibration signals.

Chapter 7

Turning with varying spindle speed

As it was mentioned in the introductory part of Chapter 6, continuous variation of the spindle speed can be used for suppressing chatter under certain conditions. In this chapter, this effect is investigated in turning processes.

7.1   Mathematical model

The mechanical model of the turning process in Figure 6.1 is to be used with mass m, damping c, stiffness k and feed speed v. The modeling of turning with varying spindle speed is more complex than the modeling of conventional turning or milling, in spite of the fact that the linear mathematical model is a T-periodic DDE of the simple form:

$$\ddot{\xi}(t) + 2\zeta\omega_n\dot{\xi}(t) + \omega_n^2\xi(t) = -\frac{wh}{m}\big(\xi(t) - \xi(t - \tau(t))\big), \quad \tau(t + T) = \tau(t), \qquad (7.1)$$

where $\omega_n = \sqrt{k/m}$ is the natural angular frequency, $\zeta = c/(2m\omega_n)$ is the relative damping of the tool, w is the depth of cut, h is the specific cutting coefficient and the time delay is a function of time with principal period T. The time delay variation $\tau(t)$ is due to the varying spindle speed $\Omega(t)$. Their connection can be described in the implicit form

$$\int_{t-\tau(t)}^{t} \Omega(s)/60\,\mathrm{d}s = 1\,. \qquad (7.2)$$

This means, that the workpiece makes one revolution in the time interval $[t - \tau(t), t]$ for any t.

Spindle speed variation means that the spindle speed is modulated around an average value:

$$\Omega(t) = \Omega_0 + \Omega_1 S(t)\,, \qquad (7.3)$$

where Ω_0 is the mean value, Ω_1 is the amplitude and the bounded function $S : \mathbb{R} \to [-1, 1]$ presents the shape of the variation. In practice, the modulation amplitude
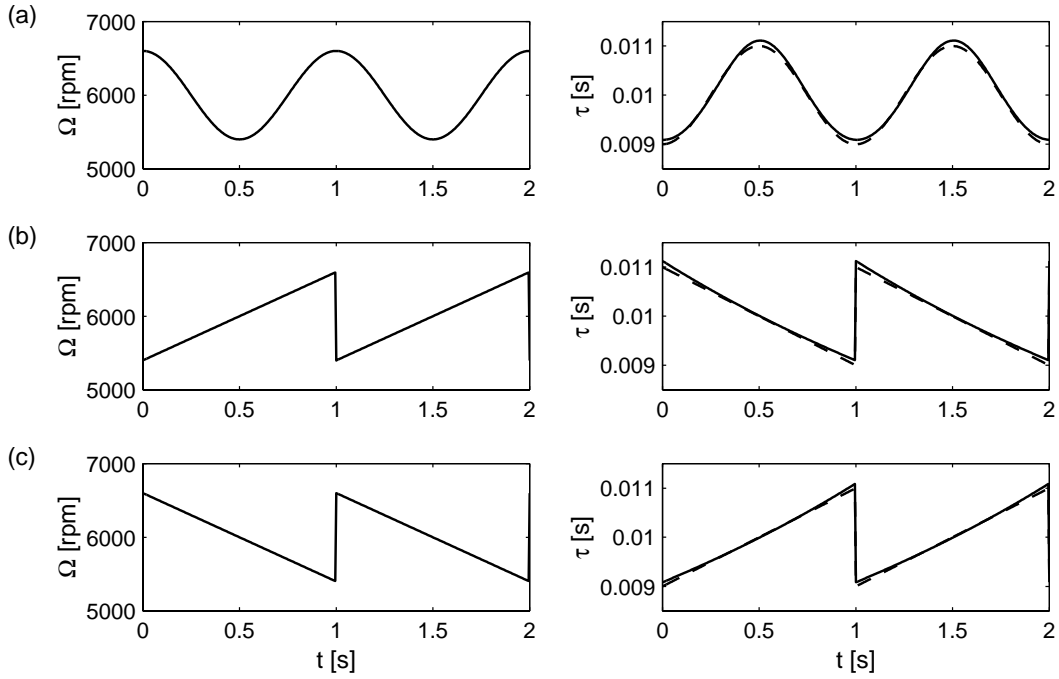
Figure 7.1: Spindle speed variations with the corresponding exact (continuous line) and approximate (dashed line) time delay variations for $\Omega_0 = 6000$ rpm, $\Omega_1 = 0.1\Omega_0$ and $T = 1$ s

cannot be greater than 20% of the mean spindle speed, i.e. $\Omega_1 < 0.2\Omega_0$. In this chapter, the following three types of spindle speed modulation are investigated (see Figure 7.1):

the cosine function: $\qquad\qquad\qquad S(t) = \cos(2\pi t/T)\,,$ $\qquad\qquad\qquad$ (7.4)

the increasing saw function: $\qquad S(t) = -1 + 2(t \bmod T)/T\,,$ $\qquad\qquad$ (7.5)

and the decreasing saw function: $\quad S(t) = 1 - 2(t \bmod T)/T\,.$ $\qquad\qquad$ (7.6)

Here, $t \bmod T$ is the residuum after the division of t by T. Although, the cosine function is the easiest to realize, the saw functions are also important cases, since they model piecewise increasing/decreasing spindle speed. These functions with discontinuities in each period cannot be generated in tool lathes, but they are useful for approximate calculations.

The exact time delay variation can be determined by solving equation (7.2) for $\tau(t)$. For the cosine type spindle speed modulation, the integration in equation (7.2) yields the implicit equation

$$\frac{1}{60}\left(\Omega_0\tau(t) + \frac{T}{2\pi}\Omega_1\Big(\sin(2\pi t/T) - \sin\big(2\pi(t-\tau(t))/T\big)\Big)\right) = 1\,. \qquad (7.7)$$

In this case, the function $\tau(t)$ cannot be given in closed form, it can only be computed

numerically.

For the saw type spindle speed modulation, the integration in equation (7.2) gives the second degree equation for $\tau(t)$:

$$\tau^2(t) + \frac{\Omega_0 T + \Omega_1\big(2(t \bmod T) - T\big)}{2\Omega}\tau(t) + \frac{60T}{\Omega_1} = 0\,, \tag{7.8}$$

where the increasing and the decreasing saw cases are given by the cases $\Omega_1 > 0$ and $\Omega_1 < 0$, respectively. The solution gives the delay variation

$$\tau(t) = \frac{\Omega_0 T + \Omega_1\big(2(t \bmod T) - T\big)}{2\Omega_1}$$
$$+ \sqrt{\left(\frac{\Omega_0 T + \Omega_1\big(2(t \bmod T) - T\big)}{2\Omega_1}\right)^2 - \frac{60T}{\Omega_1}}\,, \tag{7.9}$$

for increasing saw spindle speed, and

$$\tau(t) = \frac{-\Omega_0 T + \Omega_1\big(2(t \bmod T) - T\big)}{2\Omega_1}$$
$$- \sqrt{\left(\frac{-\Omega_0 T + \Omega_1\big(2(t \bmod T) - T\big)}{2\Omega_1}\right)^2 + \frac{60T}{\Omega_1}}\,, \tag{7.10}$$

for decreasing saw spindle speed.

As it can be seen at equation (7.7), the time delay variation $\tau(t)$ usually have no closed form, since no explicit solution of equation (7.2) can be given. Still, if Ω_1 is small enough, say, $\Omega_1 < 0.1\Omega_0$, then the approximation

$$\tau(t) \approx \tau_0 - \tau_1 S(t) \tag{7.11}$$

can effectively be used, where $\tau_0 = 60/\Omega_0$ and $\tau_1/\tau_0 = \Omega_1/\Omega_0$. In Figure 7.1, the exact time delays and the approximate ones are compared for the three types of spindle speed variation with $\Omega_1 = 0.1\Omega_0$. The maximum error of the approximations shown in Figure 7.1 is 1%, and the integrals of the exact and the approximate delay variation over the principal period T deviates by 0.5%.

If negative values of $\tau(t)$ are also allowed, then equation (7.1) is an advanced functional differential equation (AFDE), as it was mentioned in Section 2.5. In cutting processes, the advance effect cannot arise, since even in the extreme case, when $\Omega_1 > \Omega_0$, that is, when the direction of spindle rotation changes, the chip thickness may only depend on the present and a past position of the tool. This case is not important here, since the modulation is less than 20% in practice.

7.2   Stability analysis

The stability charts for turning processes with varying spindle speed can be given by analyzing the time periodic DDE (7.1).

One possible approach to this problem is to transform this equation to a DDE with periodic coefficients using a kind of power series of the delayed term. Consider the time delay in the form $\tau_0 - \tau_1 S(t)$ with a sufficiently small delay variation amplitude τ_1 and the T-periodic function $S(t)$. Then the first order Taylor series approximation with respect to τ_1 assumes the form

$$\xi\big(t - \tau_0 + \tau_1 S(t)\big) \approx \xi(t - \tau_0) + \tau_1 S(t)\dot{\xi}(t - \tau_0). \qquad (7.12)$$

The substitution of this approximation into equation (7.1) results a DDE with a constant time delay τ_0 only:

$$\ddot{\xi}(t) + 2\zeta\omega_n\dot{\xi}(t) + \omega_n^2\xi(t) = -\frac{wh}{m}\left(\xi(t) - \xi(t - \tau_0) - \tau_1 S(t)\dot{\xi}(t - \tau_0))\right). \qquad (7.13)$$

while the first derivative of the delayed term also appears with a time periodic coefficient. The mathematical justification of this approximation is quite poor, since the Taylor expansion does not converge uniformly on the set of closed intervals above the past. Also, using higher order approximation, the higher derivatives of the delayed term $\xi(t - \tau_0)$ also arise:

$$\xi\big(t - \tau_0 + \tau_1 S(t)\big) = \xi(t - \tau_0) + \tau_1 S(t)\dot{\xi}(t - \tau_0) + \frac{1}{2!}\tau_1^2 S^2(t)\ddot{\xi}(t - \tau_0)$$
$$+ \frac{1}{3!}\tau_1^3 S^3(t)\dddot{\xi}(t - \tau_0) + \dots, \qquad (7.14)$$

and neutral or advanced functional differential equations (NFDEs and AFDEs, respectively) are obtained as approximate equations. As it was mentioned in Section 2.5, the stability analysis of NFDEs is not trivial, while AFDEs are always unstable for $S(t) \equiv$ const. This also confirms that the Taylor series approach cannot be used for accurate approximation.

The semi-discretization method can effectively be used to transform equation (7.1) into an approximate discrete map, as it was shown in Chapter 5. The approximation of the time varying delay is shown in Figure 7.2. Construct the intervals $[t_i, t_{i+1})$, $i = 0, 1, \dots$ of length Δt so that $k\Delta t = T$. The delay approximation in the ith interval reads

$$\tau(t) = \left[\text{round}\left(\frac{1}{\Delta t}\int_{t_i}^{t_{i+1}}\tau(t)\mathrm{d}t - \frac{1}{2}\right)\right]\Delta t + (t - t_i). \qquad (7.15)$$

This is a kind of update of the semi-discretization from constant delay (see Figure 5.1) to time varying delay. Alternatively, it can also be considered as a special case of the
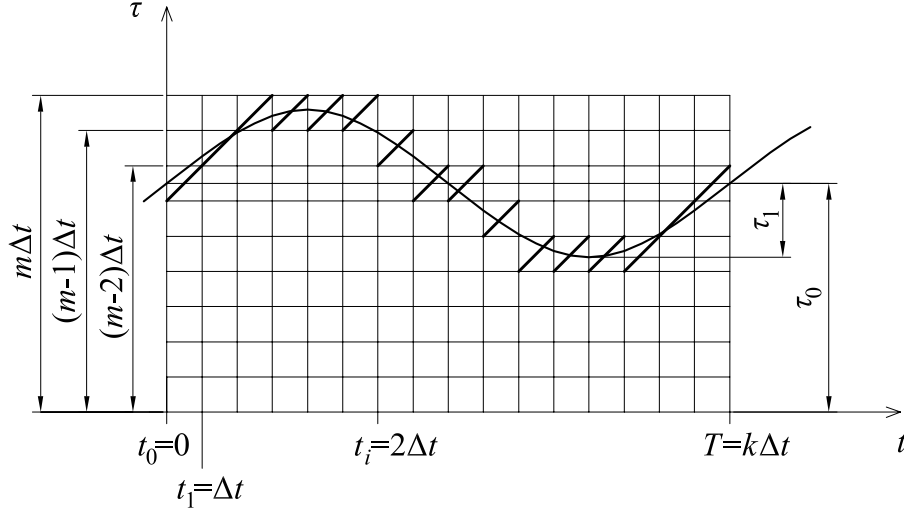
Figure 7.2: Semi-discretization of varying time delay

general method shown in Figure 5.4, since the delayed term in equation (7.1) can also be written in a Stieltjes integral form:

$$\xi(t - \tau(t)) = \int_{-\infty}^{0} f_\delta(\vartheta + \tau(t))\xi(\vartheta)d\vartheta \,, \tag{7.16}$$

where f_δ is the Dirac distribution.

Similarly to the equation (5.37), the approximate ordinary differential equation series reads

$$\ddot{\xi}(t) + 2\zeta\omega_n\dot{\xi}(t) + \left(\omega_n^2 + \frac{wh}{m}\right)\xi(t) = \frac{wh}{m}\xi(t_{i-j}) \,, \quad t \in [t_i, t_{i+1}) \,, \quad i = 0, 1, \ldots \,, \tag{7.17}$$

where

$$j = \text{round}\left(\frac{1}{\Delta t}\int_{t_i}^{t_{i+1}} \tau(t)dt - \frac{1}{2}\right) \,, \quad i = 0, 1, \ldots \,. \tag{7.18}$$

For the initial conditions $\xi(t_i) = \xi_i$, $\dot{\xi}(t_i) = \dot{\xi}_i$, the solution and its derivative at the time instant t_{i+1} can be written as

$$\xi_{i+1} = \xi(t_{i+1}) = a_{0\,0}\xi_i + a_{0\,1}\dot{\xi}_i + b_{0\,j}\,\xi_{i-j} \,, \tag{7.19}$$

$$\dot{\xi}_{i+1} = \dot{\xi}(t_{i+1}) = a_{1\,0}\xi_i + a_{1\,1}\dot{\xi}_i + b_{1\,j}\,\xi_{i-j} \,, \tag{7.20}$$

where the coefficients $a_{0\,0}$, $a_{0\,1}$, $a_{1\,0}$, $a_{1\,1}$, $b_{0\,j}$ and $b_{1\,j}$ can be computed similarly as it was done in equations (5.39) and (5.40).

Let $\max_i(j) = M$, than equations (7.19) and (7.20) defines the discrete map

$$\mathbf{y}_{i+1} = \mathbf{B}_i\mathbf{y}_i \,, \tag{7.21}$$

where the $M + 2$ dimensional vector of state variables is

$$\mathbf{y}_i = \mathrm{col}(\dot{x}_i \ \ x_i \ \ x_{i-1} \ \ \ldots \ \ x_{i-M}),\qquad(7.22)$$

and the coefficient matrix has different form for each $i = 0, 1, \ldots$ depending on the magnitude of the corresponding approximate time delay. For example, in the first interval of Figure 7.2, it is

$$\mathbf{B}_1 = \begin{pmatrix} a_{1\,1} & a_{1\,0} & 0 & \ldots & 0 & b_{1\,M-2} & 0 & 0 \\ a_{0\,1} & a_{0\,0} & 0 & \ldots & 0 & b_{0\,M-2} & 0 & 0 \\ 0 & 1 & 0 & \ldots & 0 & 0 & 0 & 0 \\ \vdots & \vdots & \vdots & \ddots & \vdots & \vdots & \vdots & \vdots \\ 0 & 0 & 0 & \ldots & 0 & 1 & 0 & 0 \\ 0 & 0 & 0 & \ldots & 0 & 0 & 1 & 0 \end{pmatrix},\qquad(7.23)$$

since

$$j = \mathrm{round}\left(\frac{1}{\Delta t}\int_{t_0}^{t_1}\tau(t)\,\mathrm{d}t - \frac{1}{2}\right) = M - 2\,.\qquad(7.24)$$

In the second interval,

$$j = \mathrm{round}\left(\frac{1}{\Delta t}\int_{t_1}^{t_2}\tau(t)\,\mathrm{d}t - \frac{1}{2}\right) = M - 1\,,\qquad(7.25)$$

and the coefficient matrix reads

$$\mathbf{B}_2 = \begin{pmatrix} a_{1\,1} & a_{1\,0} & 0 & \ldots & 0 & 0 & b_{1\,M-1} & 0 \\ a_{0\,1} & a_{0\,0} & 0 & \ldots & 0 & 0 & b_{0\,M-1} & 0 \\ 0 & 1 & 0 & \ldots & 0 & 0 & 0 & 0 \\ \vdots & \vdots & \vdots & \ddots & \vdots & \vdots & \vdots & \vdots \\ 0 & 0 & 0 & \ldots & 0 & 1 & 0 & 0 \\ 0 & 0 & 0 & \ldots & 0 & 0 & 1 & 0 \end{pmatrix}.\qquad(7.26)$$

That is, the elements $b_{0\,j}$ and $b_{1\,j}$ related to the x_{i-j} discrete variable are shifted into the $(j+2)$th column of the coefficient matrix in each interval.

Finally, the transition matrix can be given in the form

$$\mathbf{\Phi} = \mathbf{B}_{k-1}\mathbf{B}_{k-2}\ldots\mathbf{B}_0\,,\qquad(7.27)$$

and stability properties can be determined by eigenvalue investigation.

7.3 Stability charts

The turning process with a reasonable 10% spindle speed modulation is investigated. The principal period is given as a multiple of the average spindle rotation period.
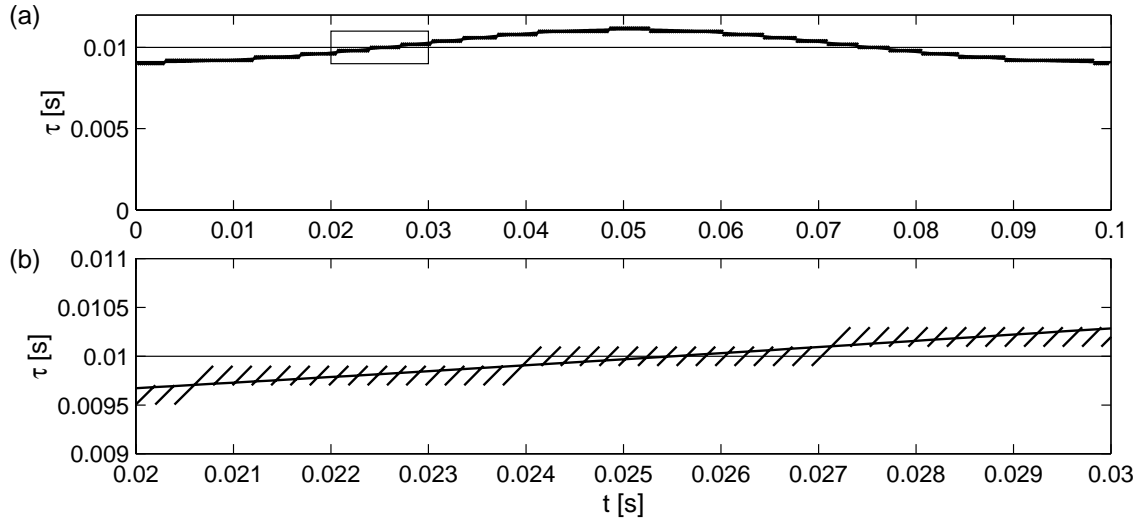
Figure 7.3: Approximation of the varying time delay for $\Omega_0 = 6000$ rpm, $T\Omega_0/60 = 10$

Stability charts are constructed for the cases $T\Omega_0/60 = 2, 10, 20$. The stability charts are presented in the plane of dimensionless spindle speed $\Omega_0/(60 f_n)$ and dimensionless depth of cut $\tilde{w} = (wh)/(m\omega_n^2)$. The relative damping is $\zeta = 0.02$.

Stability charts were constructed for approximation parameter $M = 56$. This value was chosen so that $\tau_0 = \int_0^T \tau(t)\mathrm{d}t = 50\Delta t$. The number of discretization intervals is $k = 101, 505, 1010$ according to the cases $T\Omega_0/60 = 2, 10, 20$. The approximation over the principal period and also an enlarged part of it can be seen in Figure 7.3 for the case $\Omega_0 = 6000$ rpm, $T\Omega_0/60 = 10$. The exact time delay was determined by numerical solution of the implicit equation (7.2), so the approximation (7.11) was not used.

Stability boundaries in the high-speed parameter domain (lobes 1-5) can be seen in Figures 7.4, 7.5 and 7.6 for $T\Omega_0/60 = 2$, 10 and 20, respectively. The charts denoted by (a), (b) and (c) in the figures were constructed for turning operations with cosine, increasing saw and decreasing saw spindle speed modulation, respectively. The boundary curves of the conventional turning process are also presented by thin lines, so the effect of spindle speed variation on stability can be followed. As it can be seen, the stability properties essentially improves for the case $T\Omega_0/60 = 2$, until just slight deviations arise for the cases $T\Omega_0/60 = 10$ and 20. This shows, that the effect of the speed modulation is stronger, if $T\Omega_0/60$ is small. In the opposite case, when the modulation period is large relative to the spindle rotation period $(T\Omega_0/60 \rightarrow \infty)$, the process can be considered quasi-autonomous, and the boundary curves does not deviate from the ones of the conventional turning process.

In the high-speed domain, no significant difference arises between the cosine, increasing and decreasing saw modulation.
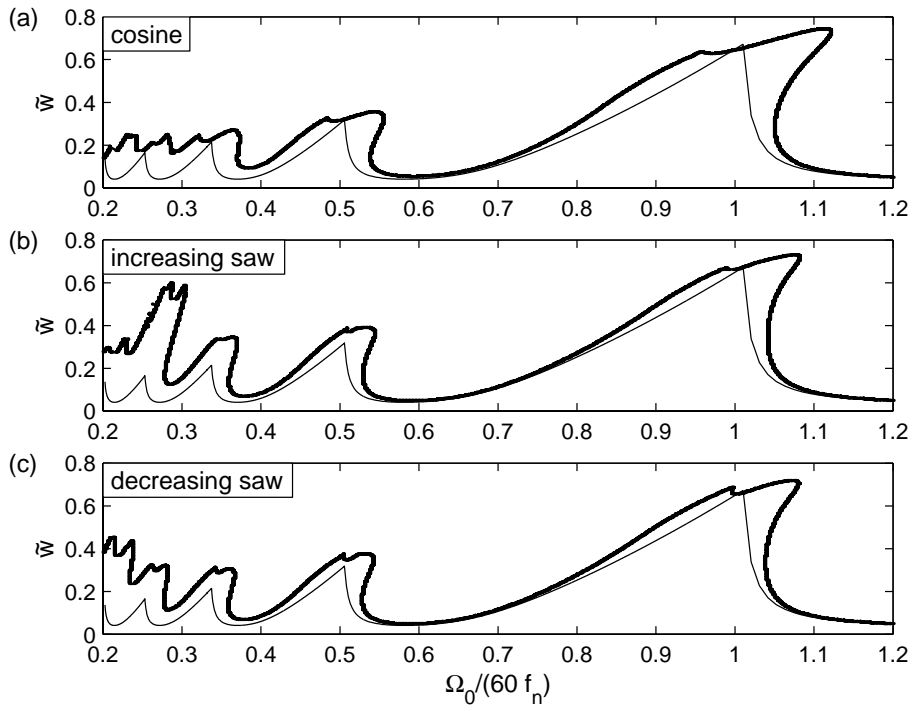
Figure 7.4: Stability charts for $T\Omega_0/60 = 2$
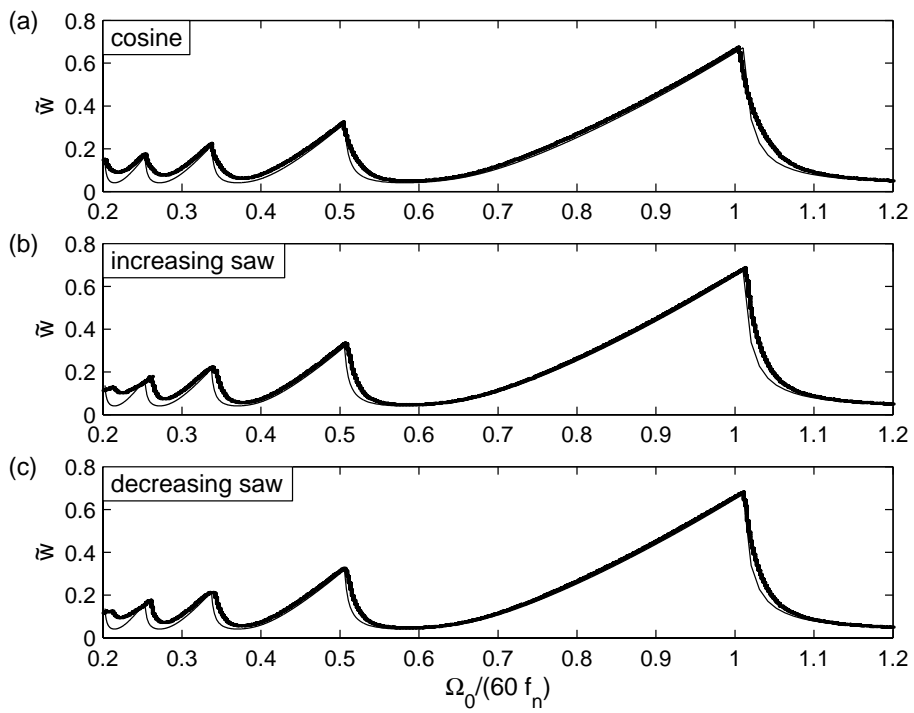
Figure 7.5: Stability charts for $T\Omega_0/60 = 10$
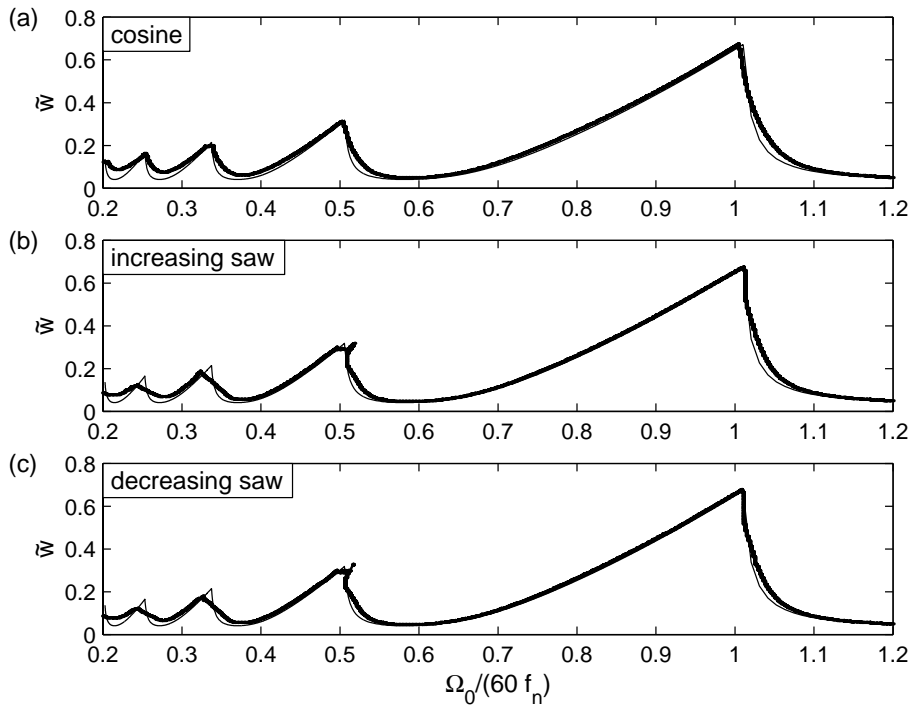
Figure 7.6: Stability charts for $T\Omega_0/60 = 20$

Although, the case $T\Omega_0/60 = 2$ results the best improvements in stability, it can hardly be realized in turning lathes, while period ratios 10 and 20 are more accessible. Also, turning operations are generally used for low spindle speed domains. In Figures 7.7 and 7.8, stability charts in the low speed parameter domain (lobes 5-11) are presented for $T\Omega_0/60 = 10$ and 20, respectively. Here, the stability improvements are more significant than in the high-speed domain. Still, these improvements are smaller in the case $T\Omega_0/60 = 20$.

In the low speed domain, the differences between the cosine, increasing and decreasing saw modulation are more conspicuous. The best improvements in stability were obtained for the cosine type modulation.
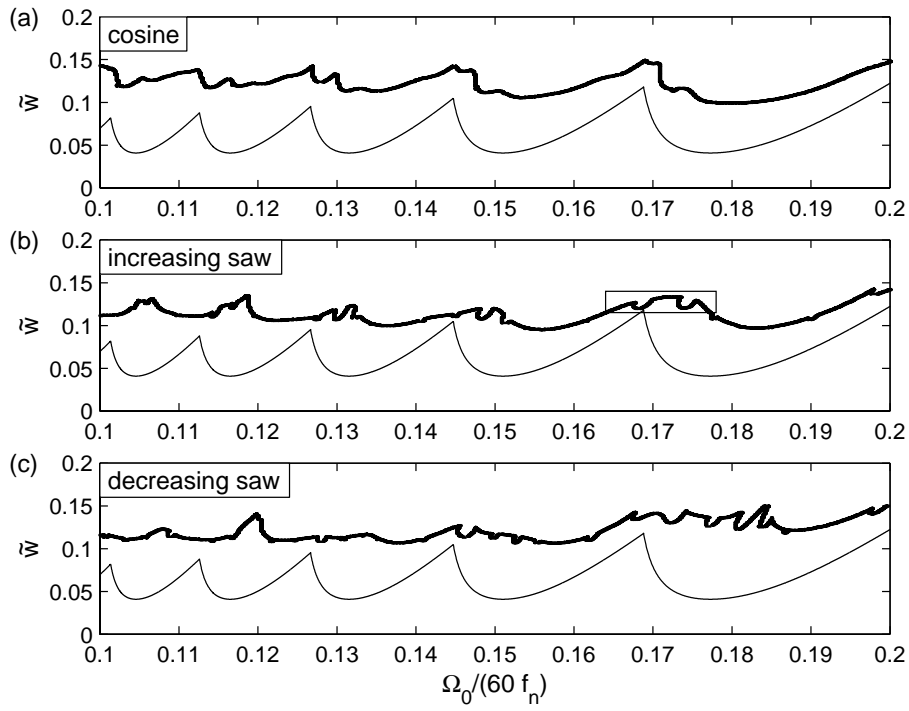
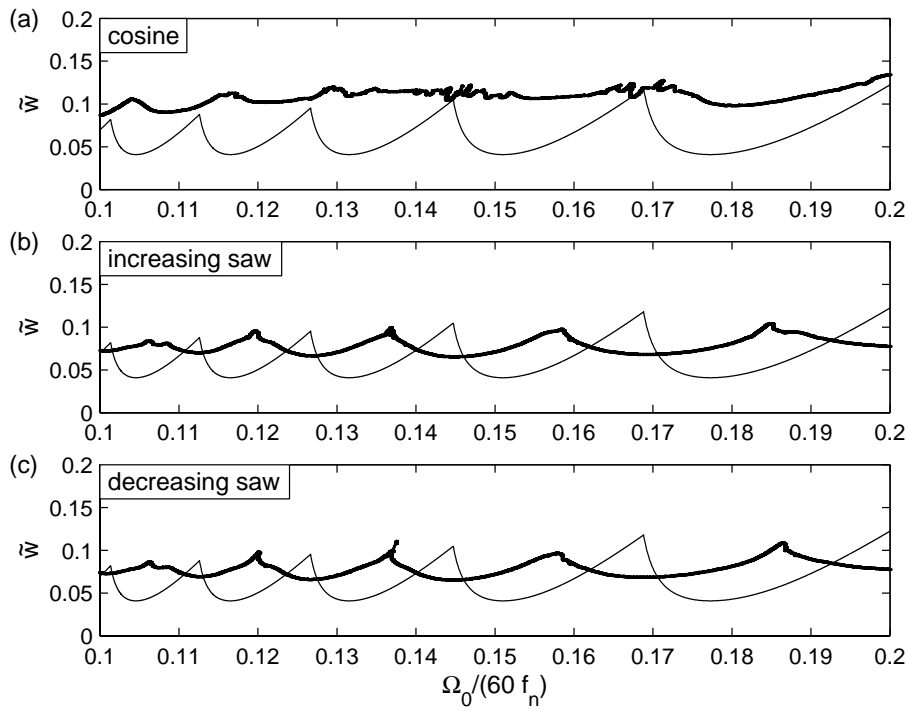Figure 7.7: Stability charts for $T\Omega_0/60 = 10$

Figure 7.8: Stability charts for $T\Omega_0/60 = 20$

7.4   Period one bifurcation in turning processes with varying spindle speed

In turning operation with varying spindle speed, another new bifurcation phenomenon arises. While, in the conventional turning processes, only Hopf bifurcation can occur, and secondary Hopf or period two (flip) can arise in conventional milling, period one bifurcations may also arise for turning with varying spindle speed. The reasoning that was used for equation (6.33) to prove that no period one bifurcation occurs for milling processes cannot be used here, since the principal period of equation (7.1) is T, and the time delayed term cannot be dropped by the substitution of $x(t - \tau(t + T)) = \mu x(t - \tau(t))$.

In milling processes, the additional flip lobes seem to arise in a clear, organized way. In turning processes with varying spindle speed, however, the new lobes has an intriguing structure. Numerical investigations of the critical characteristic multipliers shows, that boundary curves related to period one bifurcations really exist: the Hopf-type boundary curves are crossed by period one and period two type ones, one after the other. These period one and two type boundaries are not significant, since they cut off only small parts from the stable domains. Still, they are of great theoretical importance, because the arising vibrations can be either quasi-periodic (secondary Hopf bifurcation) or T-periodic (period one bifurcation) or $2T$-periodic (period two bifurcation).

In Figure 7.9, the framed part of the chart (b) in Figure 7.7 is enlarged. It presents, how a period one and a period two lobe cross the Hopf-type stability boundary.
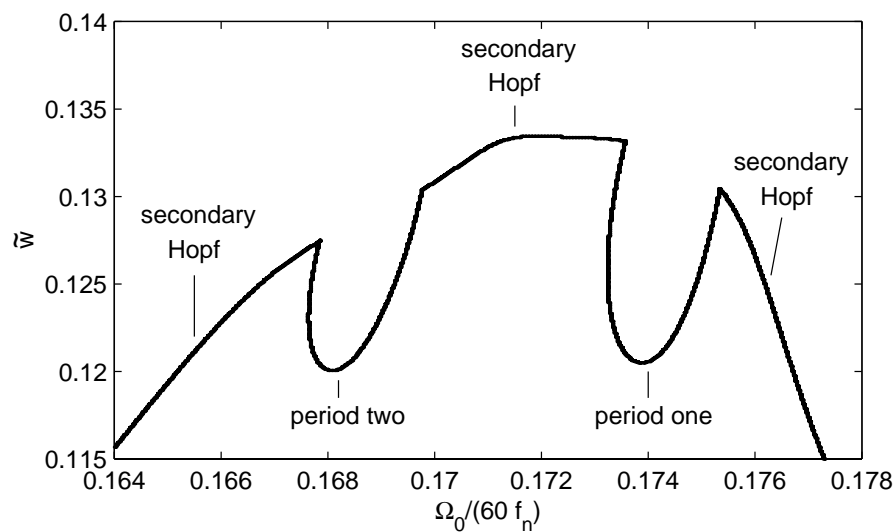
Figure 7.9: Stability boundaries and the relating bifurcation types for $T\Omega_0/60 = 10$

7.5   New results

Thesis 5 *The dynamic behavior of turning process with varying spindle speed was investigated. The connection between spindle speed variation and the resulted time varying delay in the governing equation was determined. Three types of spindle modulation was investigated, the cosine, the increasing saw and the decreasing saw.*

A range of stability charts were constructed for 10% modulation amplitude. It was shown, that the stability properties improve for low modulation period, while for high modulation period, the system can be considered quasi-autonomous, and the charts converge to the ones of the conventional turning process.

It was shown, that the stability properties improve for low mean spindle speed only, and the spindle speed variation is not an effective way of chatter suppression for high-speed cutting.

It was shown, that in addition to secondary Hopf and period two bifurcations, period one bifurcation is also a typical way of loss of stability.

Appendix A

Sampling effect

Consider the equation

$$\ddot{x}(t) + c_0 x(t) = c_1 x(t_{i-1}), \quad t \in [t_i, t_{i+1}), \quad t_{i+1} - t_i = \Delta t, \quad i \in \mathbb{Z}. \tag{A.1}$$

Use the notation $x_i = x(t_i)$, $\dot{x}_i = \dot{x}(t_i)$. The periodic RFDE (A.1) can be considered as a series of ODEs for each interval $[t_i, t_{i+1})$. The connection between x_i and $\dot{x}_i$ defines a discrete map. Stability conditions for equation (A.1) can be given by analyzing this discrete map.

The general solution of equation (A.1) in the interval $[t_i, t_{i+1})$ reads

$$x(t) = K_{1i} \cos\left(\sqrt{c_0}\right)(t - t_j)) + K_{2i} \sin\left(\sqrt{c_0}\,(t - t_j)\right) + \frac{c_1}{c_0} x_{i-1}. \tag{A.2}$$

The initial values x_i, $\dot{x}_i$ determine the coefficients K_{1i} and K_{2i}:

$$x(t_i) = K_{1i} + \frac{c_1}{c_0} x_{i-1} = x_i \qquad \Rightarrow \qquad K_{1i} = x_i - \frac{c_1}{c_0} x_{i-1}, \tag{A.3}$$

$$\dot{x}_i(t) = \sqrt{c_0} K_{2i} = \dot{x}_i \qquad \Rightarrow \qquad K_{2i} = \frac{1}{\sqrt{c_0}} \dot{x}_i. \tag{A.4}$$

Substitution of equations (A.3) and (A.4) into equation (A.2), and $t = t_{i+1}$ yield

$$x_{i+1} = \cos\left(\sqrt{c_0}\,\Delta t\right) x_i + \frac{1}{\sqrt{c_0}} \sin\left(\sqrt{c_0}\,\Delta t\right) \dot{x}_i + \frac{c_1}{c_0}\left(1 - \cos\left(\sqrt{c_0}\,\Delta t\right)\right) x_{i-1}, \tag{A.5}$$

$$\dot{x}_{i+1} = -\sqrt{c_0} \sin\left(\sqrt{c_0}\,\Delta t\right) x_i + \cos\left(\sqrt{c_0}\,\Delta t\right) \dot{x}_i + \frac{c_1}{\sqrt{c_0}} \sin\left(\sqrt{c_0}\,\Delta t\right) x_{i-1}. \tag{A.6}$$

The discrete map mentioned above can be given in the form

$$\begin{pmatrix} \dot{x}_{i+1} \\ x_{i+1} \\ x_i \end{pmatrix} = \begin{pmatrix} C & -S\sqrt{c_0} & S\,c_1/\sqrt{c_0} \\ S/\sqrt{c_0} & C & (1-C)\,c_1/c_0 \\ 0 & 1 & 0 \end{pmatrix} \begin{pmatrix} \dot{x}_i \\ x_i \\ x_{i-1} \end{pmatrix}, \tag{A.7}$$

where $C = \cos\left(\sqrt{c_0}\,\Delta t\right)$ and $S = \sin\left(\sqrt{c_0}\,\Delta t\right)$.

Stability properties are determined by the eigenvalues of the coefficient matrix. The characteristic equation reads

$$D(\mu) = \det \begin{pmatrix} C - \mu & -S\sqrt{c_0} & Sc_1/\sqrt{c_0} \\ S/\sqrt{c_0} & C - \mu & (1-C)c_1/c_0 \\ 0 & 1 & -\mu \end{pmatrix}$$

$$= -\mu \left(C^2 - 2\mu C + \mu^2 + S^2 \right) - \left(\frac{c_1}{c_0}(C-\mu)(1-C) - \frac{c_1}{c_0}S^2 \right) \tag{A.8}$$

$$= -\mu^3 + 2C\mu^2 + \left(\frac{c_1}{c_0}(1-C) - 1 \right)\mu + \frac{c_1}{c_0}(1-C) = 0 \,.$$

Equation (A.1) is asymptotically stable, if all the solutions of the characteristic equation (A.8) are in modulus less than one. To check this condition, the so-called Möbius transformation $\mu = (\eta+1)/(\eta-1)$ is used, that transforms the unit disc of the complex plane to the left half of the complex plane. Since $|\mu| < 1$ if and only if $\mathrm{Re}\,\eta < 0$, the Routh-Hurwitz criteria can be used as the condition of asymptotic stability for η.

Substitution of $\mu = (\eta + 1)/(\eta - 1)$ into equation (A.8) and multiplication with $(\eta - 1)^3$ results

$$D(\eta) = -(\eta + 1)^3 + 2C(\eta + 1)^2(\eta - 1)$$

$$+ \left(\frac{c_1}{c_0}(1-C) - 1 \right)(\eta + 1)(\eta - 1)^2 + \frac{c_1}{c_0}(1-C)(\eta - 1)^3$$

$$= 2(C-1)\left(1 - \frac{c_1}{c_0} \right)\eta^3 + 2(C-1)\left(1 + 2\frac{c_1}{c_0} \right)\eta^2 \tag{A.9}$$

$$+ \left(-2(C+1) + 2\frac{c_1}{c_0}(1-C) \right)\eta - 2(C+1) = 0 \,.$$

According to the Routh-Hurwitz criteria, stability conditions are defined by the coefficients of η^3, η^2, η^1, η^0, denoted by a_3, a_2, a_1, a_0, respectively. After the substitution of C and S defined in equation (A.7), the coefficients read

$$a_3 = (1 - \cos(\sqrt{c_0}\,\Delta t))\left(1 - \frac{c_1}{c_0} \right) , \tag{A.10}$$

$$a_2 = (1 - \cos(\sqrt{c_0}\,\Delta t))\left(1 + 2\frac{c_1}{c_0} \right) , \tag{A.11}$$

$$a_1 = \frac{c_1}{c_0}(-1 + \cos(\sqrt{c_0}\,\Delta t)) + 1 + \cos(\sqrt{c_0}\,\Delta t) , \tag{A.12}$$

$$a_0 = 1 + \cos(\sqrt{c_0}\,\Delta t) \,. \tag{A.13}$$

If the sign of all the coefficients are the same (e.g. positive, in this case), and the Hurwitz determinant H_2 is positive, than equation (A.1) is asymptotically stable. Here, the Hurwitz determinant H_2 reads

$$H_2 = a_1 a_2 - a_0 a_3$$

$$= 2\frac{c_1}{c_0^2}(1 - \cos(\sqrt{c_0}\,\Delta t))(c_0(1 + 2\cos(\sqrt{c_0}\,\Delta t)) - c_1(1 - \cos(\sqrt{c_0}\,\Delta t))) \,. \tag{A.14}$$

Now, the stability conditions are as follows

$$a_3 > 0 : \qquad 1 - \cos\left(\sqrt{c_0}\,\Delta t\right) \neq 0 \quad \Rightarrow \quad c_0 \neq \frac{(2k)^2\pi^2}{(\Delta t)^2}, \quad k = 0, 1, \ldots, \tag{A.15}$$

and

$$1 - \frac{c_1}{c_0} > 0 \quad \Rightarrow \quad c_1 < c_0, \tag{A.16}$$

$$a_2 > 0 : \qquad 1 - \cos\left(\sqrt{c_0}\,\Delta t\right) \neq 0 \quad \Rightarrow \quad c_0 \neq \frac{(2k)^2\pi^2}{(\Delta t)^2}, \quad k = 0, 1, \ldots, \tag{A.17}$$

and

$$1 + 2\frac{c_1}{c_0} > 0 \quad \Rightarrow \quad c_1 > -\frac{1}{2}c_0, \tag{A.18}$$

$$a_1 > 0 : \qquad \frac{c_1}{c_0}\left(-1 + \cos\left(\sqrt{c_0}\,\Delta t\right)\right) + 1 + \cos\left(\sqrt{c_0}\,\Delta t\right) > 0$$

$$\Rightarrow \quad c_1 < \frac{1 + \cos\left(\sqrt{c_0}\,\Delta t\right)}{1 - \cos\left(\sqrt{c_0}\,\Delta t\right)}c_0, \quad c_0 \neq \frac{(2k)^2\pi^2}{(\Delta t)^2}, \quad k = 0, 1, \ldots, \tag{A.19}$$

$$a_0 > 0 : \qquad 1 + \cos\left(\sqrt{c_0}\,\Delta t\right) > 0 \quad \Rightarrow \quad c_0 \neq \frac{(2k+1)^2\pi^2}{(\Delta t)^2}, \quad k = 0, 1, \ldots, \tag{A.20}$$

$$H_2 > 0 : \qquad \cos\left(\sqrt{c_0}\,\Delta t\right) \neq 0 \quad \Rightarrow \quad c_0 \neq \frac{(2k)^2\pi^2}{(\Delta t)^2}, \quad k = 0, 1, \ldots, \tag{A.21}$$

and

$$0 < c_1 < \frac{1 + 2\cos\left(\sqrt{c_0}\,\Delta t\right)}{1 - \cos\left(\sqrt{c_0}\,\Delta t\right)}c_0, \tag{A.22}$$

or

$$0 > c_1 > \frac{1 + 2\cos\left(\sqrt{c_0}\,\Delta t\right)}{1 - \cos\left(\sqrt{c_0}\,\Delta t\right)}c_0. \tag{A.23}$$

While condition (A.22) fulfils for the domains $0 < c_0 < 1/4$ or $(1 + 3k/2)^2 < c_0 < (2 + 3k/2)^2$, condition (A.23) is satisfied for $(1/2 + 3k/2)^2 < c_0 < (1 + 3k/2)^2$.

Finally, conditions (A.15)-(A.23) define the stability criteria for equation (A.1) as

$$c_1 < c_0, \quad c_0 \neq \frac{k^2\pi^2}{\Delta t^2}, \quad k = 0, 1, \ldots, \tag{A.24}$$

and

$$0 < c_1 < \frac{1 + 2\cos\left(\sqrt{c_0}\Delta t\right)}{1 - \cos\left(\sqrt{c_0}\Delta t\right)}c_0 \quad \text{or} \quad 0 > c_1 > \frac{1 + 2\cos\left(\sqrt{c_0}\Delta t\right)}{1 - \cos\left(\sqrt{c_0}\Delta t\right)}c_0. \tag{A.25}$$

References

[1] Altintas, Y., Budak, E. (1995) Analytical prediction of stability lobes in milling, *Annals of the CIRP*, **44**(1), pp. 357-362.

[2] Altintas, Y., Engin, S., Budak, E. (1999a) Analytical stability prediction and design of variable pitch cutters, *Journal of Manufacturing Science and Engineering*, **121**, pp. 173-178.

[3] Altintas, Y., Shamato, E., Lee, P., Budak, E. (1999b) Analytical prediction of stability lobes in ball end milling, *Journal of Manufacturing Science and Engineering*, **121**, pp. 586-592.

[4] Altintas, Y., Lee, P. (1996) A general mechanics and dynamics model for helical end mills, *Annals of the CIRP*, **45**(1), pp. 59-64.

[5] Altintas, Y., Lee, P. (1998) Mechanics and dynamics of ball end milling, *Journal of Manufacturing Science and Engineering*, **120**, pp. 684-692.

[6] Andronov, A. A., Leontovich, E. A. (1937) Some cases of dependence of limit cycles on parameters, *Uchenie Zapiski Gor'kovskovo Gos. Univ.*, **6**, pp. 3-24.

[7] Arino, O., Nosov, V. R. (1998) On stability of a class of neutral type functional differential equations, *Mathematics and Computers in Simulation*, **45**, pp. 299-307.

[8] Arnold, V. I. (1978) *Mathematical Methods of Classical Mechanics*, Springer-Verlag, Berlin.

[9] Balachandran, B. (2001) Non-linear dynamics of milling process, *Philosophical Transactions of the Royal Society*, **359**, pp. 793-820.

[10] Balachandran, B., Zhao, M. X. (2000) A mechanics based model for study of dynamics of milling operations, *Meccanica*, **35**(2), pp. 89-109.

[11] Bali, J. (1988) *Cutting* (in Hungarian), Tankkönyvkiadó, Budapest.

[12] Batzer, S. A., Gouskov, A. M., Voronov, S. A. (1999) Modeling the vibratory drilling process, *Proceedings of the 1999 ASME Design Engineering Technical Conferences, Las Vegas, Nevada*, paper no. DETC99/VIB-8024, (CD-ROM).

[13] Bauchau, O. A., Nikishkov, Y. G. (2001) An implicit Floquet analysis for rotorcraft stability evaluation, *Journal of the American Helicopter Society*, **46**, pp. 200-209.

[14] Bayly, P. V., Halley, J. E., Mann, B. P., Davies, M. A. (2001a) Stability of interrupted cutting by temporal finite element analysis, *Proceedings of the ASME 2001 Design Engineering Technical Conferences, Pittsburgh, Pennsylvania*, paper no. DETC2001/VIB-21581 (CD-ROM).

[15] Bayly, P. V., Lamar, M. T., Calvert, S. G. (2001b) Mechanics of regenerative vibration in drilling: analytical and experimental study of the formation of lobed holes, *Proceedings of the ASME 2001 Design Engineering Technical Conferences, Pittsburgh, Pennsylvania*, paper no. DETC2001/VIB-21580 (CD-ROM).

[16] Bayly, P. V., Metzler, S. A., Schaut, A. J., Young, K. A. (2001c) Theory of torsional chatter in twist drills: model, stability analysis and composition to test, *Journal of Manufacturing Science and Engineering*, **123**(4), pp. 552-561.

[17] Bayly, P. V., Young, K. A., Calvert, S. G., Halley, J. E. (2001d) Analysis of tool oscillation and hole roundness error in a quasi-static model of reaming, *Journal of Manufacturing Science and Engineering*, **123**(3), pp. 387-396.

[18] Bayly, P. V., Mann, B. P., Schmitz, T. L., Peters, D. A., Stépán, G., Insperger, T. (2002) Effects of radial immersion and cutting direction on chatter instability in end-milling, *2002 ASME International Mechanical Engineering Congress & Exposition, New Orleans, Louisiana*, submitted.

[19] Bálint. L. (1967) *Cutting Processes Design* (in Hungarian), Műszaki Könyvkiadó, Budapest.

[20] Bellman, R., Cooke, K. (1963) *Differential-Difference Equations*, Academic Press, New York.

[21] Bhatt, S. J., Hsu, C. S. (1966) Stability criteria for second-order dynamical systems with time lag, *Journal of Applied Mechanics*, **33E**(1), pp. 113-118.

[22] Broer, H. W., Hoveijn, I., van Noort, M. (1998), A reversible bifurcation analysis of the inverted pendulum, *Physica D: Nonlinear Phenomena*, **112**(1-2), pp. 50-63.

[23] Budak, E., Altintas Y. (1998a) Analytical prediction of chatter stability in milling - Part I: General formulation, *Journal of Dynamic Systems, Measurement, and Control*, **120**, pp. 22-30.

[24] Budak, E., Altintas Y. (1998b) Analytical prediction of chatter stability in milling - Part II: Application of the general formulation to common milling systems, *Journal of Dynamic Systems, Measurement, and Control*, **120**, pp. 31-36.

[25] Butcher E. A., Sinha, S. C. (1998a) Symbolic computation of secondary bifurcations in a parametrically excited simple pendulum, *International Journal of Bifurcation and Chaos*, **8**(3), pp. 627-637.

[26] Butcher E. A., Sinha, S. C. (1998b) Symbolic computation of local stability and bifurcation surfaces for nonlinear time-periodic systems, *Nonlinear Dynamics*, **17**, pp. 1-21.

[27] Campbell S. A. (1999) Stability and bifurcation of a simple neural network with multiple time delays, *Fields Institute Communications*, **21**, pp. 65-79.

[28] Campbell S. A., Ruan, S., Wei, J. (1999) Qualitative analysis of a neural network model with multiple time delays, *International Journal of Bifurcation and Chaos*, **9**(8), pp. 1585-1595.

[29] Champneys, A., Fraser, W. B. (2000) The 'Indian rope trick' for a parametrically excited flexible rod: linearized analysis, *Proceedings of The Royal Society, Mathematical Physical and Engineering Sciences*, **456**, pp. 553-570.

[30] Cooke, K. L., Turi, J., Turner, G. (1991) Stabilization of hybrid systems in the presence of feedback delays, *IMA Preprint series, #* **906**, pp. 1-15.

[31] Corpus, W. T., Endres, W. J. (2000) A high-order solution for the added stability lobes in intermittent machining, *Proceedings of the Symposium on Machining Processes, Orlando, Florida*, **MED-11**, pp. 871-878.

[32] D'Agelo, H. (1970) *Linear Time-varying System: Analysis and Synthesis*, Allyn and Bacon, Boston.

[33] Davies, M. A. (1998) Dynamic problems in hard-turning, milling, and grinding, in *Dynamics and Chaos in Manufacturing Processes*, Ed.: Moon, F.C., Wiley, New York, pp. 57-91.

[34] Davies M. A., Balachandran, B. (2000) Impact dynamics in the milling of thin-walled structures, *Nonlinear Dynamics*, **22**(4), pp. 375-392.

[35] Davies, M. A., Burns, T. J., Schmitz, T. L. (1999) High-speed machining processes: dynamics on multiple scales, *Proceedings of the Workshop of COST P4 WG2 on Dynamics and Control of Mechanical Processing, Budapest, Hungary*, pp. 7-19.

[36] Davies, M. A., Dutterer, B., Pratt, J., Schaut, A. J. (1998) On the dynamics of high-speed milling with long, slender endmills, *Annals of the CIRP*, **47**(1), pp. 55-60.

[37] Davies, M. A., Pratt, J. R., Dutterer, B., Burns, T. J. (2001) The stability of low radial immersion milling, *Annals of the CIRP*, **49**(1), pp. 37-40.

[38] Davies, M. A., Pratt, J. R., Dutterer, B., Burns, T. J. (2002) Stability prediction for low radial immersion milling, *Journal of Manufacturing Science and Engineering*, **124**(2), pp. 217-225.

[39] Denk, R. (1995) Hill's equation systems and infinite determinants, *Mathematische Nachrichten*, **175**, pp. 47-60.

[40] Diekmann, O., van Gils, S. A., Lunel, S. M. V., Walther, H.-O. (1995) *Delay Equations*, Springer-Verlag, New York.

[41] Esterling D. M., Ren, Y., Lee, Y. S. (2002) Time-domain chatter prediction for high speed machining, *Proceedings of 2002 Annual North American Manufacturing Research Conference (NAMRC XXX), West Lafayette, Indiana*, in press.

[42] Fargue, D. (1973) Réducibilité des systèmes héréditaires à des systèmes dynamiques, *Comptes Rendus de l'Académie des Sciences, Paris*, **277**B, pp. 471-473.

[43] Farkas, M. (1994) *Periodic Motions*, Springer-Verlag, New York.

[44] Farkas, M., Stépán, G. (1992) On perturbation of the kernel in infinite delay systems, *Zeitschrift für angewandte Mathematik und Mechanik*, **72**(2), pp. 153-156.

[45] Fiagbedzi, Y. A. (2001) Periodic solutions of retarded functional differential equations, *Zeitshcrift für angewandte Mathematik und Physik*, **52**, pp. 704-712.

[46] Filho, O. C. O. (1997) On the asymptotic behavior of solutions of certain differential functional equations, *Nonlinear analysis, Theory, Methods & Applications*, **30**(2), pp. 1171-1182.

[47] Floquet, M. G. (1883) Équations différentielles linéaires à coefficients périodiques, *Annales Scientifiques de l'École Normale Supérieure*, 1883, **12**, pp. 47-89.

[48] Fofana, M. S., Bukkapatnam, S. (2001) Analysis of degenerate bifurcation in machining using a nonlinear model, *Proceedings of the ASME 2001 Design Engineering Technical Conferences, Pittsburgh, Pennsylvania*, paper no. DETC2001/VIB-21582 (CD-ROM).

[49] Garay, B. M. (1996) On structural stability of ordinary differential equations with respect to discretization methods, *Numerische Mathematik*, **72**, pp. 449-479.

[50] Garay, B. M. (1998) The discretized flow on domains of attraction: a structural stability result, *IMA Journal of Numerical Analysis*, **18**, pp. 77-90.

[51] Garay, B. M., Hilger, S. (2001) Embeddability of time scale dynamics in ode dynamics, *Nonlinear Analysis*, **47**, pp. 1357-1371.

[52] Gouskov, A. M., Voronov, S. A., Paris, H., Batzer, S. A. (2001) Cylindrical workpiece turning using multiple-cutter tool heads, *Proceedings of the ASME 2001 Design Engineering Technical Conferences, Pittsburgh, Pennsylvania*, paper no. DETC2001/VIB-21431 (CD-ROM).

[53] Gradišek, J., Govekar, E., Grabec, I. (1998a) Time series analysis in metal cutting: chatter versus chatter-free cutting, *Mechanical Systems and Processing*, **12**(6), pp. 839-854.

[54] Gradišek, J., Govekar, E., Grabec, I. (1998b) Using coarse-grained entropy rate to detect chatter in cutting, *Journal of Sound and Vibration*, **214**(5), pp. 941-952.

[55] Guckenheimer, J., Holmes, P. (1983) *Nonlinear Oscillations, Dynamical Systems, and Bifurcations of Vector Fields*, Springer-Verlag, New York.

[56]   Győri, I., Pituk, M. (1997) Stability criteria for linear delay differential equation, *Differential and Integral Equations*, **10**(5), pp. 841-852.

[57]   Győri, I., Hartung, F., Turi, J. (1995) Numerical approximations for a class of differential equations with time- and state-dependent delays, *Applied Mathematics Letters*, **8**(6), pp. 19-24.

[58]   Győri, I., Hartung, F., Turi, J. (1996) Preservation of stability in delay equations under delay perturbation, *Journal of Mathematical Analysis and Application*, **220**, pp. 290-312.

[59]   Győri, I., Turi, J. (1991) Uniform approximation of a nonlinear delay equation on infinite intervals, *Nonlinear Analysis, Theory, Methods & Applications*, **17**(1), pp. 21-29.

[60]   Hahn, W. (1961) On difference differential equation with periodic coefficients, *Journal of Mathematical Analysis and Applications*, **3**, pp. 70-101.

[61]   Halanay, A. (1961) Stability theory of linear periodic systems with delay (in Russian), *Revue de Mathématiques Pures et Appliquées*, **6**(4), pp. 633-653.

[62]   Halanay, A. (1966) *Differential Equations: Stability, Oscillations, Time Lags*, Academic Press, New York.

[63]   Hale, J. K. (1977) *Theory of Functional Differential Equations*, Springer-Verlag, New York.

[64]   Hale, J. K., Lunel, S. M. V. (1993) *Introduction to Functional Differential Equations*, Springer-Verlag, New York.

[65]   Halley, J. E. (1999) *Stability of low radial immersion milling*, MSc Thesis, Washington University, St. Louis, Missouri.

[66]   Halley, J. E., Helvey, A. M., Smith, K. S., Winfough, W. R. (1999) The impact of high-speed machining on the design and fabrication of aircraft components, *Proceedings of 1999 ASME Design and Technical Conferences, Las Vegas, Nevada*, paper no. DETC99/VIB-8057 (CD-ROM).

[67]   Hanna, N. H., Tobias, S. A. (1974) A theory of nonlinear regenerative chatter, *Journal of Engineering for industry*, **96**(1), pp. 247-255.

[68]   Hassard, B. D. (1997) Counting roots of the characteristic equation for linear delay-differential systems, *Journal of Differential Equations*, **136**, pp. 222-235.

[69]   Hill, G. W. (1886) On the part of the motion of the lunar perigee which is a function of the mean motions of the sun and moon, *Acta Mathematica*, **8**, pp. 1-36.

[70]   Hirsch, M. W., Smale, S. (1974) *Differential Equations, Dynamical Systems and Linear Algebra*, Academic Press, Berkeley.

[71]   Hopf. E. (1942) Abzweigung einer periodischen Lösung von einer stationären Lösung eines Differentialsystems, *Berichte über die Verhandlungen der Saechsischen Akademie der Wissenschaften zu Leipzig, Mathematisch-Naturwissenschaftliche Klasse*, **95**, pp. 3-22.

[72]   Hosho, T., Sakisaka, N, Moriyama, I. Sato, M., Higashimoto, A., Tokugana, T., Takeyama, T. (1977) Study for practical application of fluctuating speed cutting for regenerative chatter control, *Annals of the CIRP*, **25**(1), pp. 175-179.

[73]   Hsu, C. S., Bhatt, S. J. (1966) Stability charts for second-order dynamical systems with time lag, *Journal of Applied Mechanics*, **33E**(1), pp. 119-124.

[74]   Hu, G.-Di, Hu, G.-Da (1996) Some simple criteria for stability of neutral delay-differential systems, *Applied Mathematics and Computation*, **80**, pp. 257-271.

[75]   Hurwitz, A. (1895) Über die Bedingungen unter welchen eine Gleichung nur Wurzeln mit negativen reellen Teilen besitz, *Mathematische Annalen*, **46**, pp. 74-81.

[76]   Inamura, T., Sata, T. (1974) Stability analysis of cutting under varying spindle speed, *Annals of the CIRP*, **23**(1), pp. 119-120.

[77]   Insperger, T., Horváth, R. (2000) Pendulum with harmonic variation of the suspension point, *Periodica Polytechnica, Mechanical Engineering*, **44**(1), pp. 39-46.

[78]   Insperger, T., Stépán, G. (2000a) Stability of the milling process, *Periodica Polytechnica, Mechanical Engineering*, **44**(1), pp. 47-57.

[79]   Insperger, T., Stépán, G. (2000b) Vibration frequencies in high-speed milling processes, *Journal of Manufacturing Science and Engineering*, submitted.

[80]   Insperger T., Stépán G. (2000c) Stability of high-speed milling, *Proceedings of Symposium on Nonlinear Dynamics and Stochastic Mechanics, Orlando, Florida*, **AMD-241**, pp. 119-123.

[81]   Insperger, T., Stépán, G. (2000d) Remote control of periodic robot motion, *Proceedings of the Thirteenth Symposium on Theory and Practice of Robots and Manipulators, Zakopane, Poland*, Springer, Wien, pp. 197-203.

[82]   Insperger, T., Stépán, G. (2001a) Stability of retarded systems with parametric excitation, *Zeitschrift für angewandte Mathematik und Mechanik*, **81**(2), pp. 195-196.

[83]   Insperger, T., Stépán, G. (2001b) Semi-discretization of delayed dynamical systems, *Proceedings of the ASME 2001 Design Engineering Technical Conferences, Pittsburgh, Pennsylvania*, paper no. DETC2001/VIB-21446 (CD-ROM).

[84]   Insperger, T., Stépán, G. (2001c) Comparison of stability lobes for up- and down-milling, *Proceedings of the Workshop of COST P4 WG2 on Dynamics and Control of Mechanical Processing, Budapest, Hungary*, pp. 53-57.

[85] Insperger, T., Stépán, G. (2002a) Stability chart for the delayed Mathieu equation, *Proceedings of The Royal Society, Mathematical Physical and Engineering Sciences*, **458**(2024), pp. 1989-1998.

[86] Insperger T., Stépán, G. (2002b) Semi-discretization method for delayed systems, *International Journal for Numerical Methods in Engineering*, **55**(5), pp. 503-518.

[87] Insperger, T., Stépán, G., Bayly, P. V., Mann, B. P. (2002) Multiple chatter frequencies in milling processes, *Journal of Sound and Vibration*, in press.

[88] Insperger, T., Stépán, G., Namachchivaya, S. (2001) Comparison of the dynamics of low immersion milling and cutting with varying spindle speed, *Proceedings of the ASME 2001 Design Engineering Technical Conferences, Pittsburgh, Pennsylvania*, paper no. DETC2001/VIB-21616 (CD-ROM).

[89] Jayaram, S., Kapoor, S. G., DeVor, R. E. (2000) Analytical stability analysis of variable spindle speed machining, *Journal of Manufacturing Science and Engineering*, **122**(3), pp. 391-397.

[90] Kalmár-Nagy, T., Pratt, J.R., Davies, M.A., Kennedy, M. (1999) Experimental and analytical investigation of the subcritical instability in metal cutting, *Proceedings of the 1999 ASME Design Engineering Technical Conferences, Las Vegas, Nevada*, paper no. DETC99/VIB-8060, (CD-ROM).

[91] Karsai, G. (1996) Stability of periodic operating dynamic systems, *Periodica Polytechnika, Mechanical Engineering*, **40**(1), pp. 45-57.

[92] Khusainov, D. Ya., Yun'kova, E. V. (1988) Investigation of the stability of linear systems of neutral type by the Lyapunov function method, *Differencial'niye Uravneniya*, **24**, pp. 613-621.

[93] Kim, W. S., Bejczy, A. K. (1993) Special issue on space robotics, *IEEE Transactions on Robotics and Automation*, **10**(5).

[94] Kolmanovskii, V. B., Nosov, V. R. (1986) *Stability of Functional Differential Equations*, Academic Press, London.

[95] Kordonis, I.-G. E., Philos, Ch. G. (1998) Oscillation and nonoscillation in linear delay or advanced difference equations, *Mathematical and Computer Modelling*, **27**(7), pp. 11-21.

[96] Kondo, E., Ota, H., Kawai, T. (1992) Regenerative chatter vibrations of turning workpiece, *Transactions of the Japan Society*, **58**, pp. 1251-1265.

[97] Kovács, L. L., Stépán, G. (2002) Dynamics of digital force control applied in rehabilitation robotics, *Meccanica*, in press.

[98] Kudinov, V. A. (1955) Theory of vibration generated from metal cutting (in Russian), *New Technology of Mechanical Engineering*, Moscow: USSR Academy of Sciences Publishing House, pp. 1-7.

[99]   Kudinov, V. A. (1967) *Dynamics of Tool-Lathe* (in Russian), Mashinostroenie, Moscow.

[100] Lakshmikantham, V., Trigiante, D. (1988) *Theory of Difference Equations, Numerical Methods and Applications*, Academic Press, London.

[101] Laczik, B. (1986) *Vibration monitoring of cutting processes* (in Hungarian), PhD Thesis, Technical University of Budapest, Budapest, Hungary.

[102] Li, L. M. (1988) Stability of linear neutral delay-differential systems, *Bulletin of the Australian Mathematical Society*, **38**, pp. 339-344.

[103] Listyn, E., Stavroulakis, I. P. (2001) On the oscillation of solutions of higher order Emden-Fowler state dependent advanced differential equations, *Nonlinear Analysis*, **47**, pp. 3877-3883.

[104] Ludvig, Gy. (1973) *Dynamics of Machines* (in Hungarian), Műszaki Könyvkiadó, Budapest.

[105] Mann, B. P. (2001) Personal communications.

[106] Mathieu, E. (1868) Mémoire sur le mouvement vibratoire ďune membrane de forme elliptique, *J. Math. Pure Appl.*, **13**, pp. 137-203.

[107] Márialigeti, J. (1995) Computer simulation of the influence of tooth errors on gear dynamic behaviour, *Periodica Polytechnika, Transportation Engineering*, **23**(1-2), pp. 89-105.

[108] Márialigeti, J. (1997) Simulation study of the influence of involute tip relief on gear dynamic behaviour, *Periodica Polytechnika, Transportation Engineering*, **25**(1-2), pp. 59-77.

[109] Mennicken, R. (1968) On the convergence of infinite Hill-type determinants, *Archive for Rational Mechanics and Analysis*, **30**, pp. 12-37.

[110] Metallidis, P., Natsiavas, S. (2000) Vibration of a continuous system with clearance and motion constraints, *International Journal of Non-Linear Mechanics*, **35**(4), pp. 675-690.

[111] Minis, I., Yanushevsky, R. (1993) A new theoretical approach for the prediction of machine tool chatter in milling, *Journal of Engineering for Industry*, **115,** pp. 1-8.

[112] Minorsky, N. (1942) Selfexcited oscillations in dynamical systems possessing retarded actions, *Journal of Applied Mechanics*, **9**, pp. 65-71.

[113] Moon, F.C. (1998) *Dynamics and Chaos in Manufacturing Processes*, Wiley, New York.

[114] Müller, T., Stépán, G. (1994) Stability and robustness of force controlled machines, *Zeitschrift für angewandte Mathematik und Mechanik*, **74**(4), pp. 152-153.

[115] Myshkis, A. D. (1949) General theory of differential equations with delay, *Uspehi Matematitseskih Nauk*, **4**(5), pp. 99-141. [*English Translation: AMS* (1951), **55**, pp. 1-62.]

[116] Myshkis, A. D. (1955) *Lineare Differentialgleichungen mit nacheilendem Argument*, Deutscher Verlag der Wissenschaften, Berlin.

[117] Namachchivaya, N. S., Sowers, R. B., van Roessel H. J. (2001) Unified approach for noisy nonlinear Mathieu-type systems, *Proceedings of the ASME 2001 Design Engineering Technical Conferences, Pittsburgh, Pennsylvania*, paper no. DETC2001/VIB-21590 (CD-ROM).

[118] Nayfeh, A. H., Chin, C. M., Pratt, J. (1997) Perturbation methods in nonlinear dynamics - applications to machining dynamics, *Journal of Manufacturing Science and Engineering*, **119**, pp. 485-493.

[119] Nayfeh, A. H., Mook, D. T. (1979) *Nonlinear Oscillations*, John Wiley and Sons, New York.

[120] Neimark, Ju. I. (1949) D-subdivision and spaces of quasi-polynomials (in Russian), *Prikladnaja Mathematika i Mechanika*, **13**(4), pp. 349-380.

[121] Patkó, Gy., Kollányi, T. (1999) Non-linear parametrically excited vibrations in belt drives of machine tools, *Proceedings of 10th World Congress on the Theory of Machines and Mechanisms, Oulu, Finland*.

[122] Park, Ju. H., Won, S. (2000) Stability analysis for neutral delay-differential systems, *Journal of the Franklin Institute*, **337**, pp. 1-9.

[123] Perko, L. (1996) *Differential Equations and Dynamical Systems*, Springer-Verlag, New York.

[124] Péics, H. (2000) Representation of solutions of difference equations with continuous time, *Electronic Journal of Qualitative Theory of Differential Equations: Proceedings of the 6'th Colloquium on the Qualitative Theory of Differential Equations*, No. 21., pp. 1-8.

[125] Pontryagin, L. S. (1942) On the zeros of some elementary transcendental functions (in Russian), *Izvestiya Akademiya Nauk SSSR*, **6**(3), pp. 115-134.

[126] Ramani, D. V., Rand, R. H., Keith, W. L. (2001) Perturbation solution for secondary bifurcation in the quadratically-damped Mathieu equation, *Proceedings of the ASME 2001 Design Engineering Technical Conferences, Pittsburgh, Pennsylvania*, paper no. DETC2001/VIB-21587 (CD-ROM).

[127] Rayleigh (Strutt) J. W. (1887) On the maintenance of vibrations by forces of double frequency, and on the propagation of waves through a medium endowed with a periodic structure, *Philosophical Magazine and Journal of Science*, **24**, pp. 145-159.

[128] Routh, E. J. (1877) *A Treatise on the Stability of a Given State of Motion*, Macmillan, London.

[129] von Schlippe, B., Dietrich, R. (1941) Shimmying of a pneumatic wheel, *Lilienthal-Gesellschaft für Luftfahrtforschung, Bericht*, **140**, translated for the AAF in 1947 by Meyer & Company, pp. 125-160.

[130] Schmitz, T. L., Davies, M. A., Medicus, K., Snyder, J. (2001) Improving high-speed machining material removal rates by rapid dynamic analysis, *Annals of the CIRP*, **50**(1), pp. 263-268.

[131] Seagalman, D. J., Butcher, E. A. (2000) Suppression of regenerative chatter via impendance modulation, *Journal of Vibration and Control*, **6**, pp. 243-256.

[132] Sexton, J. S., Milne, R. D., Stone, B. J. (1977) A stability analysis of single point machining with varying spindle speed, *Applied Mathematical Modelling*, **1**, pp. 310-318.

[133] Sexton, J. S., Stone, B. J. (1978) The stability of machining with continuously varying spindle speed, *Annals of the CIRP*, **27**(1), pp. 321-326.

[134] Shi, H. M., Tobias, S. A. (1984) Theory of finite amplitude machine tool instability, *International Journal of Machine Tool Design and Research*, **24**, pp. 45-69.

[135] Sinha, S. C., Wu, D. H. (1991) An efficient computational scheme for the analysis of periodic systems, *Journal of Sound and Vibration*, **151**, pp. 91-117.

[136] Sinha, S. C., Butcher, E. A. (1997) Symbolic computation of fundamental solution matrices for linear time-periodic dynamical systems, *Journal of Sound and Vibration*, **206**, pp. 61-85.

[137] Sitz, A., Schwarz U., Kurths J., Maus, D., Wiese, M., Warnecke, G. (2001) Signatures of acoustic emission signals generated during high speed cutting, *Proceedings of the ASME 2001 Design Engineering Technical Conferences, Pittsburgh, Pennsylvania*, paper no. DETC2001/VIB-21618 (CD-ROM).

[138] Smith, S., Tlusty, J. (1991) An overview of modeling and simulation of the milling process, *Journal of Engineering for Industry*, **113**, pp. 169-175.

[139] Smith, S., Tlusty, J. (1993) Efficient simulation programs for chatter in milling, *Annals of the CIRP*, **42**(1), pp. 463-466.

[140] Stephenson, A. (1908) On a new type of dynamical stability, *Memoirs and Proceedings of the Manchester Literary and Philosophical Society*, **52**, pp. 1-10.

[141] Stépán, G. (1989) *Retarded Dynamical Systems*, Longman, Harlow.

[142] Stépán, G. (1991) Varying delay and stability in dynamical systems, *Zeitschrift für angewandte Mathematik und Mechanik*, **71**(4), pp. 154-156.

[143] Stépán, G. (1998) Delay-differential equation models for machine tool chatter, in *Dynamics and Chaos in Manufacturing Processes*, Ed.: Moon, F.C., Wiley, New York, pp. 165-192.

[144] Stépán, G. (2001a) Vibrations of machines subjected to digital force control, *International Journal of Solids and Structures*, **38**(10-13), pp. 2149-2159.

[145] Stépán, G. (2001b) Modelling nonlinear regenerative effects in metal cutting, *Philosophical Transactions of the Royal Society*, **359**, pp. 739-757.

[146] Stépán, G., Haller, G. (1995) Quasiperiodic oscillations in robot dynamics, *Nonlinear Dynamics*, **8**, pp. 513-528.

[147] Stépán, G., Kalmár-Nagy, T. (1997) Nonlinear regenerative machine tool vibration, *Proceedings of the 1997 ASME Design Engineering Technical Conferences, Sacramento, California*, paper no. DETC97/VIB-4021 (CD-ROM).

[148] Stépán, G., Steven, A. (1990) Theoretical and experimental stability analysis of a hybrid position-force controlled robot, *Proceedings of the Eighth Symposium on Theory and Practice of Robots and Manipulators, Krakow, Poland*, pp. 53-60.

[149] Stépán, G., Szalai, R. (2001) Nonlinear vibrations of highly interrupted machining, *Proceedings of the 2nd Workshop of COST P4 WG2 on Dynamics and Control of Mechanical Processing, Budapest, Hungary*, pp. 59-64.

[150] Stroinski, U. (1994) Delay-independent stability criteria for neutral differential equations, *Differential Integral Equations*, **7**(1), pp. 593-599.

[151] Stuart, A. M., Humphries, A. R. (1996) *Dynamical Systems and Numerical Analysis*, Cambridge University Press, Cambridge.

[152] Szabó, Zs. (2001) Quasi-periodic motions of articulated pipes conveying flowing fluid, *Proceedings of the ASME 2001 Design Engineering Technical Conferences, Pittsburgh, Pennsylvania*, paper no. DETC2001/VIB-214242 (CD-ROM).

[153] Szabó, Zs., Lóránt, G. (2000) Parametric excitation of a single railway wheelset, *Vehicle System Dynamics*, **33**(1), pp. 49-55.

[154] Takemura, T., Kitamura, T., Hoshi, T., Okushima, K. (1974) Active suppression of chatter by programmed variation of spindle speed, *Annals of the CIRP*, **23**(1), pp. 121-122.

[155] Taylor, F. W. (1907) On the art of cutting metals, *Transactions of ASME*, **28**, pp. 31-350.

[156] Thompson, R. A. (1986a) On the doubly regenerative stability of a grinder: the theory of chatter growth, *Journal of Engineering for Industry*, **108**, pp. 74-82.

[157] Thompson, R. A. (1986b) On the doubly regenerative stability of a grinder: the mathematical analysis of chatter growth, *Journal of Engineering for Industry*, **108**, pp. 83-92.

[158] Thompson, R. A. (1992) On the doubly regenerative stability of a grinder: the effect of contact stiffness and wave filtering, *Journal of Engineering for Industry*, **114**, pp. 53-60.

[159] Tian, J., Hutton, S. G. (2001) Chatter instability in milling systems with flexible rotating spindles - a new theoretical approach, *Journal of Manufacturing Science and Engineering*, **123**(1), pp. 1-9.

[160] Tlusty, J. (1986) Dynamics of high-speed milling, *Journal of Engineering for Industry*, **108**, pp. 59-67.

[161] Tlusty, J. (2000) *Manufacturing Processes and Equipment*, Prentice Hall, New Yersey.

[162] Tlusty, J., Polacek, A., Danek, C., Spacek, J. (1962) *Selbsterregte Schwingungen an Werkzeugmaschinen*, VEB Verlag Technik, Berlin.

[163] Tlusty, J., Smith, S., Winfough, W. R. (1996) Techniques for the use of long slender end mills in high-speed milling, *Annals of the CIRP*, **45**(1), pp. 393-396.

[164] Tobias, S.A. (1965), *Machine Tool Vibration*, Blackie, London.

[165] van der Pol, F., Strutt, M. J. O. (1928) On the stability of the solutions of Mathieu's equation, *Philosophical Magazine, and Journal of Science*, **5**, pp. 18-38.

[166] Volterra, V. (1928) Sur la theorie mathematique des phenomenes hereditares, *Journal de Mathématiques Pures et Appliqués*, **7**, pp. 149-192.

[167] Whitehead, B. T., Bayly, P. V., Calvert, S. G. (2001) The effect of process damping on stability and hole form in drilling, *Proceedings of the SAE Aerospace Manufacturing Technology Conference, Seattle, Washington*, paper no. 2001-01-2605 (CD-ROM).

[168] Whitney, D. E. (1977) Force feedback control of manipulator fine motions, *Journal of Dynamics Systems, Measurement and Control*, **98**, pp. 91-97.

[169] Wiercigroch, M., Budak, E. (2001) Sources of nonlinearities, chatter generation and suppression in metal cutting, *Philosophical Transactions of the Royal Society*, **359**, pp. 663-693.

[170] Zhang, Z., Li, Q. (1998) Oscillation theorems for second-order advanced functional difference equations, *Computers & Mathematics with Applications*, **36**(6), pp. 11-18.

[171] Zhao, M. X., Balachandran, B. (2001) Dynamics and stability of milling process, *International Journal of Solids and Structures*, **38**(10-13), pp. 2233-2248.

[172] Zounes, R. S., Rand, R. H. (2001) Global behavior of a nonlinear quasiperiodic Mathieu equation, *Proceedings of the ASME 2001 Design Engineering Technical Conferences, Pittsburgh, Pennsylvania*, paper no. DETC2001/VIB-21595 (CD-ROM).